SAPIENZA
UNIVERSITÀ DI ROMA

Optimal Control of Systems with Memory

Doctorate school in Mechanical Engineering

Dottorato di Ricerca in Meccanica Teorica e Applicata – XXXI Ciclo

Candidate

Elena Paifelman

ID number 1326268

Thesis Advisor

Prof. Antonio Carcaterra

Co-Advisor

Ing. Francesco La Gala

October 2018

Optimal Control of Systems with Memory
Ph.D. thesis. Sapienza – University of Rome

This thesis has been typeset by LaTeX and the Sapthesis class.

Version: February 2, 2019

Author's email: elena.paifelman@uniroma1.it

To convolution

Abstract

The “Optimal Control of Systems with memory” is a PhD project that is borne from the collaboration between the Department of Mechanical and Aerospace Engineering of Sapienza University of Rome and CNR-INM the Institute for Marine Engineering of the National Research Council of Italy (ex INSEAN). This project is part of a larger EDA (European Defence Agency) project called ETLAT: Evaluation of State of the Art Thin Line Array Technology. ETLAT is aimed at improving the scientific and technical knowledge of potential performance of current Thin Line Towed Array (TLA) technologies (element sensors and arrays) in view of Underwater Surveillance applications.
A towed sonar array has been widely employed as an important tool for naval defence, ocean exploitation and ocean research. Two main operative limitations costrain the TLA design such as: a fixed immersion depth and the stabilization of its horizontal trim. The system is composed by a towed vehicle and a towed line sonar array (TLA). The two subsystems are towed by a towing cable attached to the moving boat. The role of the vehicle is to guarantee a TLA’s constant depth of navigation and the reduction of the entire system oscillations. The vehicle is also called "depressor" and its motion generates memory effects that influence the proper operation of the TLA. The dynamic of underwater towed system is affected by memory effects induced by the fluid-structure interaction, namely: vortex shedding and added damping due to the presence of a free surface in the fluid. In time domain, memory effects are represented by convolution integral between special kernel functions and the state of the system. The mathematical formulation of the underwater system, implies the use of integral-differential equations in the time domain, that requires a nonstandard optimal control strategy. The goal of this PhD work is to developed a new optimal control strategy for mechanical systems affected by memory effects and described by integral-differential equations. The innovative control method presented in this thesis, is an extension of the Pontryagin optimal solution which is normally applied to differential equations. The control is based on the variational control theory implying a feedback formulation, via model predictive control.
This work introduces a novel formulation for the control of the vehicle and cable oscillations that can include in the optimal control integral terms besides the more conventional differential ones. The innovative method produces very interesting results, that show how even widely applied control methods (LQR) fail, while the present formulation exhibits the advantage of the optimal control theory based on integral-differential equations of motion.

Acknowledgments

I would first like to thank my thesis supervisor, Prof. Antonio Carcaterra, who has always inspired me and instilled me the passion for research. I would also like to thank my collegue and friend Gianluca Pepe for helping me and supported along all the doctoral period.
Thank to Francesco La Gala who gave me the chance to do this work, stimulating me with new technical-scientific challenges. I thank also Prof. Aldo Sestieri and Elena Ciappi for their kindness and for the very useful advices on drafting this thesis.
I thank my colleagues of CNR-INM Fabrizio and Luca for their sympathy and support during all these years. Thank to my doctoral collegues in Sapienza for sharing and supporting each other during this, sometimes hard, journey. I would like to thank especially, Lina, Federica and Manuel for their patience, cigarettes and friendship.
Thank to Francesca and Silvia my friends of all time for always trusting me. Finally, I must express my very profound gratitude to my parents, my sister and my boyfriend for providing me with unfailing support and continuous encouragement throughout my years of study and through the process of researching and writing this thesis. This accomplishment would not have been possible without them. Thank you.

Index of contents

List of Figures

List of Tables

Chapter 1

Introduction

The goal of this work is to develop a new optimal control strategy for mechanical systems affected by memory effects and described by integral-differential equations. In particular, tha main engineering application presented in this work concerns the control of typical underwater systems for underwater surveillance applications.
This PhD project is borne from the collaboration between the Vibrations, Mechatronics and Vehicle Dynamics Research Group of the Department of Mechanical and Aerospace Engineering of Sapienza University of Rome and the Council of National Research Institute of Marine engineering CNR-INM (ex CNR-INSEAN) of Rome.

1.1 The ETLAT project

This work is part of a European project, ETLAT: Evaluation of State of the Art Thin Line Array Technology (TLA) which goal is to improve the design of the TLAs systems. These systems and their dynamical behaviour have been evaluated during this project by comparing numerical simulations with experimental hydrodynamic tests performed by INM.
The presented work is framed in the major landscape of underwater surveillance. My personal contribution does not concern only the definition of a control law, main focus of the present thesis, but it futher involves all those activities necessary to successfully complete the project.
In this regard, experimental campains have been carried out so to test the dynamical behaviour of the mechanical system (induced vibrations and self noise) and to evaluate their hydrodynamic properties (drag force).
Eventually, the data post-processing was the final operation, crucial to extract and determine the dynamic parameters that have to be compared with the numerical simulations made by the other partner involved in the project.

1.2 Limitations of engineering system

The underwater mechanical system tests in this project, is composed by a towed vehicle and a towed line sonar array (TLA)[1–4].

The towed sonar array has been an important tool for naval defence, ocean exploitation and ocean research [5–9].
The TLA is an underwater array in which sonar, accelerometer and hydrophone sensors are used to make acoustic, dynamic, vibrational underwater measurements [10, 11].
The study of underwater arrays has been an area of considerable research effort. Cables are extensively used for many ocean applications. Just a few examples of ocean systems that make wide use of cables are the ocean mooring systems, towed array sonar systems and remotely operated vehicles (ROV) shown in Figure 1.1. The

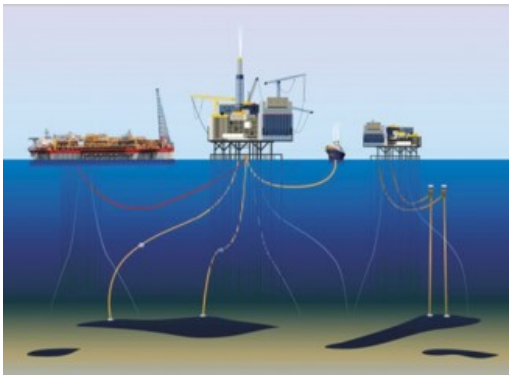

(a) mooring lines

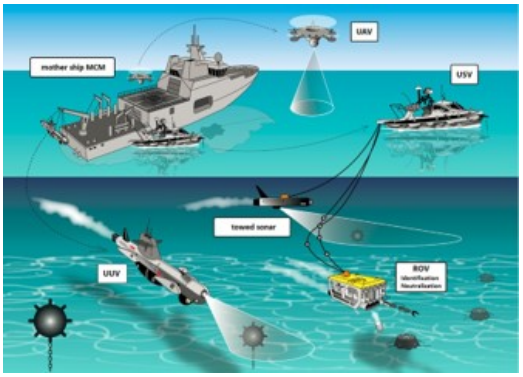

(b) ROV

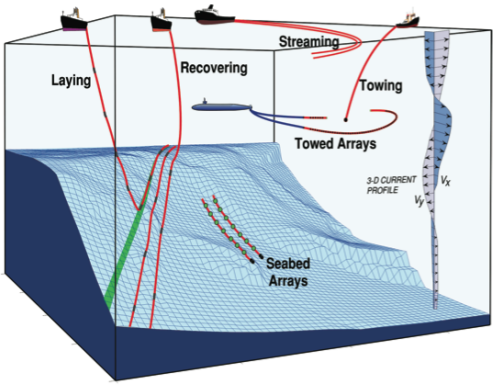

(c) towed arrays

Figure 1.1. Underwater cable applications

static cable problems have found application in the design of buoy [12] , mooring lines [13] , suspended pipelines and marine riser [14]. Many theories have been developed for the static response of submarine cable as [15–18].
The underwater cables are characterized by an unstable dynamic when they are towed in the fluid flow. The main underwater instabilities can be divided in (i) flow induced vibrations and vortex shedding [19–22] (ii) hydroelastic instabilities [23, 24].
Vortex induced vibrations (VIV) occur in many engineering situations, such as bridges, stacks, transmission lines, aircraft control surfaces, offshore structures,

thermowells, engines, heat exchangers, marine cables, towed cables, drilling and production risers in petroleum production, mooring cables, moored structures, tethered structures, buoyancy and spar hulls, pipelines, cable-laying, members of jacketed structures, and other hydrodynamic and hydroacoustic applications.
One of the classical open-flow problems in fluid mechanics concerns the flow around a circular cylinder, or more generally, a bluff body. At very low Reynolds numbers (based on the diameter of the circular member) the streamlines of the resulting flow is perfectly symmetric as expected from potential theory. However, as the Reynolds number is increased the flow becomes asymmetric and the so-called Kármán vortex street occurs. The Strouhal number relates the frequency of shedding multiply by a characteristic dimension of the body (diameter in the case of a cylinder) to the velocity of the flow. It is defined as $St = f_{st}D/U$, where f_{st} is the vortex shedding frequency (or the Strouhal frequency) of a body at rest, D is the diameter of the circular cylinder, and U is the velocity of the ambient flow.
The second effect of instability is the hydroelasticity or flexible fluid-structure interaction (FSI) which concernes the motion of deformable bodies into fluids. The theory of hydroelasticity has been adapted from aeroelasticity, to describe the effect of structural response of the body on the fluid around it. The interaction between the elastic behavior of the TLA and the flow field around it generates vortex instabilities.
A good survey on the dynamical behavior of underwater arrays can be found in [25–29].
Due to the unstable nature of the TLA and the presence of acoustic sensors inside the array, the TLA's operating requires specific costrains. One typical application of the TLA regards the oil detection under the seabed. Many TLA arrays, long kilometers, are towed in ocean by a moving boat, the hydrophone sensors inside the TLA are used to emit acoustic waves. Reflection at the seabed implies the presence or not mineral or gas underwater resources.
The acoustic sensors functioning depends on the TLA dynamic implying operative limitations on the TLA as:

- *An Operative frequency range* which is directly correlated to the correct measurements by sensors.
- *A Stable dynamic*, because dynamical instabilities could add noise to the measurements (self noise).
- *A Fixed sensing depth* which is important to reconstruct the position of the sensors and to correlated the respective signals recorded.

For these reasons, two main engineering requirements costrain the TLA design such as: a fixed immersion depth and the stabilization of its horizontal trim [30–32].
During my partecipation in the experimental campain performed in the frame of the ETLAT project, we faced with these dynamic unstabilities. The tests were performed at INM on different TLAs geometry (lenght, diameter, material). In order to reduce these effects during experiments was necessary to adjust the TLA configuration by adding tail or similar bouy part.
To better deal with those phenomena, has been established to convert the passive

vehicle into a controlled one.
The role of the vehicle is to guarantee a TLAs constant depth of navigation and the reduction of the entire system oscillations [17, 33]. The vehicle is also called depressor and its motion generates memory effects which influence the proper operation of the TLA [34].
Memory effects are frequently induced by fluid-structure interaction. In this work two main phenomena claim for these effects in the model: (i) vortex wake and (ii) added damping due to the presence of a free surface in the fluid.
Underwater autonomous or remotely operated vehicles are examples [35–41]. The vorticity can be generated by the motion of the vehicle as well as by the presence of cables (ROV-Sonar array), [2, 42, 43]. A vehicle moving close to the water free surface induces waves which, in turn, influence the motion of the vehicle [44–47].
In time domain, memory effects are represented by convolution integral between special kernel functions and the vehicle state [48–50]. In fact, the depressor motion which is affected by these two kind of memory effects is represented by an integral-differential mathematical model. In this work an optimal control law for the underwater depressor motion which guarantees the engineering costrains of the TLA's design is developed. The presence of convolution terms in the model requires a nonstandard optimal control strategy.

1.3 Overview of integral-differential control literature

Robust control techniques are often used to control underwater vehicle [51–54]. Normally, the underwater vehicles are represented by nonlinear rigid body models [55–57] and these techniques do not involved integral memory effects.
The optimal control applications applied to underwater vehicle present in literature normally do not take in account memory effects into the model. These effects are neglected or approximated by small external system perturbations [58–61].
Many problems in economics, biology, epidemiology and memory effects can be modeled as Volterra control problems which are solvable by dynamic programming methods [62–66].
The optimal control techniques applied on integral-differential equations present in literature are mainly based on direct methods.
There are two classes of methods employed to solve the optimal control system design problems: (i) indirect and (ii) direct optimal control methods.
The indirect methods are based on the variational method of optimal control theory, which typically consists in the calculus of variations and Pontryagin's methods [67, 68], that can be used to derive a set of necessary conditions that must be satisfied by an optimal control law and its associated state-control equations. These necessary conditions of optimality lead to a (generally nonlinear) boundary-value problem (BVP) that must be solved to determine the explicit expression for the optimal control. Except in some special cases, the solution of this BVP is difficult, and in some cases not practical to obtain. In simple cases the BVP may be solved analytically, but in more general cases it must be discretized and solved numerically, [69].
Direct optimal control methods take the opposite approach, where the optimal control problem is discretized at the first step. The state and/or control of the

original optimal control problem are approximated in some appropriate manner. In the case where only the control is approximated, the method is called a *control parameterization method*. When both the state and control are approximated the method is called a *state and control parameterization method*. The state space equations are discretized to form a system of algebraic equations (known as defect equations or defect constraints, similar to residual functions). The result is a nonlinear program (NLP) that can be solved using standard large-scale optimization algorithms [70–75].
Direct methods are particularly effective for highly nonlinear systems, problems with inequality constraints, or other situations where indirect methods fall short [71, 76].
The principal optimal control direct method applied to integral-differential equations with a quadratic performance index is founded in [72, 77–79].
The direct methods applied to IDEs optimal control problem present in literature are divided into different categories on the basis of the kind of discretization used [80].

- **Control parametrization methods**
  - *Direct shooting method* is a control parameterization method where the control is parameterized using a specified functional form, e.g:

$$u(t) \approx \sum_{i=1}^{m} a_i \phi_i(t) \tag{1.1}$$

    where $\phi_i(t)$ are known functions and a_i are the parameters to be determined from the optimization. The NLP that arises from direct shooting minimizes the cost subject to any path and interior-point constraints.
    The most straightforward of the direct methods is singleshooting [81]; state trajectories are obtained for every NLP function evaluation by solving the defect equations using forward simulation. The control is parameterized using either a polynomial approximation or another appropriate method. Given a set of initial conditions and a control parameterization, the optimization is then performed with respect to the control parameters (e.g., polynomial coefficients).
  - In the *Direct multishooting method*, the time interval is divided into subintervals. The direct shooting method is applied in each time subinterval with the values of the state at the beginning of each subinterval and the unknown coefficients in the control parameterization being unknowns in the optimization. It is seen that the direct multiple-shooting method increases the size of the optimization problem because the values of the state at the beginning of each subinterval are parameters in the optimization. Despite the increased size of the problem due to these extra variables, the direct multiple-shooting method is an improvement over the standard direct shooting method because the sensitivity to errors in the unknown initial conditions are reduced because integration is performed over significantly smaller time intervals.

- **State-Control parametrization methods**
  - *Direct collocation method* is a state and control parameterization method where the state and control are approximated using a specified functional form. The two most common forms of collocation are local collocation and global collocation. Local collocation has been employed using one of two categories of discretization: Runge-Kutta methods, [82], and orthogonal collocation methods.
  - *Pseudospectral (Global Orthogonal Collocation) Methods* is a global form of orthogonal collocation, i.e., in a pseudospectral method the state is approximated using a global polynomial and collocation is performed at chosen points. Thus, as opposed to local collocation, where the degree of the polynomial is fixed and the number of meshes is varied, in a pseudospectral method the number of meshes is fixed and the degree of the polynomial is varied.

Both the collocation and the pseudospectral methods depend on the choise of the basis functions used in the discretizations of the system. Some collocation techniques for solving the optimal control problem governed by Volterra integral equations imply the use of orthogonal functions [83].
The orthogonal functions have received considerable attention dealing with various optimal control problems. The approach is to convert the underlying differential equation into an integral equation through integration, approximating various signals involved in the equation by truncated orthogonal functions, and using the operational matrix of integration to eliminate the integral operations. This matrix can be uniquely determined based on the particular orthogonal functions. Among piecewise constant basis functions, block-pulse functions are found to be very attractive, in view of their properties of simplicity and disjointedness, among orthogonal polynomials, the shifted Legendre polynomials is computationally more effective [84–86]. Elnagar and Razzaghi in [87] have presented a pseudospectral Legendre method for linear quadratic optimal control problems .
The Bernoulli polynomials and Taylor series are not based on orthogonal functions, nevertheless, they possesses the operational matrices of integration. However, since the integration of the cross product of two Taylor series vectors is given in terms of a Hilbert matrix, which are known to be ill conditioned, the applications of Taylor series are limited.
In recent years the hybrid functions consisting of the combination of block-pulse functions [88] with Chebyshev polynomials [72, 85, 89–92] , Legendre polynomials [93–96] or Taylor [97, 98] or Fourier [83, 99] series have been shown to be a mathematical power tool for discretization of selected problems. Mashayekhi in [100] reduces the optimal control problem on IDEs to a NLP one by first expanding the state rate vector and the control vector as a hybrid function with unknown coefficients. These hybrid functions consist of block-pulse functions and Bernoulli polynomials.
A suitable method with Lipschitz controls has been suggested for Volterra control problems by Belbas in [64], and a method based on approximating the

controlled Volterra integral equations by a sequence of systems of controlled ODEs has been presented in [66].
Maleknejad in [101] exploits the structural properties of triangular orthogonal functions for reducing the optimal control problem to a set of algebraic equations by expanding the state vector and control vector as triangular orthogonal functions in a direct method without any integration.
Shen applies the Galerkin finite element methods to the optimal control problem governed by an elliptic integral-differential IDEs with random field [102–105]. A gradient algorithm based on the pre-conditioner conjugate gradient algorithm (PCG) is developed for this optimal control problem. This algorithm can transform a part of the state equation matrix and co-state equation matrix into block diagonal matrix and then solve the optimal control systems iteratively. Other application of the Galerkine finite element method to the optimal control of IDEs can be found in [106, 107].

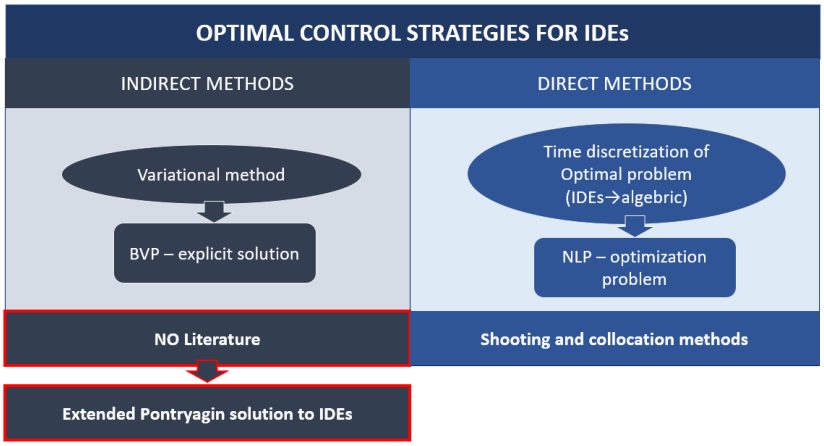

Figure 1.2. Optimal control methods on integral-differential equations

The scheme in Figure 2.4 shows a short resume of the principal optimal control methods applied on integro-differential equations. It is clear from the literature studies that, there is not an optimal control indirect method which implies a variational approach to IDEs.
Only direct and nonlinear programming methods are used to control integro-differential equations of motion.
The great power of the optimal control method theorized in this work is the fomrulation of a novel indirect variational optimal control approach for IDEs.
In fact, as already explained, these problems are generally approached with direct control methods and a general variational theory is missing in the global optimal control theory of IDEs panorama.
The control method proposed in this work, is an extension of the Pontryagin optimal solution, normally applied to differential equations.
The present approach, based on the VFC-variational feedback implying a feedback formulation. This control logic has been applied in recent investigations of car mechatronics [108, 109]. Moreover the same approach can be applied to optimal

control problems of damping in structural dynamics as well [110–113]. More specifically, in this work, a feedback via model predictive control (MPC) is formulated for integral-differential system model. Normally the MPC method is applied to differential equations [114, 115].

This work is divided into five Chapters. In Chapter 2 the prototypical control problem is described. The engineering problem and a possible control strategy are discussed. The introduction of memory effects and the novel variational calculus on convolution terms is illustred in details (Section 2.4).
The integral-differential equations of motion of the underwater depressor affected by memory effects is explained in Chapter 3. Starting from the potential theory, the general equation of motion is illustred. Two main mathematical models are considered: the 1-Dof motion of the depressor in which the added damping memory effect and the release of vorticity are modelled; and the classical 2-Dof hydrofoil model by Theodorsen that models the vortex wake generation of the control surface of the vehicle.
In Chapter 4 the novel optimal control theory applied to IDEs is shown. The new control algorithm is presented as an extension of the Pontryagin classical theory underlying the principal differences between the two approach (Section 4.2). The implicit solution of the optimal control problem is illustred in Section 4.3 and the feedback formulation via a novel integral model predictive control is founded in Section 4.4.
Finally, the numerical results of the integral optimal control applied to different depressor IDE models are shown in Chapter 5. The novel algorithm exhibits better results in comparison to the standard LQR (linear quadratic regulator) optimal control strategy.

Chapter 2

Overall description of the control problem with memory

In this Chapter the engineering problem analyzed in this work is illustred in details. The physical and the related mathematical complexities of the system are introducted. The necessity of the control of the depressor is justified by introducing the problems related to the operation of the entire underwater system. The presence of memory effects in the model due to the fluid-solid interaction implies the presence of convolution terms in the model that suggests a nonstandard optimal control strategy.
Finally, the variational calculus is extended to a general convolution term. This is the first novel result of this work, the starting point of the variational approach used to extend the Pontryagin's solution to the optimal control of IDEs.

2.1 Introduction to the problem formulation

A classical towed mechanical system used in ocean exploration and military applications, is composed by a towed vehicle V and a towed line array (TLA) sonar [116, 117]. The two subsystems are towed by the towing cable attached to the moving

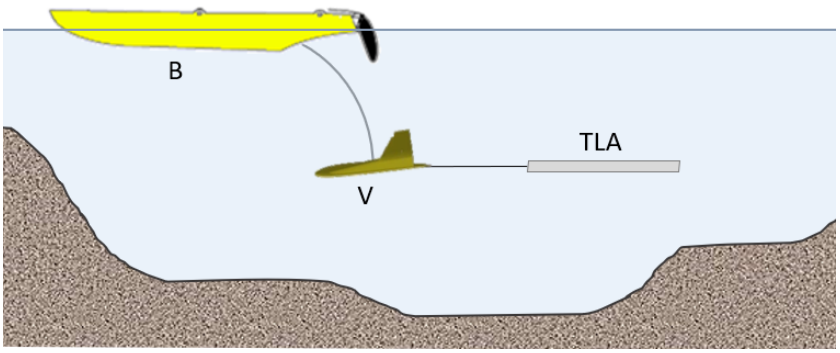

Figure 2.1. Underwater towed system

boat, B (Figure 2.1). The TLAs, employed for the ocean detection, are plastic arrays

in which are located sonar and accelerometer sensors (Figure2.2).

Figure 2.2. Thin line array (TLA)

As explained in detail in Chapter 1, the correct use of the TLAs is influenced by:

- an operative frequency range (self noise)
- an unstable dynamic
- a stable sensing depth

and operative limitations are required to gaurantee a correct utilization:

- a fixed immersion depth
- the stabilization of the horizontal configuration

The goal of the vehicle V (Figure 2.3) is to guarantee a TLA's constant depth of navigation and the reduction of the entire system oscillations [17, 118, 119]. Figure 2.3 shows the prototype and the final design of the depressor. The vehicle has been designed and created by 3D printing technology by INM. Moreover, CFD simulations have been carried out to compute the hydrodynamic forces on the depressor for different configurations (angle of attack). Preliminary experimental tests have been also developed to validate the numerical simulations. The main goal of these tests was to check the depressor's dynamic stability and the reaching of a fixed navigation depth [17].

The depressor is characterized by a great stability at varying towing speed and maneuvers. Accelerometers, IMU and GPS sensors are inside the vehicle in order to reconstruct its motion and compute its vibrations during experiments.

The problem's formulation imply a very high physical complexity which introduces complexities in the mathematical model. The presence of different underwater subsystems interacting each other generates fluid-structure interaction phenomena. This effects, that are the main contribution on which this thesis is focused, are formulated as convolution integrals in the model. Also the presence of cables in the system (towing cable and TLA) make the system highly nonlinear. Moreover, the presence of incident waves have as mathematical counterpart external random forces. Finally, the hydroelasticity arises by the interaction between the fluid and the TLA dynamic makes the model's operator stochastic.

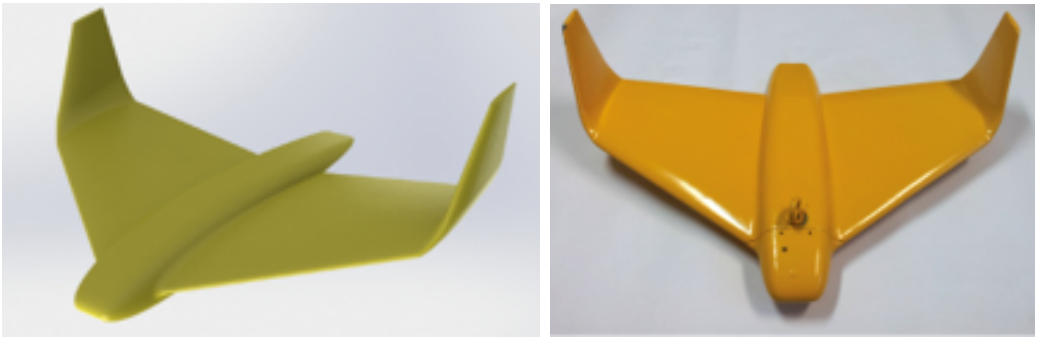

Figure 2.3. Finned depressor

The huge mathematical complexities of the model give a final equation of motion that is a set of nonlinear partial differential equations combined with a set of integro-differential equations with stochastic operators and external loads (see Figure 2.4).

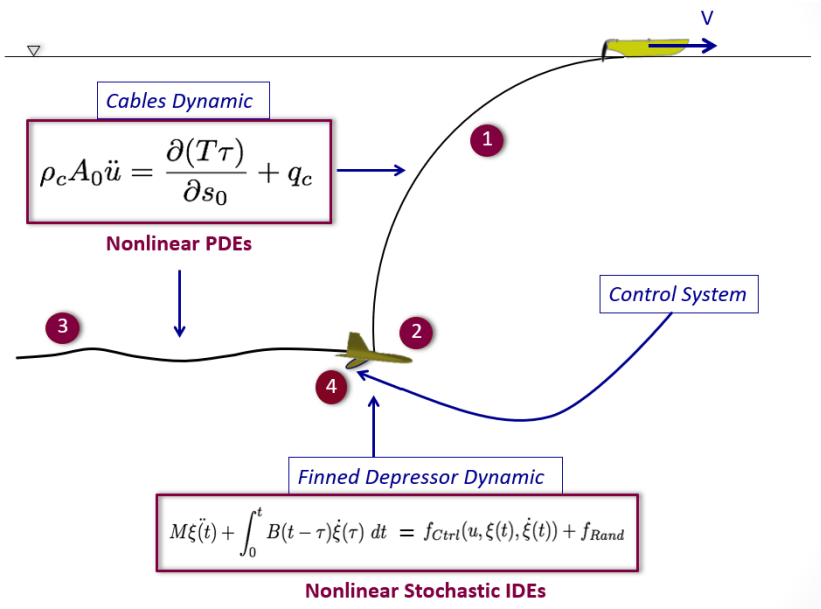

Figure 2.4. Mathematical complexity of entire system

2.2 Outline of a possible strategy of optimal control

The complexity of the model makes difficult an optimal control strategy on the depressor's motion. To control a set of nonlinear PDEs combining with a set of IDEs with stochastic operator and external loads, it's necessary formulated a complicated nonstandard optimal control formulation.
Expressing this model as:

$$\dot{x} = f(x, u, y) \tag{2.1}$$

where x is the state, u the control variable and y the external forces acting on the system. The critical components that characterized this optimal control problem can be summarized as:

- f nonlinear (hydrodynamic forces, cables);
- **f** integro-differential (memory effects);
- **y** stochastic (waves, cables hydroelasticity).

At first step of analysis only the fluid-structure interaction has been considered in the model. In fact, this phenomena has a principal role in the generation of the dynamical unstabilities of the underwater system. So the focus is only on the criticality that considers the system **f** integro-differential.
In the future, also the other effects will be insered in to the mathamtical model.
The role of the depressor is to reach the TLA's operative conditions that are:

(i) the minimization of the TLA's vibrations $min(v)$ ($v_2 < v_1$);

(ii) the reaching of a stable sensing depth (H_2) as shown in Figure 2.5.

V is also called "depressor" [33] and its motion generates memory effects that influence the proper operation of the TLA [120].
For these reasons, the goal of this work is to developed an optimal control law on the depressor dynamic in order to:

- minimize its vibrations induced by memory effects that influence the proper operation of the TLA;
- guarantee the reaching of its fixed depth.

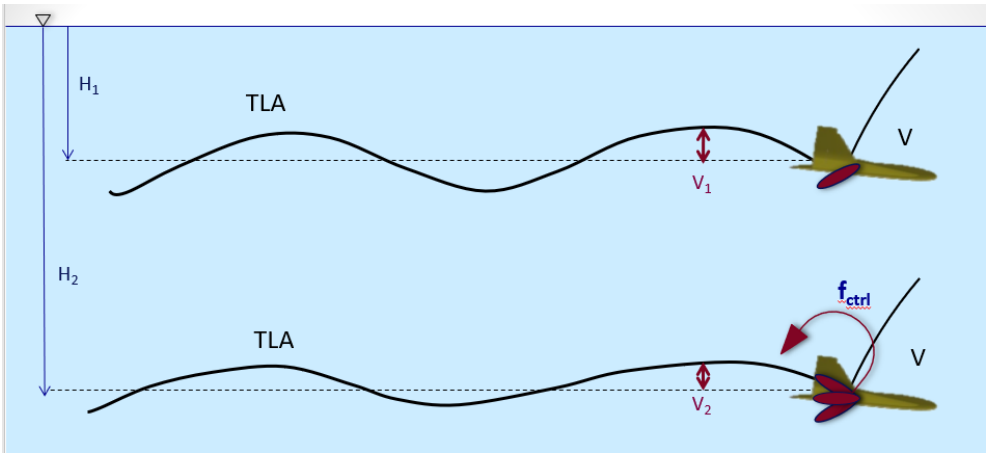

Figure 2.5. Control system overview

The presence of memory effects which affected the depressor motion, implies the use of integral-differential equations in the time domain, that requires a nonstandard optimal control strategy.

2.3 Memory effects

Memory effects are frequently induced by the fluid-structure interaction.
The hydrodynamic load on a body moving into an ideal fluid in waves contains the memory of the motion history in terms of memory effects.
In this work two main phenomena claim for these effects in the model: vortex shedding and added damping.
If the vehicle moves close to the free surface, memory effect called added damping is borne. An oscillating underwater body closed to the free surface radiates out waves, these will affect the fluid pressure changing the forces applied by the fluid on the body during all the subsequent time. This "circular" interation phenomena starts the so called added damping memory effect. The dynamic of the vehicle is affected by these effects because the distance of the body from the free surface is less than its chord length (h<$2b$). Moreover, the depressor motion could induce the release of vortex wake which influence the stability of the TLA.
This effect is induced by the interactions between the inertial, elastic, and hydrodynamic forces that occur when an elastic body is moving into a fluid flow. The modelling of the vortex wake will be exposed in Chapter 3.1.2.
The two kind of memory effects are represented in the depressor model by convolution integrals in time domain:

$$F_{memory} = \int_{-\infty}^{t} \boldsymbol{K}(t-\tau)\boldsymbol{y}(\tau)d\tau \tag{2.2}$$

These terms are the convolutions between "special" kernel function, $\boldsymbol{K}(t)$, and the "memory" of the past motion of the underwater depressor, $\boldsymbol{y}(t)$. The kernel functions, positive defined, depend on the geometry of the body and can computed by experimental test or by using panel numerical method. For simple geometry these functions are well known in literature [121].

2.4 Variations for memory effects

In order to develop an indirect variational optimal control algorithm for these kind of problems, the first innovative result of this work is the variations for the memory effects terms.
At this step of the study this was the first problematic with we faced. In fact, in literature is not present a general variational formulation for convolution integrals. So in this Section, an original variational calculus is proposed for a general convolution integral.
These results will be foundamental in the mathematical formulation of the integro-differential optimal control theory proposed.
The variations of the following expression:

$$\int_{-\infty}^{T} \boldsymbol{g}^T(t) \left[\delta \int_{-\infty}^{t} \boldsymbol{K}(t-\tau)\boldsymbol{y}(\tau)\, d\tau\right] dt \tag{2.3}$$

are computed with respect to the state variable $\boldsymbol{y}(t)$ when a general convolution term is multiplied by a general time function $\boldsymbol{g}(t)$ and the kernel matrix $\boldsymbol{K}(t)$ is a

time function.
Note that the causality of the impulse response implies $\boldsymbol{K}(t-\tau) = 0$ if $\tau > t$, and:

$$\int_{-\infty}^{t} \boldsymbol{K}(t-\tau)\boldsymbol{y}(\tau)\, d\tau = \int_{-\infty}^{T} \boldsymbol{K}(t-\tau)\boldsymbol{y}(\tau)\, d\tau \tag{2.4}$$

Expression (2.3) becomes:

$$\int_{-\infty}^{T} \boldsymbol{g}^T(t) \left[\delta \int_{-\infty}^{T} \boldsymbol{K}(t-\tau)\boldsymbol{y}(\tau)\, d\tau\right] dt \tag{2.5}$$

Changing the order of integration:

$$\int_{-\infty}^{T}\int_{-\infty}^{T} \boldsymbol{g}^T(t)\boldsymbol{K}(t-\tau)\, dt\, \delta\boldsymbol{y}(\tau)\, d\tau = \int_{-\infty}^{T}\int_{\tau}^{T} \boldsymbol{g}^T(t)\boldsymbol{K}(t-\tau)\, dt\, \delta\boldsymbol{y}(\tau)\, d\tau \tag{2.6}$$

where the causality property of $\boldsymbol{K}(t)$ has been used. It permits to conclude:

$$\int_{-\infty}^{T} \boldsymbol{g}^T(t) \left[\delta \int_{-\infty}^{t} \boldsymbol{K}(t-\tau)\boldsymbol{y}(\tau)\, d\tau\right] dt = \int_{-\infty}^{T}\int_{t}^{T} \delta\boldsymbol{y}^T(t)\boldsymbol{K}^T(\tau-t)\boldsymbol{g}(\tau)\, d\tau\ dt \tag{2.7}$$

Chapter 3

Fluid-body interaction control: A physical example of memory effects

In this chapter the integral-differential model of the finned depressor is described. The general equations of motion of an underwater body moving close to the free surface is briefly illustred in the frame of the potential theory formulation. The general mathematical contributes of the memory effect, added mass and damping, is discussed in Section 3.1. Meanwhile, the Theodorsen model is analysed in Section 3.1.2.
Starting from the formulation of a general integral-differential model of an underwater body motion affected by the presence of memory effects, two different models are analysed in detail.
A prototype 1-Dof model, which describes the depressor heave motion when it is moving close to the free surface releasing wake is presented (Section 3.3). The second model is the classical 2-Dof hydroelastic Theodorsen model which characterize the unsteady hydrodynamic forces on an oscillating hydrofoil vehicle's control surface affected by memory effects (Section 3.4).
Both the depressor models are integro-differentials precluding the use of classical optimal control techniques by requiring a new nonstandard optimal control formulation. A general N-Dof extension of these models is proposed that will be the IDE model on which the optimal control theory is applied.

3.1 Mathematical formulations of memory effects

In this section the equations of motion of a general submerged body in waves, in the frame of the potential theory are briefly illustred. This theory concerns a potential, incompressible, irrotational and inviscid fluid. The potential problem with the

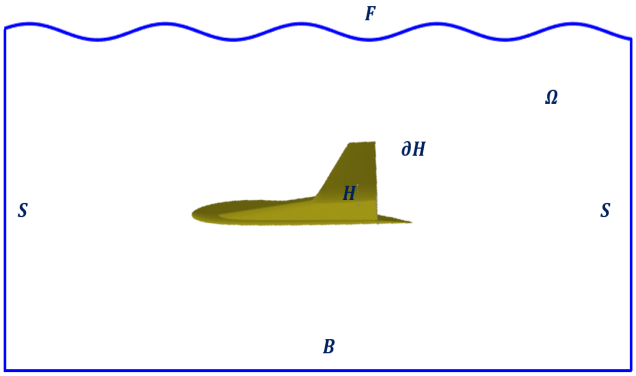

Figure 3.1. Fluid domain

linearized boundary conditions, is described by the general resolutive system [121]:

$$\begin{cases} \nabla^2\phi_j \quad \text{in } \Omega \\ \frac{\partial\phi_j}{\partial n} = V_j \cdot n_j \quad \text{on } \partial H \\ \frac{\partial\phi_j}{\partial n} = 0 \quad \text{on B} \\ \frac{\partial^2\phi_j}{\partial^2 t} + g\frac{\partial\phi_j}{\partial n} = 0 \quad \text{on F} \\ \frac{\partial\phi_j}{\partial R} = (-\frac{1}{2R} + i^*k)\phi_j \quad \text{on } S \end{cases} \tag{3.1}$$

where the Ω is the fluid domain, H is the body surface, B is the ocean seabed, F is the sea free surface and S is the far-field (see Figure 3.1). The body motion in terms of potential velocity is $\phi_j = A_j e^{-i\sigma t}$ where j indicates a generic degree of freedom of the body, $\xi_j(t),\ j \in [1,6]$ as show in Figure 3.2 (1=surge, 2=sway, 3=heave, 4=roll, 5=pitch, 6=yaw).

From the potential theory, the hydrodynamic forces acting on a body moving in waves is based on the superposition of the radiation forces (R) due to the body motion in an undisturbed sea and diffraction forces (D) due to the wave forces on a non-moving body.

$$F^W = F^R + F^D \tag{3.2}$$

In this work the focus is on the radiating component of the forces which is due to the fluid-structure interaction and generates memory effects. The diffracted force can be neglected as the length of the body is smaller with respect to the wavelength. The radiating forces, due to the fluid-structure interaction can be computed as:

$$F^R = -\int_S \rho\phi n dS \tag{3.3}$$

the integral over the fluid domain surface of the potential velocity.

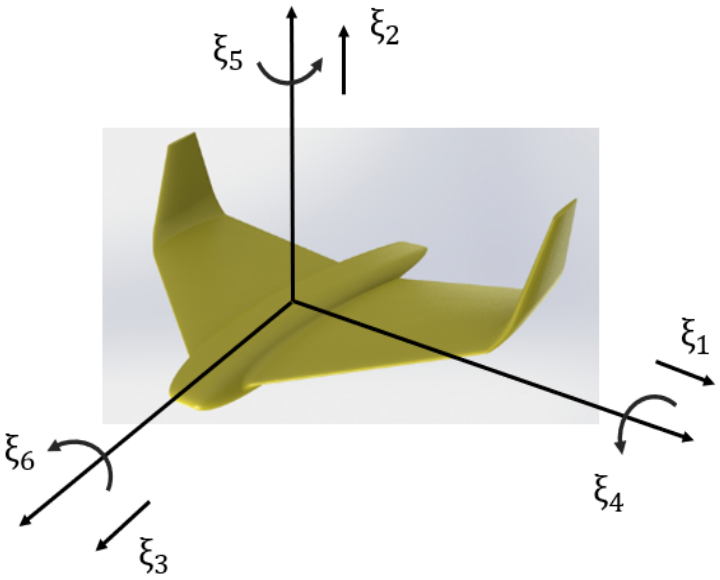

Figure 3.2. Sketch of 6-Dof depressor

3.1.1 Added damping

When the body is forced to oscillate, waves will propagate outward from the body. This will affect the fluid pressure and change the fluid momentum hence the body force for all subsequent times. This physical memory effect is obviously due to the presence of the free surface. This effect is taken in account because the vehicle is moving at a distance from the free surface (h) lower than its chord length ($2b$). In

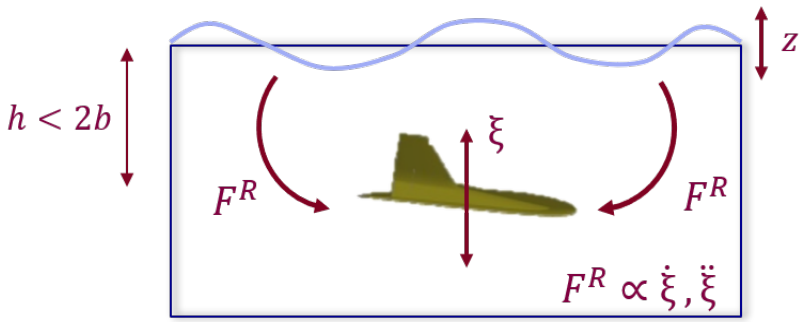

Figure 3.3. Generation of added mass and damping effects

Figure 3.3, the generation of this kind of memory effect has been schematized. The inclusion of the memory effects in the radiating forces has been theorized by Ogilvie in frequency domain [122]. Moreover, this model is not suitable for controller design because its coefficients are frequency dependent. For these reasons, the radiating

force are modelled by Cummins [123] in the time domain as:

$$\boldsymbol{F^R} = -\boldsymbol{A}\,\ddot{\boldsymbol{\xi}}(t) - \int_{-\infty}^{t} \boldsymbol{K_D}(t-\tau)\dot{\boldsymbol{\xi}}(\tau)\,d\tau \tag{3.4}$$

The hydrodynamic coefficents A and K_D are the infinite frequency costant added mass matrix ($\omega \to \infty$) and added damping function in the time domain, respectively. The memory effects are rapresented by the convolution integral over the previous history of the fluid motion. The kernel $\boldsymbol{K_D}(t-\tau)$ can be interpreted as the impulse force, at time t, due to a delta-function body velocity at an earlier time τ.
Added mass value and added damping function in time are known for different oscillating body's geometry [121].

3.1.2 Vortex wake model

In this section the general theory of hydrodynamic instability and the mechanism of the vortex wake release modelled by Theodorsen is shortly described. The vortex wake model is now presented for a general two degree of freedom hydrofoil oscillating in heave and pitch $\boldsymbol{\xi}=[\upsilon, \alpha]^T$ that model the control surface of the underwater vehicle. Figures in 3.4 show two sketches of the hydofoil vortex wake generation where F_C are the circular memory forces. The Theodorsen theory implies

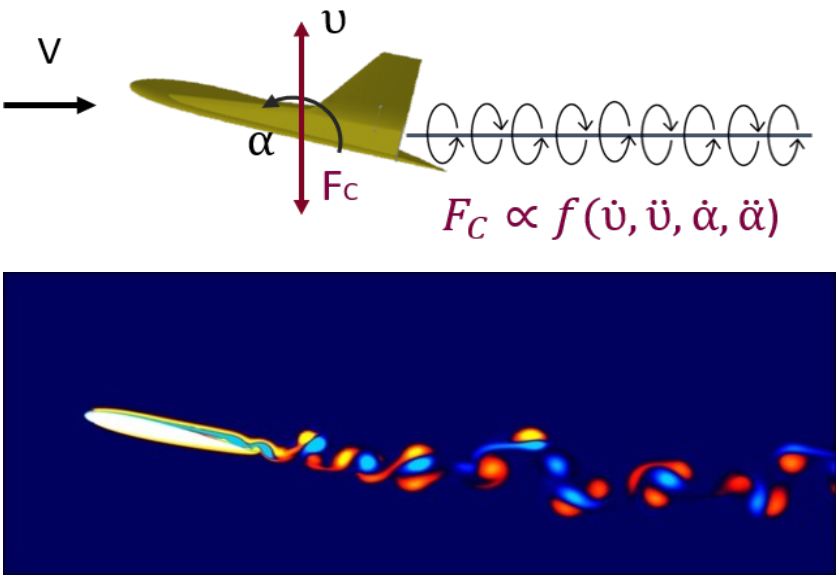

Figure 3.4. Vortex wake release

the definition of the velocity potential due to the flow around the hydrofoil [48]. The hydrodynamic forces and moments are obtained by integration starting from the velocity potential definition. The lift force, L and the pitching moment, M_α, acting on the hydrofoil are composed by two different contributions:

$$\boldsymbol{L} = \boldsymbol{L^{NC}} + \boldsymbol{L^{C}} \tag{3.5}$$

$$M_\alpha = M_\alpha^{NC} + M_\alpha^C \tag{3.6}$$

the noncirculatory (NC) and circulatory (C) part of the forces.
The expressions of the hydrodynamic forces will be illustred in details in next Section 3.4. Meanwhile, in this section the focus is on the circulatory part of the hydrodynamic forces due to the wake generation.
The circulatory part of the lift and pitching moment are:

$$L^C = -2\pi\rho U b C(\omega) \tag{3.7}$$

$$M_\alpha^C = 2\pi\rho U b^2 \left[\left(a + \frac{1}{2}\right) C(\omega) - \frac{1}{2}\right] \tag{3.8}$$

where a, b are geometrical hydrofoil parameters that will be illustred in Section 3.4. Moreover, ρ is the water density and U is the inflow velocity. Finally, $C(\omega)$ is a complex function in frequency domain, named Theodorsen function. This function is a combination of Bessel functions [48, 50]. The Theodorsen vortex wake model, originally formulated in the frequency domain, can be transposed in terms of integro-differential equations in the time domain. The circolatory part of the hydrodynamic forces can be written in terms of Wagner function, $K_W(t)$, [50]. Expressions (3.7) and (3.8) become:

$$L^C = -2\pi\rho U b \int_{-\infty}^{t} K_W(t-\tau)\dot{w}_{3/4}(\tau)\, d\tau \tag{3.9}$$

$$M_\alpha^C = 2\pi\rho U b^2 \left[\left(a + \frac{1}{2}\right) \int_{-\infty}^{t} K_W(t-\tau)\dot{w}_{3/4}(\tau)\, d\tau - \frac{1}{2}\right] \tag{3.10}$$

where $w_{3/4}(t)$ is the downwash [50] that is function of the degrees of freedom of the body and will be illustred in details in 3.4.

3.2 General integro-differential equation of motion

The final equations of motion of the finned underwater depressor affects by memory effects in the time domain is represented by the general equations:

$$\begin{aligned}(M + A)\,\ddot{\xi}(t) + \int_{-\infty}^{t} K_D(t-\tau)\dot{\xi}_j(\tau)\, d\tau + \\ \int_{-\infty}^{t} K_W(t-\tau)\dot{w}(\tau)_{3/4}\, d\tau = f_{Ctrl}(u, \xi(t), \dot{\xi}(t))\end{aligned} \tag{3.11}$$

The depressor model (3.11) is an integral-differential system which is completed with the initial conditions $\xi(\tau)$=$\xi_0(\tau)$, $\tau \in (-\infty, t]$. One can add in the model the loads f_{ctrl} which represent the control forces on the depressor. The control forces are dependent on the state $\xi(t)$, the depressor velocity $\dot{\xi}(t)$ and the control variable u.
From this theoretical general integro-differential model, two different models are formulated in details:

- 1-dof prototype model, starting from eq. (3.11) in which the control is made on heave motion;

- 2-dof Theodorsen model: the coupled heave/pitch depressor's control surface motion induces the generation of the vortex wake and the control of all the degree of freedom is made by applying a torque applied to the pitch dof.

3.3 1-Dof integro-differential prototype model

In this section a prototype model of the underwater finned depressor motion affected by both memory effects is described. In particular we refer our analysis to the body response in waves in the frame of the linear potential theory by Newmann [121].
An engineering control application which presents a single degree of freedom is here investigated (see Figure 3.5).

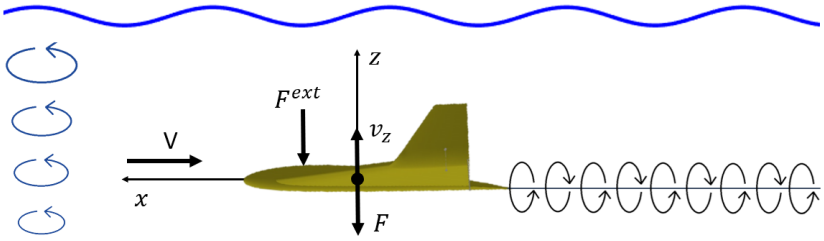

Figure 3.5. Force balance on finned vehicle - 1-Dof prototype

The x-axis is chord-wise and the z-axis is the heave direction. The equation of motion is written as:

$$m\ddot{z} = -F^{ext} - F \tag{3.12}$$

where m is the mass of the vehicle, $\dot{z}$ the heave velocity, F^{ext} the external hydrodynamic forces and F the control force along the z-axis. $F^{ext} = L + F_H$ where L is the lift force due to the wake generation and F_H the hydrodynamic load due to the presence of the free surface. For an incompressible one-dimensional flow, the following expression for the lift L is found, [48]

$$L = \frac{\ddot{z}}{\mu} + \frac{2V}{\mu}\int_{-\infty}^{t} K_W(t-\tau)\ddot{z}(\tau)\,d\tau \tag{3.13}$$

where $\mu = \pi\rho b^2/m$ is the mass ratio, $K_W(t)$ the Wagner function [50], V the dimensionless inflow velocity along the x-axis. The first term is the added inertial force, and the integral represents the circulatory part of the lift, due to the wake. A second effect contributing to the memory effects is borne when the vehicle V navigates close to the free surface [121]. The general expression of the hydrodynamic load in this case can be represented as

$$F_H = a\ddot{z} + \int_{-\infty}^{t} K_D(t-\tau)\dot{z}(\tau)\,d\tau \tag{3.14}$$

where a is costant infinite frequency added mass and the convolution term is the the added damping to which $K_D(t)$ remain associated [121]. The final equation of

motion of the vehicle is

$$\left(m + a + \frac{1}{\mu}\right)\ddot{z} + \int_{-\infty}^{t} K_W(t-\tau)\ddot{z}(\tau)\,d\tau + \int_{-\infty}^{t} K_D(t-\tau)\dot{z}(\tau)\,d\tau + F = 0 \quad (3.15)$$

Using the property of the convolution, equation (3.15) becomes:

$$M\ddot{z} + \int_{-\infty}^{t} K(t-\tau)\dot{z}(\tau)\,d\tau + F = 0 \quad (3.16)$$

where $M = m + \frac{1}{\mu} + a$ and $K(t) = \dot{K}_W(t) + K_D(t)$. Using standard notation in control theory, eq. (3.16) becomes:

$$\dot{x} = bu + b\int_{-\infty}^{t} K(t-\tau)x(\tau)\,d\tau \quad (3.17)$$

where $x = \dot{z}$, F=bu which $b = -\frac{1}{M}$ and u is the control variable. Equation (3.17) is completed with the initial conditions $x(\tau)$=$x_0(\tau)$, $\tau \in (-\infty, t]$.

3.4 2-Dof integro-differential model

An engineering control application of a two degree of freedom hydrofoil is here investigated. Theodorsen's theory [48] for this problem is employed to achieve the mathematical model of the hydrodynamic problem. This theory provide the generalized unsteady hydrodynamic forces due to an arbitrary motion of the hydrofoil that represent the vehicle's control surface which releases vortex wake. As shown in Section 3.1.2, the Theodorsen model, originally formulated in the frequency domain, can be transposed in terms of integral-differential equations in the time domain.
The x-axis is chord-wise axis (positive towards the trailing edge) and E is the center

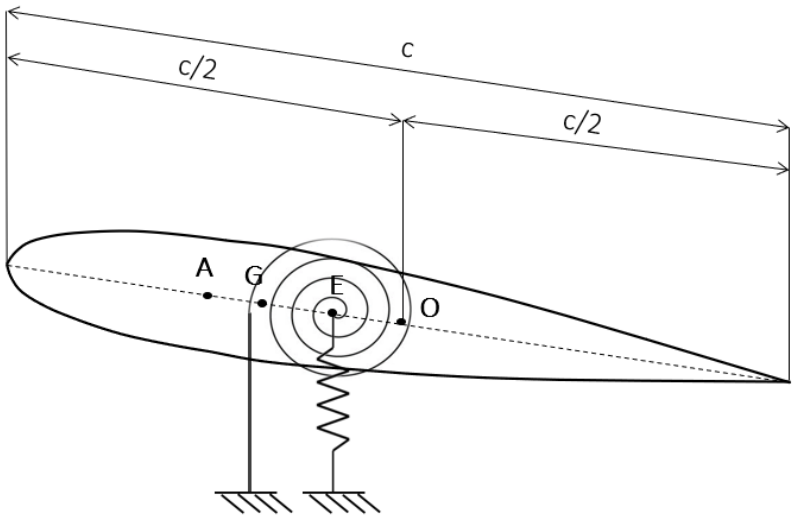

Figure 3.6. Sketch of the typical-section hydrofoil model

of rotation. The hydrofoil is studied in this way as a simple two degree-of-freedom

system, elastically constrained by a pair of translational and torsional equivalent linear springs, oscillating in plunge and pitch (Figure 3.6). By using standard notations, the non-dimensional plunge deflection at the elastic center is denoted by v meanwhile α represents the pitch motion. The elastic axis, E, is located at a distance $OE = a_h c/2$ from the mid-chord (a_h is the dimensionless distance, considered with respect to the half-cord length, $c/2$, between the center of the hydrofoil, O, and the elastic axis), while the mass center, G, is located at a distance $EG = x_\alpha c/2$ from the elastic axis.
With these assumptions, the hydroelastic equations of the typical section are:

$$\begin{cases} \ddot{v} + x_\alpha \ddot{\alpha} + \Omega^2 v = -p(v,\alpha) \\ \\ \dfrac{x_\alpha}{r_\alpha^2}\ddot{v} + \ddot{\alpha} + \alpha = r(v,\alpha) \end{cases} \tag{3.18}$$

where $\Omega = \omega_v/\omega_\alpha$, being ω_v and ω_α the uncoupled natural frequencies of heave and pitch modes, respectively; $r_\alpha = \sqrt{4J/mc^2}$ is the dimensionless radius of gyration about the elastic axis where m and J are the mass and the moment of inertia per unit length (with respect to the elastic center), respectively. For an incompressible two-dimensional flow, the following hydrofoil expressions for the lift p and the pitching moment r, are respectively, [49]:

$$\begin{aligned} p(v,\alpha) &= (\ddot{v} - a_h\ddot{\alpha} + U\dot{\alpha})\frac{1}{\mu} + \frac{2U}{\mu}\int_{-\infty}^{t} K_W(t-\tau)\dot{w}(\tau)_{3/4}\,d\tau \\ r(v,\alpha) &= [a_h(\ddot{v} - a_h\ddot{\alpha}) + \frac{1}{2}U(1-a_h)\dot{\alpha} - \frac{1}{8}\ddot{\alpha}]\frac{1}{\mu r_\alpha^2} - \frac{U(1+2a_h)}{\mu r_\alpha^2}\int_{-\infty}^{t} K_W(t-\tau)\dot{w}(\tau)_{3/4}\,d\tau \end{aligned} \tag{3.19}$$

where $\mu = \pi\rho c^2/4m$ is the mass ratio, $w_{3/4}(t)$ is the downwash, $K_W(t)$ is the Wagner function [50], $U = 2V/c\omega_\alpha$ the dimensionless inflow velocity and V is the inflow velocity, oriented along the x-axis. The integral terms represent the circulatory part of the lift, due to the wake generation.

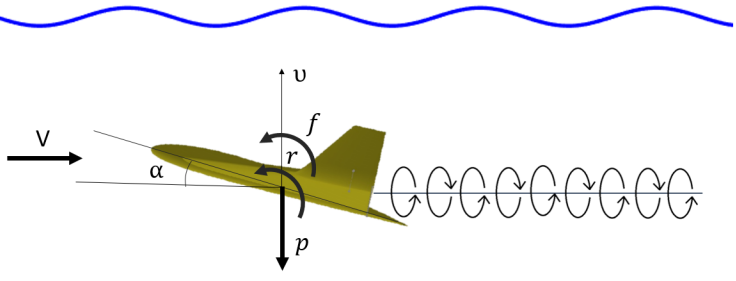

Figure 3.7. Force balance on finned vehicle - 2-Dof Theodorsen

In this case we want to reduce the release of vorticity induced by the depressor heave motion by controlling the pitch motion. The control, f, is now inserted into

the model as torque applied on the pitch dof (Figure 3.7). $M^{tot} = r - f$.
The equations of motion becames:

$$\begin{cases} \ddot{v} + x_\alpha \ddot{\alpha} + \Omega^2 v + (\ddot{v} - a_h \ddot{\alpha} + U\dot{\alpha})\dfrac{1}{\mu} + \dfrac{2U}{\mu}\displaystyle\int_{-\infty}^{t} K_W(t-\tau)\dot{w}(\tau)_{3/4}\, d\tau = 0 \\ \dfrac{x_\alpha}{r_\alpha^2}\ddot{v} + \ddot{\alpha} + \alpha - [a_h(\ddot{v} - a_h\ddot{\alpha}) + \dfrac{1}{2}U(1-a_h)\dot{\alpha} - \dfrac{1}{8}\ddot{\alpha}]\dfrac{1}{\mu r_\alpha^2} + \\ -\dfrac{U(1+2a_h)}{\mu r_\alpha^2}\displaystyle\int_{-\infty}^{t} K_W(t-\tau)\dot{w}(\tau)_{3/4}\, d\tau = f \end{cases} \tag{3.20}$$

The downwash function is $w_{3/4}(t) = \dot{v}(t) - (1/2 - a_h)\dot{\alpha}(t) + U\alpha(t)$ and using the property of the convolution, the system in matrix form becames:

$$\begin{bmatrix} 1 + \frac{1}{\mu} & x_\alpha - \frac{a_h}{\mu} \\ \frac{x_\alpha}{r_\alpha^2} - \frac{a_h}{\mu r_\alpha^2} & 1 + \frac{a_h^2}{\mu r_\alpha^2} + \frac{1}{8\mu r_\alpha^2} \end{bmatrix} \begin{Bmatrix} \ddot{v} \\ \ddot{\alpha} \end{Bmatrix} + \begin{bmatrix} 0 & \frac{U}{\mu} \\ 0 & 1 + \frac{U(1-a_h)}{2\mu r_\alpha^2} \end{bmatrix} \begin{Bmatrix} \dot{v} \\ \dot{\alpha} \end{Bmatrix} + \begin{bmatrix} \Omega^2 & 0 \\ 0 & 1 \end{bmatrix} \begin{Bmatrix} v \\ \alpha \end{Bmatrix} +$$

$$\begin{bmatrix} \frac{2U}{\mu}\ddot{K}_W & \frac{2U}{\mu}[(a_h - \frac{1}{2})\ddot{K}_W + U\dot{K}_W] \\ -\frac{(1+2a_h)U}{\mu r_\alpha^2}\ddot{K}_W & -\frac{(1+2a_h)U}{\mu r_\alpha^2}[(a_h - \frac{1}{2})\ddot{K}_W + U\dot{K}_W] \end{bmatrix} * \begin{Bmatrix} v \\ \alpha \end{Bmatrix} = \begin{Bmatrix} 0 \\ f \end{Bmatrix} \tag{3.21}$$

where $*$ is the convolution product. The final expression of the system is:

$$\boldsymbol{M\ddot{q} + C\dot{q} + Kq + \Psi(t) * q = \widetilde{f}} \tag{3.22}$$

where $\boldsymbol{q} = \{v, \alpha\}^T$ is the state vector, $\boldsymbol{M}$, $\boldsymbol{C}$, $\boldsymbol{K}$, $\boldsymbol{\Psi(t)}$ are the mass, damping, stiffness and the kernel square matrix, respectively. The matrix have $n \times n$ dimension. In this case n=2 where n is the number of the degree of freedom of the model. The $\widetilde{f}$ is the vector of the external force.
Using a standard notation in control theory, defining a new state vector $\boldsymbol{x} = \{\boldsymbol{x_1}, \boldsymbol{x_2}\}^T$ as:

$$\begin{cases} \boldsymbol{x_1 = q} \\ \boldsymbol{x_2 = \dot{q}} \end{cases} \tag{3.23}$$

The equation of motion becomes:

$$\begin{cases} \boldsymbol{\dot{x}_1 = x_2} \\ \boldsymbol{\dot{x}_2 = -M^{-1}Cx_2 - M^{-1}Kx_1 - M^{-1}[\Psi(t) * x_1] + M^{-1}\widetilde{f}} \end{cases} \tag{3.24}$$

The system (3.24) in matrix form is

$$\boldsymbol{\dot{x}} = \begin{bmatrix} \boldsymbol{0} & \boldsymbol{I} \\ \boldsymbol{-M^{-1}K} & \boldsymbol{-M^{-1}C} \end{bmatrix} \begin{Bmatrix} \boldsymbol{x_1} \\ \boldsymbol{x_2} \end{Bmatrix} + \begin{bmatrix} \boldsymbol{0} & \boldsymbol{0} \\ \boldsymbol{M^{-1}\Psi(t)} & \boldsymbol{0} \end{bmatrix} * \begin{Bmatrix} \boldsymbol{x_1} \\ \boldsymbol{x_2} \end{Bmatrix} + \begin{Bmatrix} \boldsymbol{0} \\ \boldsymbol{M^{-1}} \end{Bmatrix} \widetilde{f} \tag{3.25}$$

Defining the control variable, f=u equation (3.25) becames:

$$\dot{\boldsymbol{x}} = \boldsymbol{A}\boldsymbol{x} + \boldsymbol{\Sigma}(\boldsymbol{t}) * \boldsymbol{x} + \boldsymbol{b}\boldsymbol{u} \tag{3.26}$$

where $\boldsymbol{A}$ is the dynamical matrix and $\boldsymbol{\Sigma}(\boldsymbol{t})$ the convolution matrix which have $2n \times 2n$ dimension. The vector $\boldsymbol{b}$ is defined as:

$$\boldsymbol{b} = \begin{bmatrix} 0 \\ 0 \\ \boldsymbol{M^{-1}}(1,2) \\ \boldsymbol{M^{-1}}(2,2) \end{bmatrix} \tag{3.27}$$

which dimension is $2n \times 1$. Equation (3.26) is completed with the initial conditions $\boldsymbol{x}(\tau)$=$\boldsymbol{x_0}(\tau)$, $\tau \in (-\infty, t]$.

3.5 N-Dof integro-differential model

The presented model can be extend to a general N-Dof integral-differential model. Equations (3.26) becomes:

$$\dot{\boldsymbol{x}} = \boldsymbol{A}\boldsymbol{x} + \boldsymbol{\Sigma}(\boldsymbol{t}) * \boldsymbol{x} + \boldsymbol{B}\boldsymbol{u} \tag{3.28}$$

with initial conditions $\boldsymbol{x}(\tau)$=$\boldsymbol{x_0}(\tau)$, $\tau \in (-\infty, t]$.
Where $\boldsymbol{x}$ is the state vector composed by the N degree of freedom which dimension is $2N \times 1$, $\boldsymbol{A}$ is the dynamical matrix of the N-Dof system which dimension is $2N \times 2N$ and $\boldsymbol{B}$ is the $2N \times 2N$ control matrix. Moreover, $\boldsymbol{u}$ is the general N-Dof control vector.
This case is formulated in a general way in order to permitt the control of the N-Dof of the body with the possibility to apply the control forces on whatever degree of freedom is preferred. The kernel matrix $\boldsymbol{\Sigma}(t)$ implies the convolution between the kernel function and all the N-Dof of the system and it has dimension $2N \times 2N$.
The proposed optimal control algorithm will be formulated for this N-Dof equations of motion.

Chapter 4

A novel Optimal Control of integral-differential equations

In this Chapter the proposed new control logic applied to integro-differential equations is illustrated in detail. The optimal control theorized in this work is an extension of the Pontryagin optimal control theory normally applied to differential equations.
An overview of the optimal control theory by Pontryagin is shortly described in the first part of the Chapter.
The mathematical formulation of the new integral optimal control algorithm is deeply discussed by emphasising its novelty from the classical Pontryagin theory (Section 4.2). The open loop control is founded solving the variational ID optimal control problem (Section 4.3). Finally, the integral-differential control law is switched into a feedback control by formulating a novel integral *model predictive control*, integral MPC (Section 4.4).
This novel optimal control theory applied to integral-differential equations of motion and it is developed for the N-Dof matricial form of the IDE model in Section 3.5.
The same formulation applie to the scalar model is reported in Appendix C.

4.1 Overview on Standard Pontryagin Theory

Optimal Control can be seen as a generalization of the classical calculus of variations. The statement of the problem is formulated as:

$$\begin{aligned} &min\ J = \int_0^T L(\boldsymbol{x}, \boldsymbol{u}, \boldsymbol{y})\ dt \\ &\text{subjected to} \\ &\dot{\boldsymbol{x}} - f(\boldsymbol{x}, \boldsymbol{u}, \boldsymbol{y}) = 0, \quad \boldsymbol{x}(0) = \boldsymbol{x_0} \end{aligned} \tag{4.1}$$

The goal of the optimal control problem is to determine the controller design, $\boldsymbol{u(t)}$, and the associated evolution of the controlled system state, $\boldsymbol{x(t)}$ which minimize the value of the KPI-key performance index. The definition of the KPI is crucial in

the optimal control theory because it defines quantitatively the goal of the designed system. The KPI is the integral over the observation time T of J, it is a real number. J is the cost functional which depend on the state of the system $\boldsymbol{x(t)}$, the control evolution $\boldsymbol{u(t)}$ and sometimes also on the external uncontrollable forces $\boldsymbol{y(t)}$. The function L is the Lagrangian that is chosen by the designer. The second equation represents the dynamic of the controlled system, $\dot{\boldsymbol{x}} - f(\boldsymbol{x}, \boldsymbol{u}, \boldsymbol{y}) = 0$ with the initial conditions $\boldsymbol{x}(0) = \boldsymbol{x_0}$. The most important and powerful tool to look for an explicit solution to an Optimal Control Problem is the well known Pontryagin method that gives a first order necessary condition for optimality.
Pontryagin theory is very powerful and implies the following conditions:

- L is an algebraic operator.
- f is a differential costrain, ODEs.
- The optimality criterion implies a minimization or maximization of the functional J.

The problem of minimizing a functional depending on other functions constrained by differential equations, is treated by introducing the Lagrangian multipliers $\boldsymbol{\lambda}$. The modified functional is introduced in the form:

$$min\ \widetilde{J} = \int_0^T L(\boldsymbol{x}, \boldsymbol{u}, \boldsymbol{y}) - \boldsymbol{\lambda}^T[\dot{\boldsymbol{x}} - f(\boldsymbol{x}, \boldsymbol{u}, \boldsymbol{y})]\ dt = \int_0^T \widetilde{L}(\boldsymbol{x}, \dot{\boldsymbol{x}}, \boldsymbol{u}, \boldsymbol{\lambda}, \boldsymbol{y})\ dt \tag{4.2}$$

that must be minimized or maximized with respect to the three variables $\boldsymbol{x}, \dot{\boldsymbol{x}}, \boldsymbol{u}, \boldsymbol{\lambda}$. The minimization of the functional implies the perturbation of the three functions $\delta\boldsymbol{x}, \delta\dot{\boldsymbol{x}}, \delta\boldsymbol{u}, \delta\boldsymbol{\lambda}$ that produce an associated perturbation of the the functional, $\delta\widetilde{J}$ as shown in eq. (4.3).

$$\delta\widetilde{J} = \int_0^T \delta\widetilde{L}(\boldsymbol{x}, \dot{\boldsymbol{x}}, \boldsymbol{u}, \boldsymbol{\lambda}, \boldsymbol{y})\ dt = \int_0^T \frac{\partial\widetilde{L}}{\partial\boldsymbol{x}}\delta\boldsymbol{x} + \frac{\partial\widetilde{L}}{\partial\dot{\boldsymbol{x}}}\delta\dot{\boldsymbol{x}} + \frac{\partial\widetilde{L}}{\partial\boldsymbol{u}}\delta\boldsymbol{u} + \frac{\partial\widetilde{L}}{\partial\boldsymbol{\lambda}}\delta\boldsymbol{\lambda}\ dt \tag{4.3}$$

If $\boldsymbol{x}, \boldsymbol{u}, \boldsymbol{\lambda}$ are the optimal functions that make the functional minimum, then the functional perturbation should be zero:

$$\delta\widetilde{J} = \int_0^T \frac{\partial\widetilde{L}}{\partial\boldsymbol{x}}\delta\boldsymbol{x} + \frac{\partial\widetilde{L}}{\partial\dot{\boldsymbol{x}}}\delta\dot{\boldsymbol{x}} + \frac{\partial\widetilde{L}}{\partial\boldsymbol{u}}\delta\boldsymbol{u} + \frac{\partial\widetilde{L}}{\partial\boldsymbol{\lambda}}\delta\boldsymbol{\lambda}\ dt = 0 \tag{4.4}$$

The associated Euler-Lagrange equations are:

$$\begin{cases} \dfrac{\partial\widetilde{L}}{\partial\boldsymbol{x}} - \boldsymbol{\lambda}\dfrac{\partial f}{\partial\boldsymbol{x}} - \dot{\boldsymbol{\lambda}} = 0 \\ \dfrac{\partial\widetilde{L}}{\partial\boldsymbol{u}} - \boldsymbol{\lambda}\dfrac{\partial f}{\partial\boldsymbol{u}} = 0 \\ \dot{\boldsymbol{x}} - f(\boldsymbol{x}, \boldsymbol{u}, \boldsymbol{y}) = 0 \\ \boldsymbol{x}(0) = \boldsymbol{x}_0 \\ \boldsymbol{\lambda}(T) = \boldsymbol{0} \end{cases} \tag{4.5}$$

The final system is a two boundary problem, composed by two differential equations (the first and the third). The solution of the evolution of the system is in terms of time evolution $\boldsymbol{x(t)}, \boldsymbol{u(t)}, \boldsymbol{\lambda(t)}$. The Pontryaging solution is in terms of control program, and not a feedback control $\boldsymbol{u(x)}$, as it would be preferred from an engineering point of view. Therefore, the problem depends on two opposite boundary conditions: $\boldsymbol{x}(0) = \boldsymbol{x_0}$ and $\boldsymbol{\lambda}(T) = \boldsymbol{0}$ in the time domain.
The Pontryagin optimal control theory presents, for these reasons, two main disadvantages which are:

- The Pontryagin result in equation (4.5) gives a control program solution, open loop control, $\boldsymbol{u(t)}$.
- The associated Euler-Lagrange equations represents a two boundary conditions problem.
- The solution depends only on the initial condition of the state. (no dynamical measures by sensors).

To overcame the disadvantages of the Pontryagin method the use of *model predictive control* techniques are required. The switch from an open loop solution to a feedback control, using MPC methods, increases the numerical computational costs proportionally to the numbers of the degrees of freedom of the system.

4.2 An extended version of the Pontryagin theory to integral-differential equations

In this Section the Pontryagin method is extended to the control of integro-differential equations. The optimal control starting conditions, explained for the standard Pontryagin method in the Section 4.1, are now modified:

- L is an algebraic operator.
- **f is an integro-differential costrain, IDEs.**
- The optimality criterion implies a minimization or maximization of the functional J.

To generalize the Pontryagin control theory including convolution terms, it is necessary to formalize the variations of the integral part of the equation. This crucial first and innovative result is expressed by equation (2.7).
The integral control theory is now formulated for the integral-differential equation of motion equation (3.28) completed with the initial conditions $\boldsymbol{x}(\tau) = \boldsymbol{x_0}$, $\tau \in (-\infty, t]$. $\boldsymbol{A}$ and $\boldsymbol{B}$ can be time dependent coefficent matrix, precluding the use of Laplace domain based control techniques.
The cost function of the variational optimal control problem is described by the

quadratic functional $\widetilde{J}$, and the optimal control problem is stated as:

$$\begin{aligned} &min\ \widetilde{J} = \int_{-\infty}^{T} \frac{1}{2}\boldsymbol{x^T Q x} + \frac{1}{2}\boldsymbol{u^T R u}\ dt \\ &\text{subjected to} \\ &\boldsymbol{\dot{x} = Ax + \Sigma(t) * x + Bu} \end{aligned} \tag{4.6}$$

Introducing the Lagrange multiplier vector $\boldsymbol{\lambda}$, the cost function becomes:

$$J = \int_{-\infty}^{T} \frac{1}{2}\boldsymbol{x^T Q x} + \frac{1}{2}\boldsymbol{u^T R u} + \boldsymbol{\lambda^T}(\dot{\boldsymbol{x}} - \boldsymbol{Ax} - \boldsymbol{\Sigma(t) * x} - \boldsymbol{Bu})\ dt \tag{4.7}$$

where $\boldsymbol{Q}$ and $\boldsymbol{R}$ are the gain parameters. The minimization of the functional J implies:

$$\delta J = \delta \int_{-\infty}^{T} L(\boldsymbol{x}, \dot{\boldsymbol{x}}, \boldsymbol{\lambda}, \boldsymbol{u})\ dt - \delta \int_{-\infty}^{T} \boldsymbol{\lambda^T \Sigma(t) * x}\ dt \tag{4.8}$$

that when expressed in terms of the variations $\delta\boldsymbol{x}^T$, $\delta\dot{\boldsymbol{x}}^T$, $\delta\boldsymbol{\lambda}^T$, $\delta\boldsymbol{u}^T$, produces:

$$\begin{aligned} \delta J = \ & \int_{-\infty}^{T} \tfrac{\partial L}{\partial \boldsymbol{x}^T}\delta\boldsymbol{x^T} + \tfrac{\partial L}{\partial \dot{\boldsymbol{x}}^T}\delta\dot{\boldsymbol{x}}^T + \tfrac{\partial L}{\partial \boldsymbol{\lambda}^T}\delta\boldsymbol{\lambda}^T + \tfrac{\partial L}{\partial \boldsymbol{u}^T}\delta\boldsymbol{u}^T\ dt - \int_{-\infty}^{T} \delta\boldsymbol{\lambda}^T\boldsymbol{\Sigma(t) * x}\ dt + \\ & - \int_{-\infty}^{T} \boldsymbol{\lambda}^T\ \delta\left(\boldsymbol{\Sigma(t) * x}\right)\ dt = 0 \end{aligned} \tag{4.9}$$

or (using integration by parts of $\frac{\partial L}{\partial \dot{\boldsymbol{x}}}\delta\dot{\boldsymbol{x}}$)

$$\begin{aligned} \delta J = \ & \int_{-\infty}^{T} \delta\boldsymbol{x}^T\left(\boldsymbol{Qx} - \dot{\boldsymbol{\lambda}} - \boldsymbol{A}^T\boldsymbol{\lambda}\right) + \boldsymbol{\lambda}^T\left(\dot{\boldsymbol{x}} - \boldsymbol{Ax} - \boldsymbol{\Sigma(t) * x} - \boldsymbol{Bu}\right) + \\ & + \delta\boldsymbol{u}^T\left(\boldsymbol{Ru} - \boldsymbol{B}^T\boldsymbol{\lambda}\right)\ dt - \int_{-\infty}^{T} \boldsymbol{\lambda}^T\ \delta\left(\boldsymbol{\Sigma(t) * x}\right)\ dt = 0 \end{aligned} \tag{4.10}$$

and $\boldsymbol{\lambda}(T) = 0$.
The variations of the last term of equation are shown in (2.7). The stationary condition in (4.10) for J becomes:

$$\begin{aligned} \delta J = \ & \int_{-\infty}^{T} \delta\boldsymbol{x}^T\left(\boldsymbol{Qx} - \dot{\boldsymbol{\lambda}} - \boldsymbol{A}^T\boldsymbol{\lambda} - \int_{t}^{T} \boldsymbol{\Sigma}^T(\tau - t)\boldsymbol{\lambda}\ d\tau\right) + \\ & + \delta\boldsymbol{\lambda}^T\left(\dot{\boldsymbol{x}} - \boldsymbol{Ax} - \boldsymbol{\Sigma(t) * x} - \boldsymbol{Bu}\right) + \delta\boldsymbol{u}^T\left(\boldsymbol{Ru} - \boldsymbol{B}^T\boldsymbol{\lambda}\right)\ dt = 0 \end{aligned} \tag{4.11}$$

and the associated Euler-Lagrange equations are:

$$\begin{cases} \dot{\boldsymbol{\lambda}} = \boldsymbol{Qx} - \boldsymbol{A}^T\boldsymbol{\lambda} - \int_{t}^{T} \boldsymbol{\Sigma}^T(\tau - t)\boldsymbol{\lambda}(\tau)\ d\tau \\ \boldsymbol{Ru} - \boldsymbol{B}^T\boldsymbol{\lambda} = 0 \\ \dot{\boldsymbol{x}} = \boldsymbol{Ax} + \boldsymbol{Bu} + \int_{-\infty}^{t} \boldsymbol{\Sigma}(t - \tau)\boldsymbol{x}(\tau)\ d\tau = 0 \\ \boldsymbol{x}(\tau) = \boldsymbol{x_0}(\tau),\ \tau \in (-\infty, t] \\ \boldsymbol{\lambda}(T) = 0 \end{cases} \tag{4.12}$$

The system (4.12) consists of two integral-differential equations (the first and the third) and one linear algebraic equation (the second), this last providing $\boldsymbol{u} = \boldsymbol{R^{-1}B^T\lambda}$, that permits to reduce the system as:

$$\begin{cases} \dot{\boldsymbol{\lambda}} = \boldsymbol{Qx} - \boldsymbol{A}^T\boldsymbol{\lambda} - \displaystyle\int_t^T \boldsymbol{\Sigma}^T(\tau - t)\boldsymbol{\lambda}(\tau)\, d\tau \\ \dot{\boldsymbol{x}} = \boldsymbol{Ax} + \boldsymbol{BR^{-1}B^T\lambda} + \displaystyle\int_{-\infty}^t \boldsymbol{\Sigma}(t-\tau)\boldsymbol{x}(\tau)\, d\tau = 0 \\ \boldsymbol{x}(\tau) = \boldsymbol{x_0}(\tau),\ \tau \in (-\infty, t] \\ \boldsymbol{\lambda}(T) = 0 \end{cases} \tag{4.13}$$

This statement of the problem shows that, theoretically, its solution is possible only based on the knowledge of $\boldsymbol{x}(\tau) = \boldsymbol{x_0}(\tau),\ \tau \in (-\infty, t]$, i.e. only based on the past values for the trajectory $\boldsymbol{x}(t)$. However, engineering practice suggests a different operative solution, as pointed out later. Stability considerations for the system of integral-differential equations (4.13) is illustrated in Appendix D.

4.3 Implicit solution of the variational problem

Equations (4.13) can be solved by numerical techniques, for example based on forward finite differences formulation:

$$\begin{cases} \dfrac{\boldsymbol{\lambda_{i+1}}}{\Delta T} - \dfrac{\boldsymbol{\lambda_i}}{\Delta T} - \boldsymbol{Qx_i} + \boldsymbol{A}^T\boldsymbol{\lambda_i} + \displaystyle\sum_{j=i}^{N} \boldsymbol{\Sigma}_{j-i}^T\boldsymbol{\lambda}_j\Delta T \\ \dfrac{\boldsymbol{x_i}}{\Delta T} - \dfrac{\boldsymbol{x_{i+1}}}{\Delta T} + \boldsymbol{Ax_i} + \boldsymbol{BR^{-1}B^T\lambda_i} + \displaystyle\sum_{j=1}^{i} \boldsymbol{\Sigma}_{i-j}\boldsymbol{x}_j\Delta T = 0 \\ \boldsymbol{x}_j = \boldsymbol{x_0},\ j \in (-\infty, i] \\ \boldsymbol{\lambda_T} = 0 \end{cases} \tag{4.14}$$

with $N = \frac{T}{\Delta T}$ and Δt the discretization time interval.
We start with the vector of unknowns as $\{\boldsymbol{\chi_x^{(1,N)}}, \boldsymbol{\chi_\lambda^{(0,N-1)}}\}^T$, $\boldsymbol{\chi_x^{(1,N)}}$=$\{\boldsymbol{x_1, ..., x_i, ..., x_N}\}^T$, $\boldsymbol{\chi_\lambda^{(0,N-1)}}$=$\{\boldsymbol{\lambda_0, \lambda_1, ..., \lambda_i, ..., \lambda_{N-1}}\}^T$, where *(N,M)* indicates dependence on the time values of t_i for $i \in [N, M]$. Analogously, $\{\boldsymbol{\zeta_x^{(0)}}, \boldsymbol{0}\}^T$ where $\boldsymbol{\zeta_x^{(0)}}$=$\{\boldsymbol{x_0}\}$. Equation (4.14) in matrix form becomes:

$$\boldsymbol{\Omega}^{(0,N-2)} \begin{Bmatrix} \boldsymbol{\chi_x^{(1,N)}} \\ \boldsymbol{\chi_\lambda^{(0,N-1)}} \end{Bmatrix} = \boldsymbol{\Lambda}^{(0,N-1)} \begin{Bmatrix} \boldsymbol{\zeta_x^{(0)}} \\ \boldsymbol{0} \end{Bmatrix} \tag{4.15}$$

with obvious solution:

$$\begin{Bmatrix} \boldsymbol{\chi_x^{(1,N)}} \\ \boldsymbol{\chi_\lambda^{(0,N-1)}} \end{Bmatrix} = \boldsymbol{\Omega}^{(0,N-2)^{-1}} \boldsymbol{\Lambda}^{(0,N-1)} \begin{Bmatrix} \boldsymbol{\zeta_x^{(0)}} \\ \boldsymbol{0} \end{Bmatrix} \tag{4.16}$$

The structure of the matrices are shown in Appendix A.
Equation (4.16) reveals that the system response depends only on the initial condition of the system. As it is usual in optimal control problems, the solution of

equations (4.13) or (4.14) is expressed in terms of a control program $\boldsymbol{x}(t)$, $\boldsymbol{u}(t)$, $\boldsymbol{\lambda}(t)$, i.e, through a prescribed time-dependent control $\boldsymbol{u}(t)$. Theoretically, this would not be a problem if the model of the physical investigated system is error-free. In this case equations (4.13) or (4.14) make use only of the past values of the state that are known: $\boldsymbol{x}(\tau) = \boldsymbol{x_0}(\tau),\ \tau \in (-\infty, t]$. All the remaing part of the trajectory is determined on this basis. This way of solving the problem, has a strong engineering weakness. In fact, models are not perfect and the $\boldsymbol{u}(t)$ determined by solving (4.13) or (4.14) is based, at the end, only on (i) the past known values $\boldsymbol{x}(\tau) = \boldsymbol{x_0}(\tau),\ \tau \in (-\infty, t]$ and (ii) the theoretical model of the system represented by $\boldsymbol{A}, \boldsymbol{b}, \boldsymbol{\Sigma}(t)$. When sensor measurements are available, a technique that makes use of all the acquired information by the sensor over $(-\infty, t]$ is much more robust. This process modifies the exposed technique, switching from a control program to a feedback control, as illustrated in the following Section.

4.4 Feedback via model predictive control

The key strategy does not imply the use of the complete solution $\{\chi_x^{(1,N)}, \chi_\lambda^{(0,N-1)}\}^T$ and $\boldsymbol{u} = \frac{B}{R}\chi_\lambda^{(0,N-1)}$ along the time interval $[0, T]$ determined in the previous section. We use only the first output for $\boldsymbol{u}$, associated at the time $t = t_0$, to which is also associated the first output for the state at the time $t = t_1$. Therefore, at the time $t = t_1$ we know $\boldsymbol{x_0}$, $\boldsymbol{x_1}$, $\boldsymbol{\lambda_0}$ (and $\boldsymbol{u_0}$). This terms are collected into the vector $\{\zeta_x^{(0,1)}, \zeta_\lambda^{(0)}\}^T$ and the unknowns are reduced to $\{\chi_x^{(2,N)}, \chi_\lambda^{(1,N-1)}\}^T = \{\boldsymbol{x_2, x_3 ..., x_N, \lambda_1, ..., \lambda_{N-1}}\}^T$. The matrix $\boldsymbol{\Omega}^{(1,N-2)}$ reduces obviously its dimensions (Appendix B), following the reduction of the number of the unknowns. The matrix $\boldsymbol{\Lambda}^{(1,N-1)}$ increases its dimension (Appendix B), following the increase of the known term $\{\zeta_x^{(0,1)}, \zeta_\lambda^{(0)}\}^T$. We can iterate this process and at the generic *k-th* step one obtains:

$$\begin{Bmatrix} \chi_x^{(k,N)} \\ \chi_\lambda^{(k-1,N-1)} \end{Bmatrix} = \boldsymbol{\Omega}^{(k-1,N-2)^{-1}} \boldsymbol{\Lambda}^{(k-1,N-1)} \begin{Bmatrix} \zeta_x^{(0,k-1)} \\ \zeta_\lambda^{(0,k-2)} \\ \boldsymbol{0} \end{Bmatrix} \tag{4.17}$$

For the reasons explained in Section 4.3, in equation (4.13) an external disturbance $\boldsymbol{n_x}(t)$ is introduced which models an error in the theoretical modelling of the system or/and an external not controllable force. In fact, the solution of the two boundary problem in (4.13) precludes the knowledge of these external disturbances along the entire time domain $[0, T]$, that would imply the knowledge of the future values for $\boldsymbol{n_x}(t)$.
Introducing $\boldsymbol{n_x}(t)$ equation (3.26) becomes:

$$\dot{\boldsymbol{x}} = \boldsymbol{Ax} + \boldsymbol{\Sigma(t)} * \boldsymbol{x} + \boldsymbol{Bu} + \boldsymbol{n_x}(t) \tag{4.18}$$

with the initial condition $\boldsymbol{x}(\tau) = \boldsymbol{x_0}(\tau),\ \tau \in (-\infty, t]$. Equation (4.18) corresponds to the model of the system that includes the noise (model or/and disturbance), while equation (4.13), that is the best representation of the system, is used to determine the control law to be applied to equation (4.18). The scheme in Figure 4.1 shows how the open loop optimal control has been converted into an integral feedback

MPC, taking into account the past history of the state which represents the initial condition of (4.18).

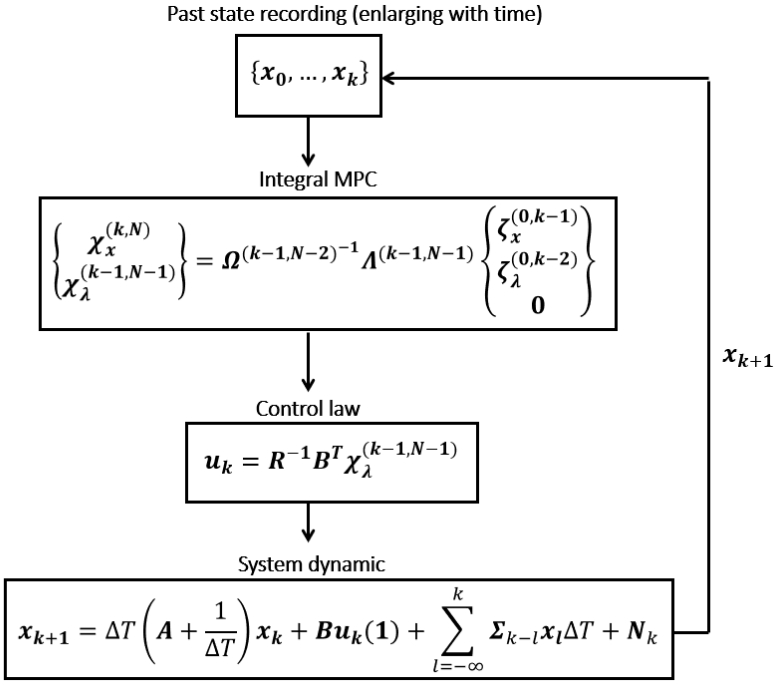

Figure 4.1. Integral MPC scheme

Chapter 5

Numerical simulations

In this Chapter the numerical results of the integral optimal control simulations applied to different integro-differential models are illustred.
The results obtained from the integral MPC simulations are compared with the standard LQR solution. The simulations have been performed with Matlab and Simulink software.
Preliminary simulations have been developed to study the stability of both the models. The tuning of dynamic and control parameters of the systems has been done in order to chose the ones which guarantee the stability of the systems. Finally, the integral MPC simulations are compared with the LQR classical method for different value of external noise. In this Chapter only few kind of disturbance (deterministic or random) are considered.

5.1 Vibrations optimal control of the 1-Dof underwater finned depressor with memory effects

The theorized integral MPC control, which includes memory effects, is applied to the control of the heave motion of the underwater 1-Dof vehicle.
This optimal control starting from an initial known value of the vehicle velocity, is finalized to reach a given immersion depth.
This optimal control problem is solved with the integral MPC method illustred in Section 4.4. The optimal control theory proposed applied to this scalar example is shown in Appendix C.
Starting from the prototype model introduced in Section 3.3, the external disturbances $n_x(t)$ have been included into the dynamic equation of motion in eq. (3.17):

$$\dot{x} = ax + bK * x + bu + n_x(t) \tag{5.1}$$

$n_x(\mu, \sigma)$ is a random variable described by Gaussian normal distribution, μ its mean value, σ its standard deviation and *H(t)* is the heaviside function. The values of the parameters which characterize the dynamic of the model are shown in Table 5.1. The choice of the matrices Q and R, following Bryson [124], is tuned with the maximum

value expected for v_z and F as::

$$\begin{aligned} Q &= diag(q_i) \\ R &= diag(r_i) \end{aligned} \tag{5.2}$$

where

$$\begin{aligned} q_i &= \frac{1}{{v_{z,i}}_M{}^2} \\ r_i &= \frac{1}{{F_i}_M{}^2} \end{aligned} \tag{5.3}$$

In the present case q=r=1, since the maximum values for the vehicle velocity and the control force are 1 m/s and 1 N, respectively.

Parameter	Value	Unit
m	10	kg
ρ	1000	$\frac{kg}{m^3}$
$x_0(\tau)$	1	$\frac{m}{s}$
ΔT	0.1	s
T	15	s

Table 5.1. System parameter - 1-Dof

Different kind of external disturbances are considered deterministic or stochastic. When n_{v_z} is a random variable described by Gaussian normal distribution it is expressed as $n_{v_z}(\mu, \sigma)$ where μ its mean value and σ its standard deviation. Table 5.2 shows the expression of the disturbances inserted into the simulated dynamic system, where *H(t)* is the heaviside function, in particular $H_1(t) = 0.35[H(t-1) - H(t-3)] + 0.4[H(t-4.5) - H(t-7)]$, $H_2(t) = 0.9[H(t) - H(t-8)] + 0.2[H(t-14) - H(t-7)]$, $H_1^{'}(t) = 0.3[H(t-3) - H(t-1)] - 0.4[H(t-7) - H(t-4.5)]$ and $H_2^{'}(t) = H_1^{'}(t)(t) + H(t-11) - H(t-10.5)$.
The analytical expression of the kernel function has been chosen as: $K(t) = -2.954 \cdot 10^{-9} exp(0.801t) + 4.688 \cdot 10^{-10} exp(0.9289t)$.
The performance of the integral MPC are compared with the LQR solution. The efficency of the integral MPC is measured by the merit parameter:

$$Q_{MPC,LQR} = \frac{J_{MPC} - J_{LQR}}{J_P} \cdot 100 \tag{5.4}$$

where J_{MPC} and J_{LQR} represent the cost function of the integral MPC and the LQR solution, respectively and J_P is the cost function of the optimal Pontryagin's solution.

Disturbances	Expression
Zero	$n_{v_z} = 0$
Gaussian random + $H_1(t)$	$n_{v_z} = N(0, 0.5) + H_1(t)$
Gaussian random + $H_2(t)$	$n_{v_z} = N(0, 0.3) \cdot H_2(t)$
Discrete 1	$n_{v_z} = H_1^{'}(t)$
Discrete 2	$n_{v_z} = H_1^{'}(t) + H_2^{'}(t)$
Sinusoidal	$n_{v_z} = 0.6\ sin(0.4\pi t)$
Gaussian random $\sigma = 0.2$	$n_{v_z} = N(0, 0.2)$
Gaussian random $\sigma = 0.5$	$n_{v_z} = N(0, 0.5)$
Gaussian random $\sigma = 0.8$	$n_{v_z} = N(0, 0.8)$

Table 5.2. External modeled disturbances 1-Dof

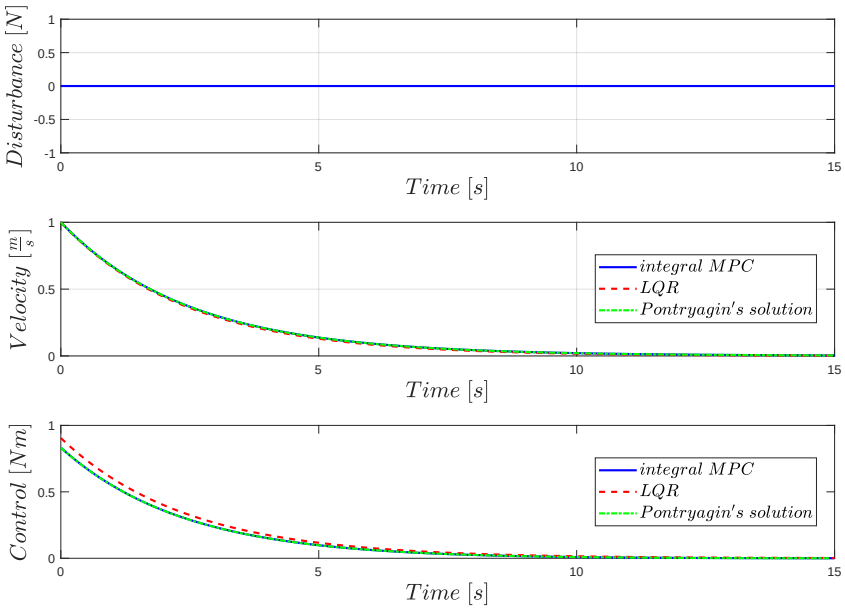

Figure 5.1. Zero external disturbances

The numerical results have been published in [125].

Figures 5.1 show the heave velocity and the control force for $n_x = 0$. In this case the integral MPC matches with the Pontryagin solution and presents best performaces than the LQR control method. The performance of the integral MPC are compared with the LQR solution. Figures 5.2 and 5.3 show the comparison between the two control methods where an external force is a combination of a random signal and of the deterministic signals $H_1(t)$ and $H_2(t)$, as described in Table 5.2, acting on the vehicle dynamic. Different levels of the disturbance in terms of standard deviation σ are considered: $\sigma = 0.2$ (Figure 5.4), $\sigma = 0.5$ (Figure 5.5)

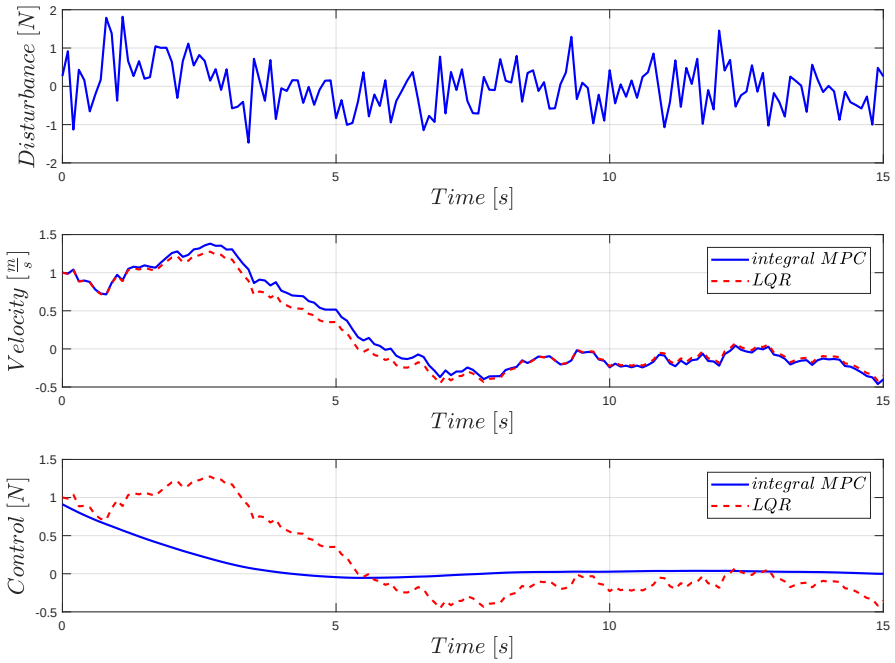

Figure 5.2. Gaussian random + $H_1(t)$

and $\sigma = 0.8$ (Figure 5.6).
Discrete (Figures 5.13 and 5.8) and both continuous deterministic signals (Figure 5.9) have been applied in the integro-differential model.
It appears that the integral MPC shows better performances with respect to the benchmark LQR method for any type of test. Table 5.4 shows the comparison between the Q's, defined by eq. (5.4).

Simulation	$Q_{MPC,LQR}$
Zero disturbances	7.3
Discrete 1	48
Discrete 2	55
Sinusoidal	153
Gaussian random + $H_1(t)$	102.9
Gaussian random + $H_2(t)$	72.4
Gaussian random $\sigma = 0.2$	24.4
Gaussian random $\sigma = 0.5$	58.1
Gaussian random $\sigma = 0.8$	101.5

Table 5.3. Merit parameter [%] - 1-Dof

Figure 5.10 shows the cost function values J for each solution method for increasing random noise levels. The random external disturbance applied to the system

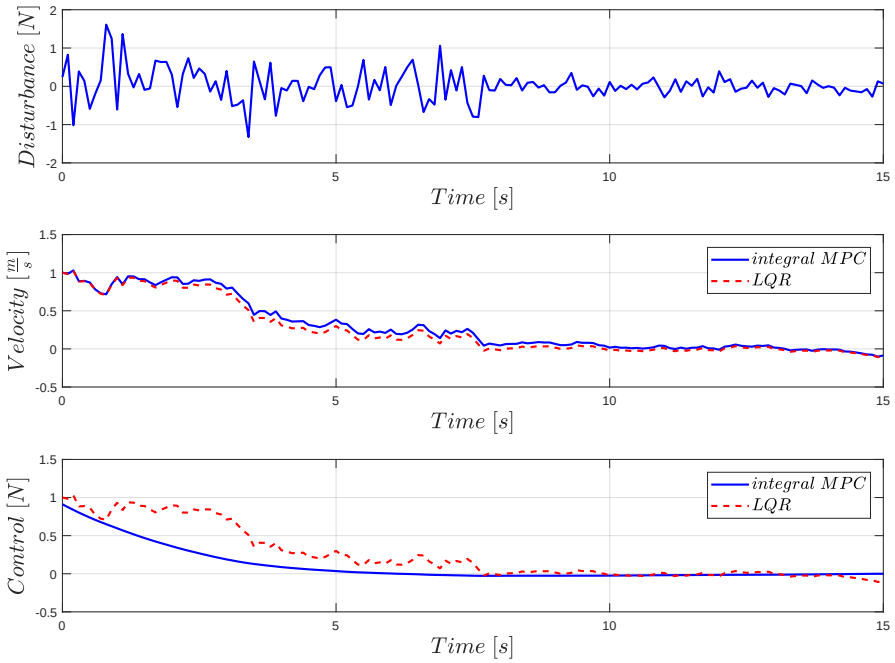

Figure 5.3. Gaussian random + $H_2(t)$

$n_x(\mu, \sigma)$ has zero mean value μ and a standard deviation, σ, from zero value up to 1. The results show higher performaces in term of minimization of cost function of the integral MPC method respect to the LQR one for any kind of external disturbance.

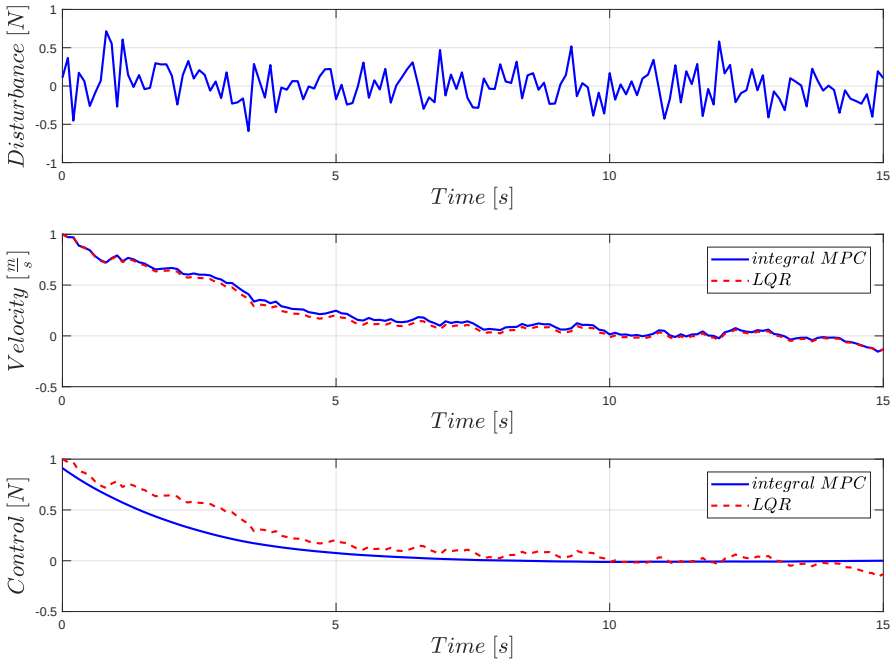

Figure 5.4. Gaussian random disturbances $\sigma = 0.2$

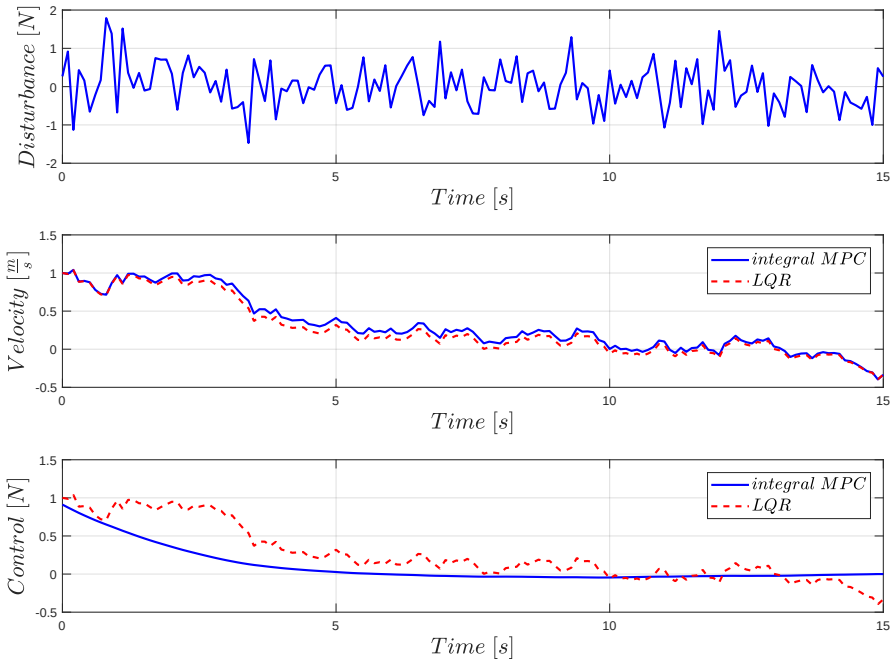

Figure 5.5. Gaussian random disturbances $\sigma = 0.5$

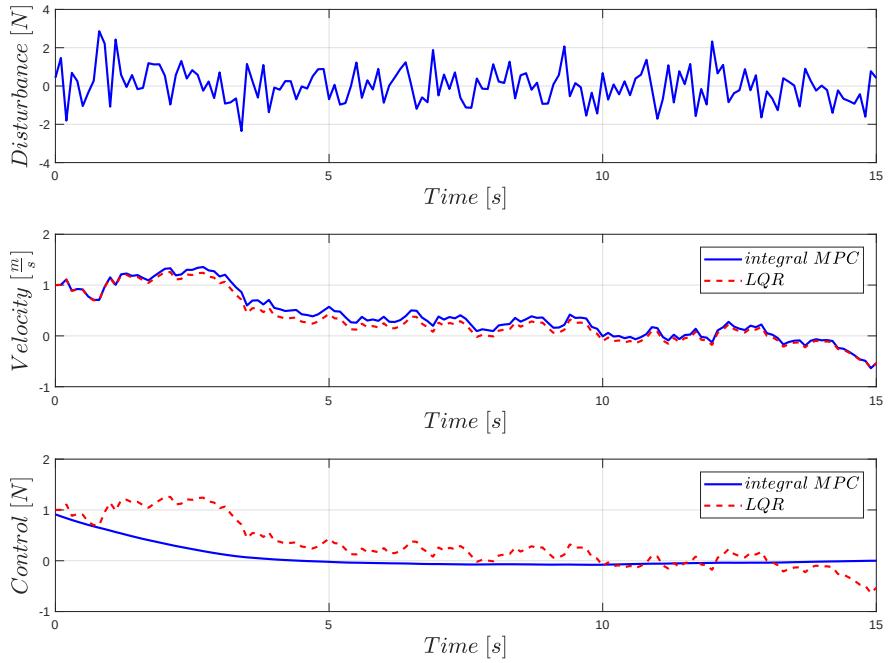

Figure 5.6. Gaussian random disturbances $\sigma = 0.8$

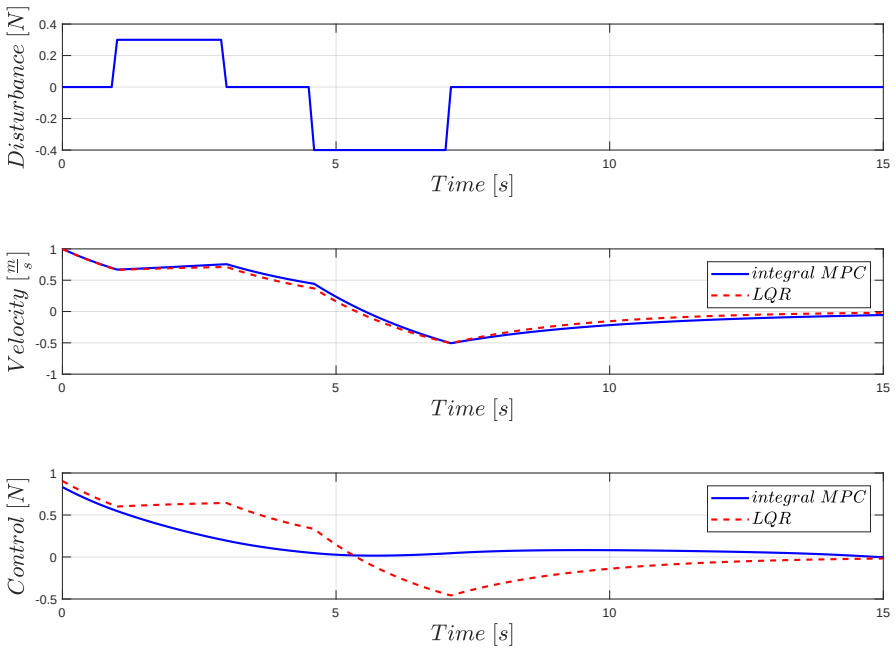

Figure 5.7. Discrete 1

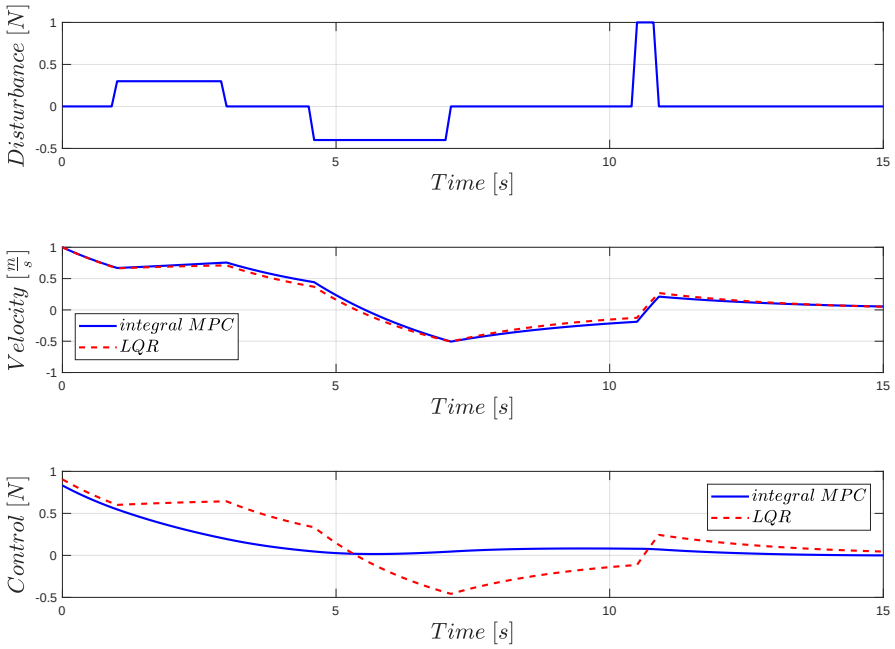

Figure 5.8. Discrete 2

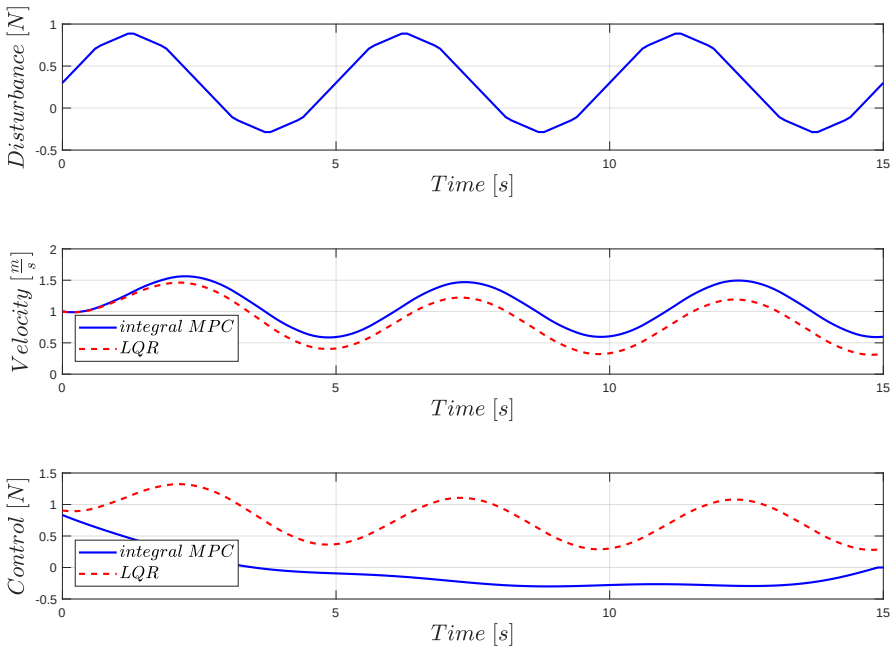

Figure 5.9. Sinusoidal

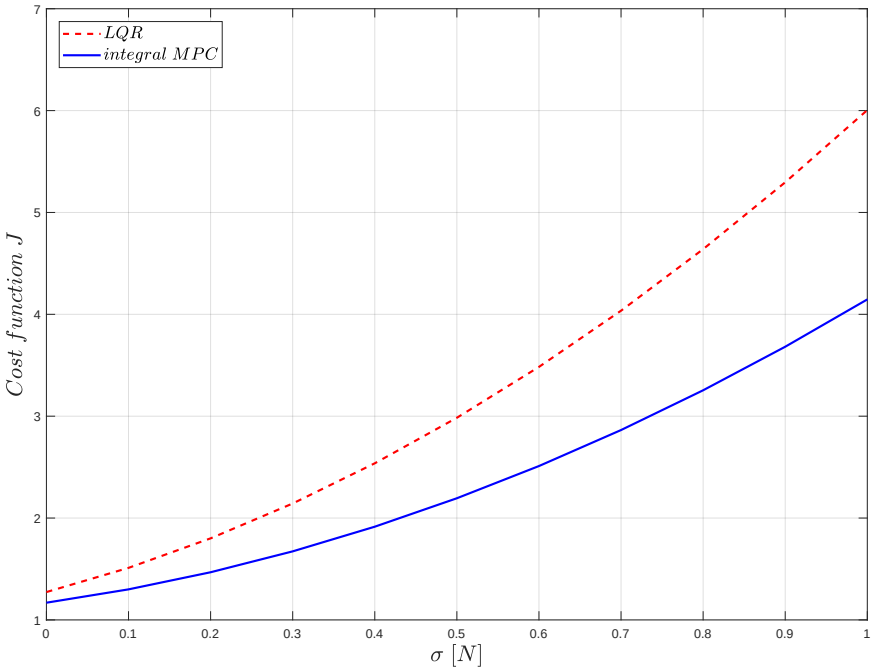

Figure 5.10. Cost function J at different disturbance levels - 1-Dof

5.2 Fluttering control of the 2-Dof underwater depressor control surfaces

The integral optimal control algorithm is now applied on the integro-differential Theodorsen model shown in Section 3.4. In this model the convolution term represents the release of wake vorticity induced by the coupled heave/pitch motion of an hydrofoil in a fluid flow.
The hydroil model can approximate the underwater depressor 2-Dof motion when the release of vortex wake is induced by the motion of the control lifting surface of the vehicle.
This control problem has as goal the minimization of all the degrees of freedom by applying a control torque on the pitch degree of freedom, as shown in Section 3.4. Starting from the equation of motion in (3.26) external random disturbances have been inserted into the IDEs model:

$$\dot{\boldsymbol{x}} = \boldsymbol{A}\boldsymbol{x} + \boldsymbol{\Sigma}(\boldsymbol{t}) * \boldsymbol{x} + \boldsymbol{b}\boldsymbol{u} + \boldsymbol{n}_{\boldsymbol{x}}(t) \tag{5.5}$$

$\boldsymbol{n}_{\boldsymbol{x}}(\mu, \sigma)$ is a random vector described by Gaussian normal distribution, μ its mean value, σ its standard deviation.
The geometrical parameter (Figure 5.11) of the hydrofoil that are referred to the

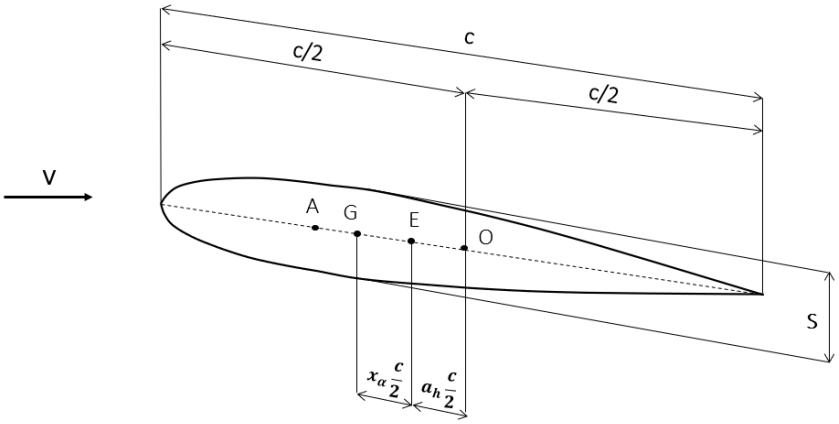

Figure 5.11. Hydrofoil geometrical parameters

geometry in Section 3.4, are expressed in next table 5.4 where S and m are the thickness and the mass of the hydrofoil, respectively.
Table 5.5 shows the dynamical system parameters chosen in the simulation where ω_v, ω_α are the uncoupled frequency of heave and pitch degree of freedom, respectively. Moreover, $\boldsymbol{x}_0(\tau)$ are the initial condition of the system, ΔT is the time step and T is the final time of simulation.

Parameters	Value	Unit
ρ	1000	$\frac{kg}{m^3}$
c	1	m
S	0.1	m
m	30	kg
V	10	$\frac{m}{s}$
x_α	0.2	$-$
a_h	0.2	$-$

Table 5.4. Hydrofoil geometrical parameters

Parameters	Value	Unit
ω_v	0.5	Hz
ω_α	0.9	Hz
$\boldsymbol{x}_0(\tau)$	1	$\frac{m}{s}$
ΔT	0.1	s
T	15	s

Table 5.5. Simulation parameters - 2-Dof

The mass moment of inertia of the hydrofoil has been computed by the Huygens–Steiner theorem:

$$J = J_c + md^2 \tag{5.6}$$

where J_c is the mass moment of inertia referred to the hydrofoil center, O, and d is the distance between the elastic center and the center of the wing ($d = a_h \frac{c}{2}$).
The hydrofoil is composed by an interior part make by foam and the external coverage in aluminium as shown in Figure 5.12.
The mass moment of inertia referred to the hydrofoil center is computed as:

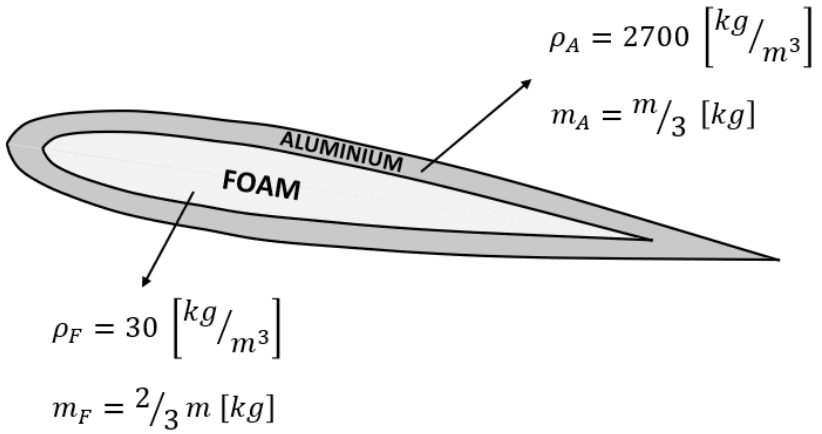

Figure 5.12. Hydrofoil material composition

$$J_c = \rho_{eq} * c * I \tag{5.7}$$

where I is the geometrical mass moment of inertia, c is the wing length and the equivalent density of the hydrofoil is:

$$\rho_{eq} = \frac{\rho_F * \rho_A}{\rho_A * m_F + \rho_F * m_A} m \tag{5.8}$$

where ρ_F, m_F, ρ_A, m_A are the density and the mass of the foam and aluminium, respectively (Figure5.12). The geometrical mass moment of inertia is [126]:

$$I = 0.0384 c S^3 \tag{5.9}$$

The model parameter obtained from the geometrical and dynamical parameter are shown in Table 5.6.

Parameter	Value	Unit
$\mu = \frac{\pi\rho c^2}{4m}$	26.2	kg
$\Omega = \frac{\omega_v}{\omega_\alpha}$	0.55	–
$r_\alpha = \sqrt{\frac{4J}{mc^2}}$	0.22	–
$U = \frac{2V}{c\omega_\alpha}$	22	$\frac{m}{s}$

Table 5.6. Derivate model parameters - 2-Dof

The control gain, **Q** and r, choosen to control the IDEs 2-Dof hydrofoil model are:

$$Q = \begin{bmatrix} 0.3 & 0 & 0 & 0 \\ 0 & 0.3 & 0 & 0 \\ 0 & 0 & 0.4 & 0 \\ 0 & 0 & 0 & 0.01 \end{bmatrix} \qquad r = 0.03 \tag{5.10}$$

Different kind of external disturbances are considered. Table 5.7 shows the expression of the disturbances inserted into the simulated dynamic system, where $H_3(t) = 0.35H(t-6)$ and $H_4(t) = [H(t-11) - H(t-9)] \cdot -0.4[H(t-8) - H(t-4)]$. The analytical expression of the kernel function has been chosen as: $K(t) = 1 - 0.165exp(-0.0455t) - 0.335exp(-0.3t)$.

Disturbances	Expression
Zero	$\boldsymbol{n_x} = 0$
Gaussian random + $H_3(t)$	$\boldsymbol{n_x} = N(0, 0.2) + H_3(t)$
Gaussian random + $H_4(t)$	$\boldsymbol{n_x} = N(0, 0.2) \cdot H_2(t)$
Gaussian random $\sigma = 0.2$	$\boldsymbol{n_x} = N(0, 0.2)$
Gaussian random $\sigma = 0.6$	$\boldsymbol{n_x} = N(0, 0.6)$
Gaussian random $\sigma = 0.9$	$\boldsymbol{n_x} = N(0, 0.9)$

Table 5.7. External modeled disturbances - 2-Dof

The performances of the integral MPC are measured by the same merit parameter used for the 1-Dof model in eq. 5.4.
Figures 5.13 - 5.14 show the heave and pitch motion, their associated velocities and the control force applied on the pitch dof, respectively, for $\boldsymbol{n_x} = 0$. In this case the integral MPC matches with the Pontryagin's solution and presents best performaces than the LQR control method.

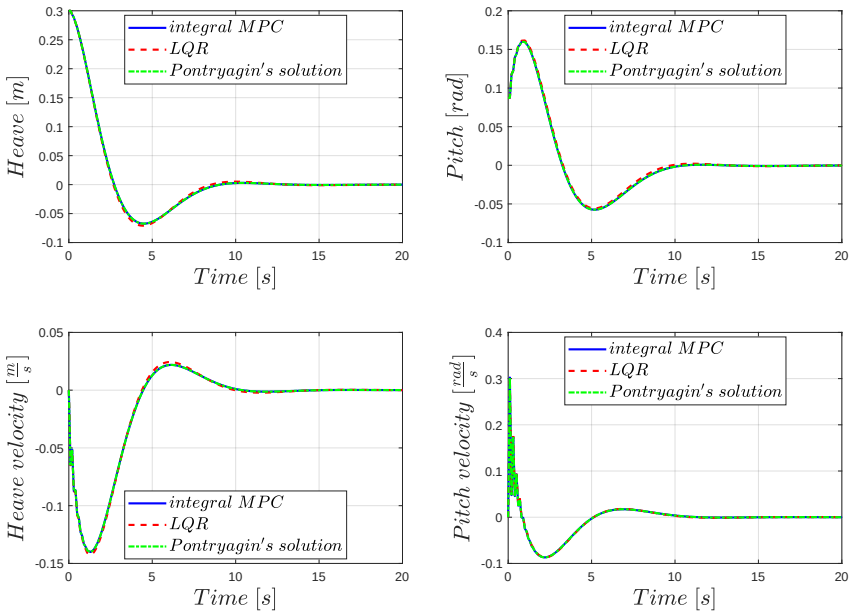

Figure 5.13. Zero external disturbance: Heave and Pitch

The performance of the integral MPC are compared with the LQR solution. Figures 5.15 - 5.18 show the comparison between the two control methods where an external force is a combination of a random signal and of the deterministic signals $H_3(t)$ and $H_4(t)$, as described in Table 5.7, acting on the vehicle dynamic. Different levels of the disturbance in terms of standard deviation σ are considered: $\sigma = 0.2$ (Figure 5.19 - 5.20), $\sigma = 0.6$ (Figure 5.21 - 5.22) and $\sigma = 0.9$ (Figure 5.23 - 5.24).

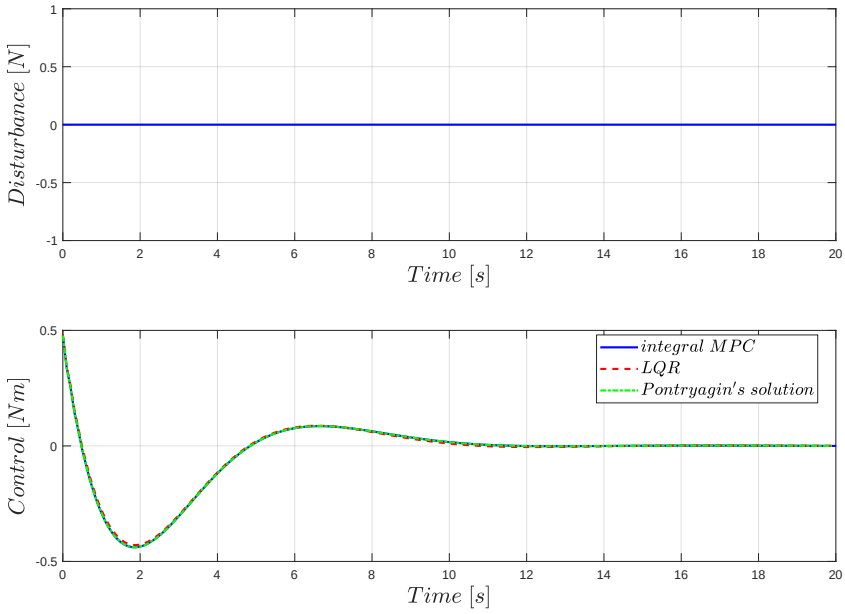

Figure 5.14. Zero external disturbance: Pitch control

It appears that the integral MPC shows better performances with respect to the benchmark LQR method for any type of test. Table 5.8 shows the comparison between the Q's, defined by eq. (5.4). Figure 5.25 shows the cost function values J

Simulation	$Q_{MPC,LQR}$
Zero disturbances	1
Gaussian random + $H_3(t)$	129
Gaussian random + $H_4(t)$	6
Gaussian random $\sigma = 0.2$	22
Gaussian random $\sigma = 0.6$	164
Gaussian random $\sigma = 0.9$	435

Table 5.8. Merit parameter [%] - 2-Dof

for each solution method for increasing random noise levels. The random external disturbance applied to the system $n_x(\mu, \sigma)$ has zero mean value μ and a standard deviation, σ, from zero value up to 1. The results show higher performaces in term of minimization of cost function of the integral MPC method respect to the LQR for any type of external random disturbance.

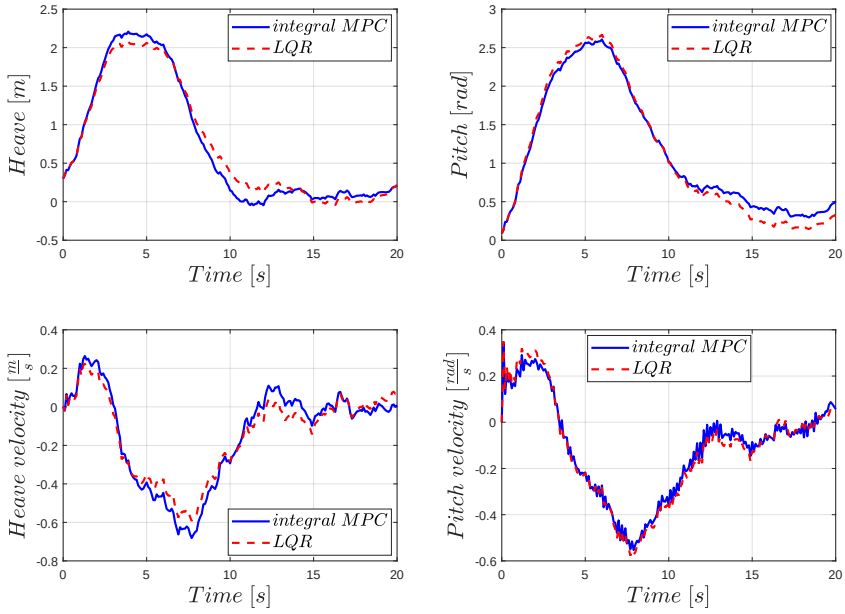

Figure 5.15. Gaussian random + $H_3(t)$: Heave and Pitch

An insteresting application of the proposed algorithm is the optimal control of the hydrofoil flutter instabilities. In fact, Theodorsen 2-Dof hydrofoil model is in general used to study this phenomena when the hydrofoil is moving in water with the velocity of its flutter speed.
For the hydrofoil geometry chosen in the simulations before illustred, the fluttering speed is $0.1m/s$.
In Figures (5.26) and (5.27) the control law and the system response are illustred when the system is not controlled and when the integral MPC control method is applied. In the simulation external disturbance are not acting on the system. The goodness of the proposed method is also compare to the LQR logic, as for the other simulations. It is clear from the results, in Figure (5.26), that with the proposed control algorithm it possible to totally control che instabilities due to the fluttering condition of the hydrofoil. The value of the merit parameter respect to the LQR performance is $Q_{MPC,LQR} = 7\%$, so the integral MPC shows even in this case better results in term of cost function minimization.

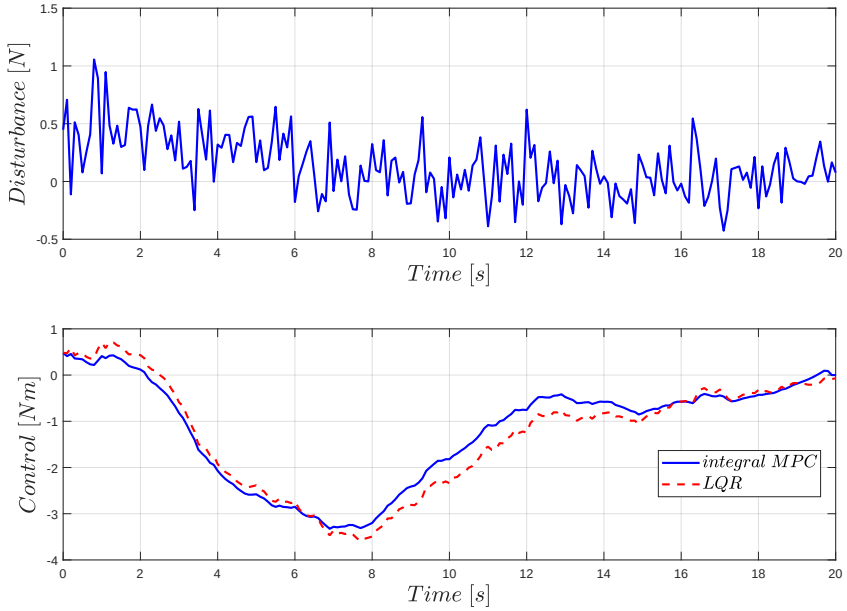

Figure 5.16. Gaussian random + $H_3(t)$: Pitch control

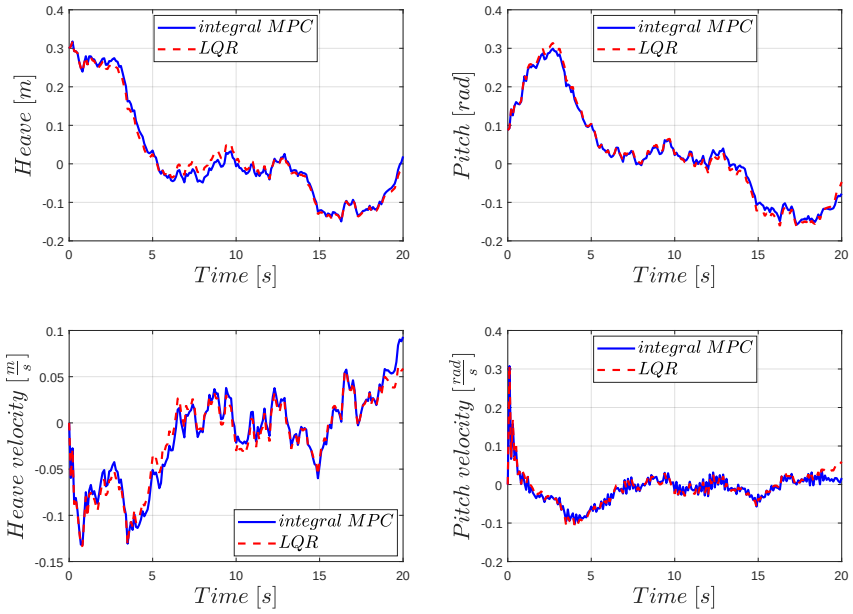

Figure 5.17. Gaussian random + $H_4(t)$: Heave and Pitch

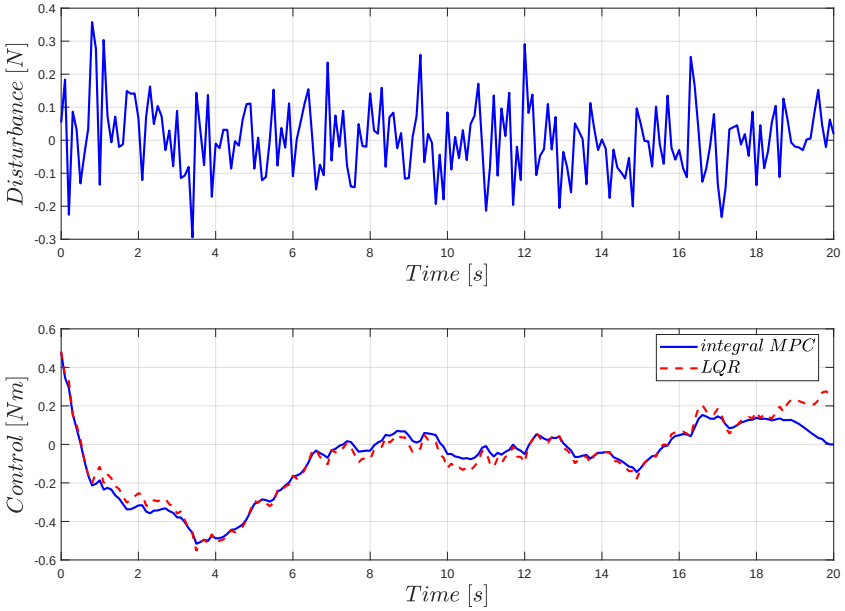

Figure 5.18. Gaussian random + $H_4(t)$: Pitch control

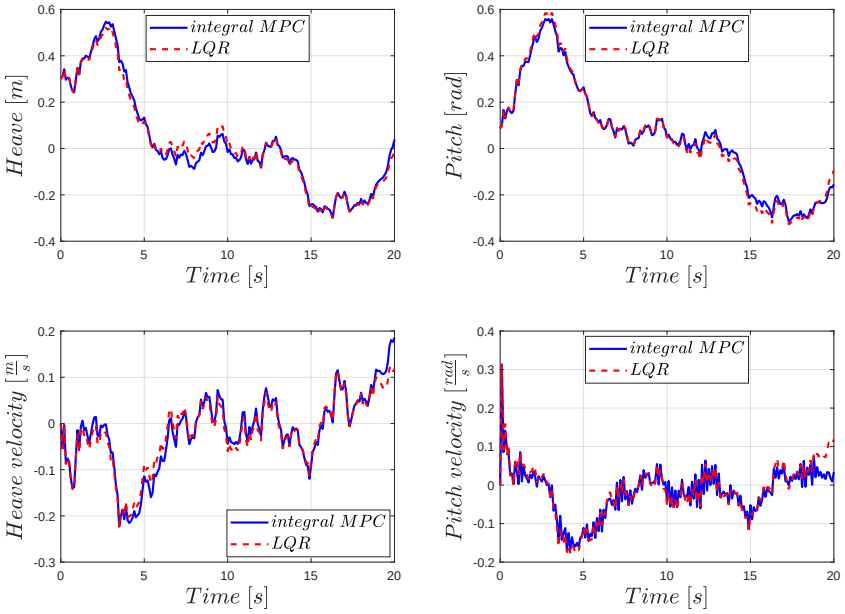

Figure 5.19. Gaussian random $\sigma = 0.2$: Heave and Pitch

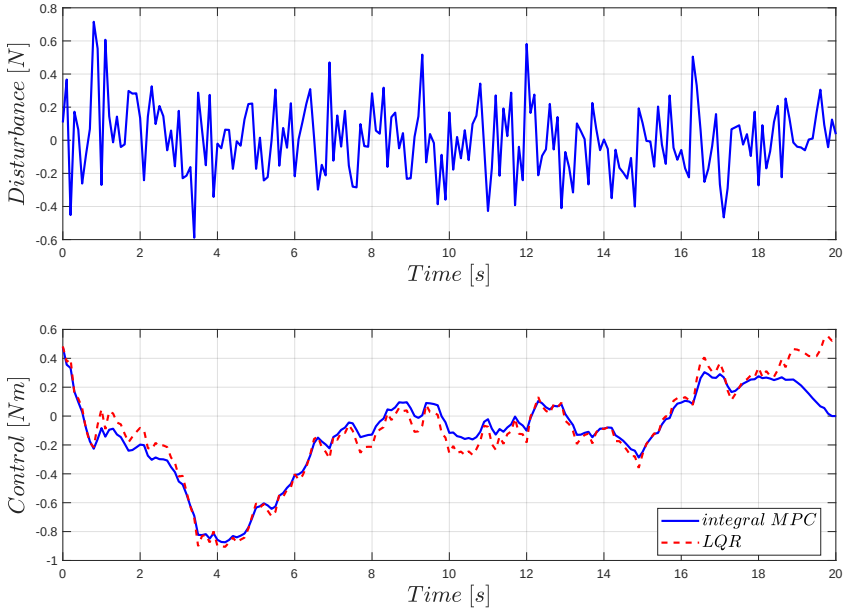

Figure 5.20. Gaussian random $\sigma = 0.2$: Pitch control

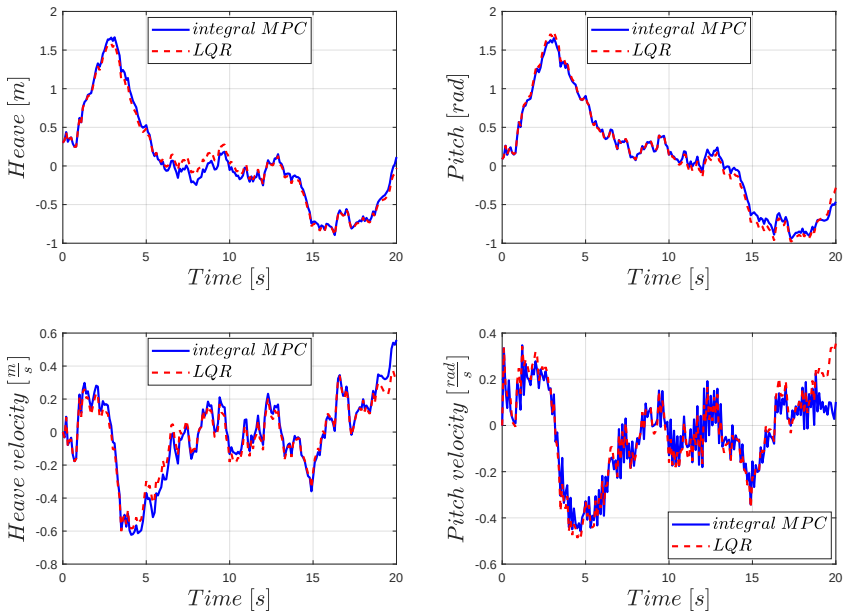

Figure 5.21. Gaussian random $\sigma = 0.6$: Heave and Pitch

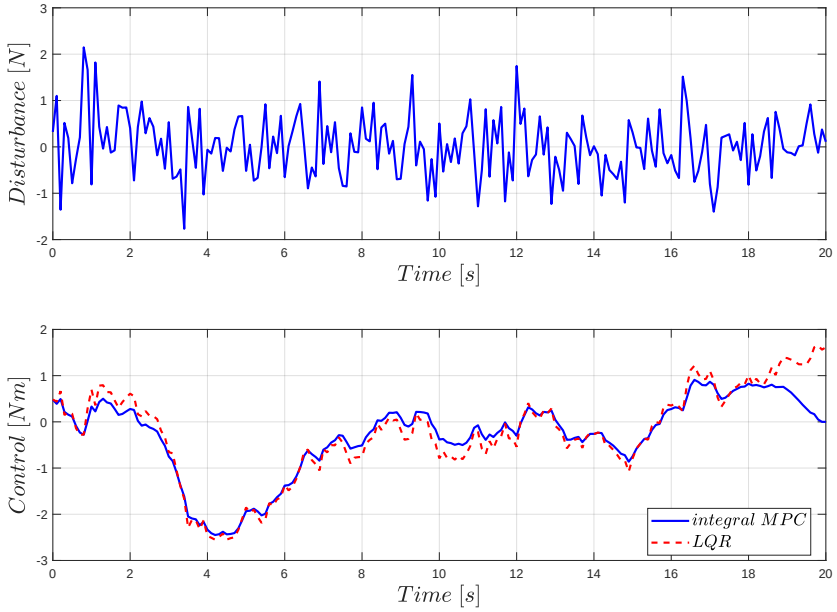

Figure 5.22. Gaussian random $\sigma = 0.6$: Pitch control

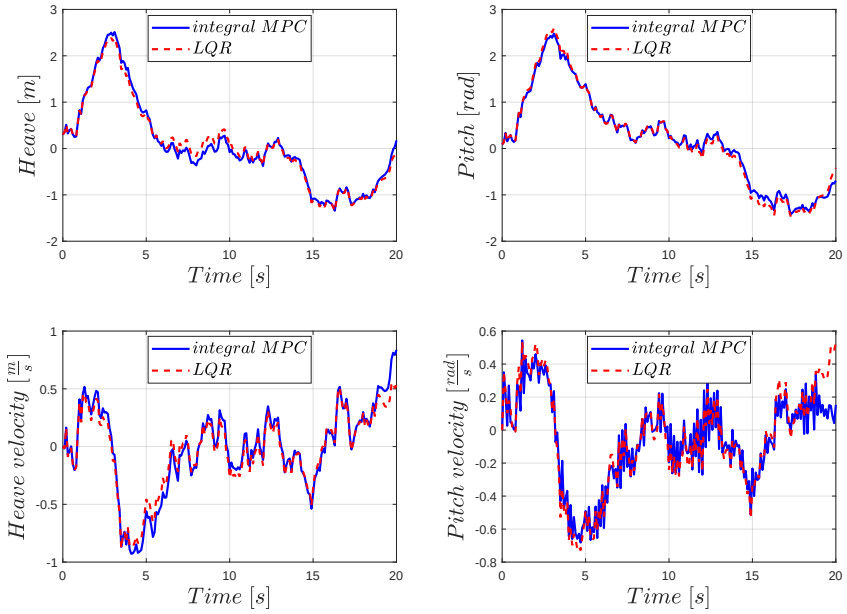

Figure 5.23. Gaussian random $\sigma = 0.9$: Heave and Pitch

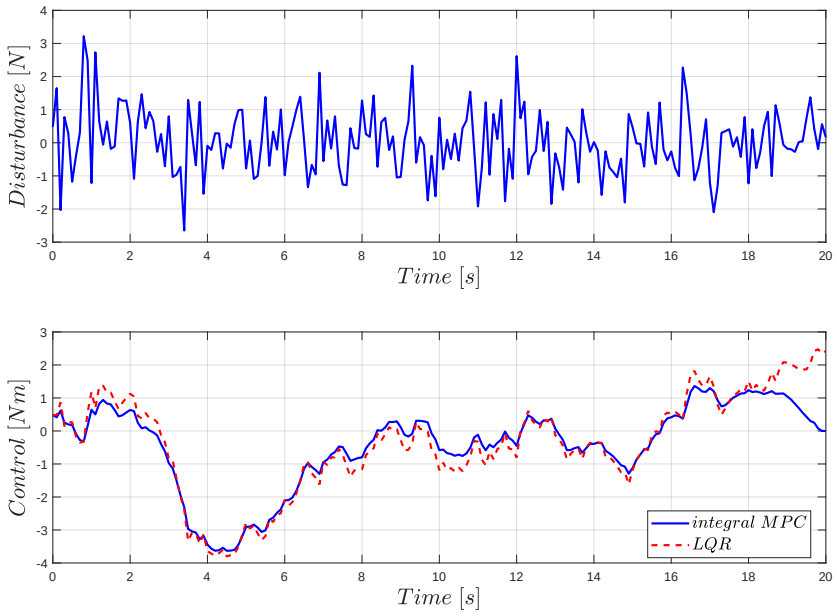

Figure 5.24. Gaussian random $\sigma = 0.9$: Pitch control

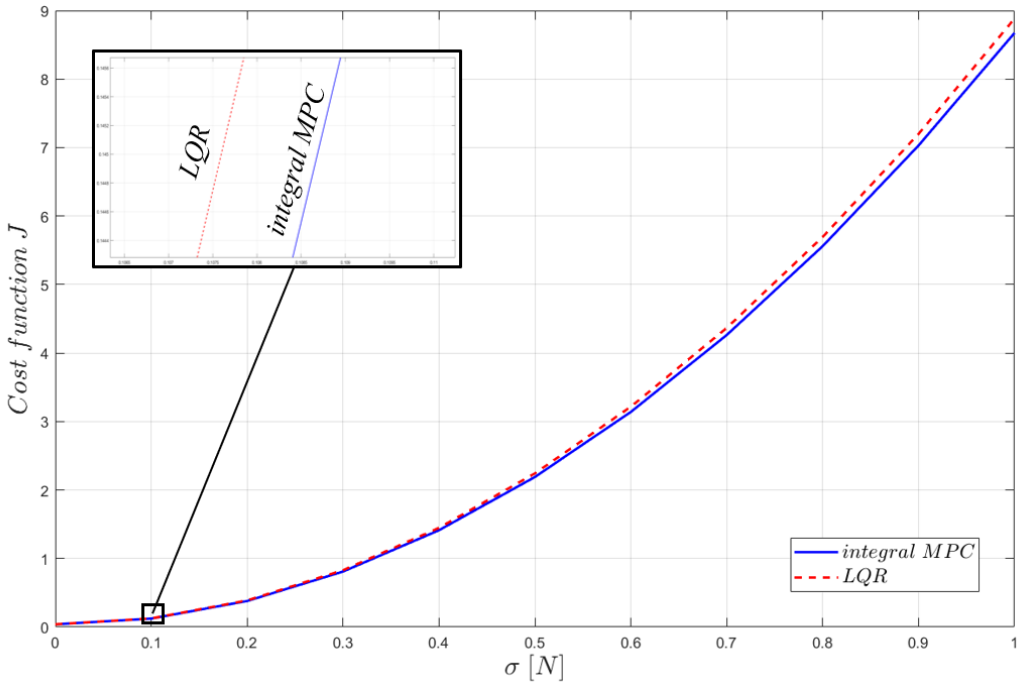

Figure 5.25. Cost function J at different disturbance levels - 2-Dof

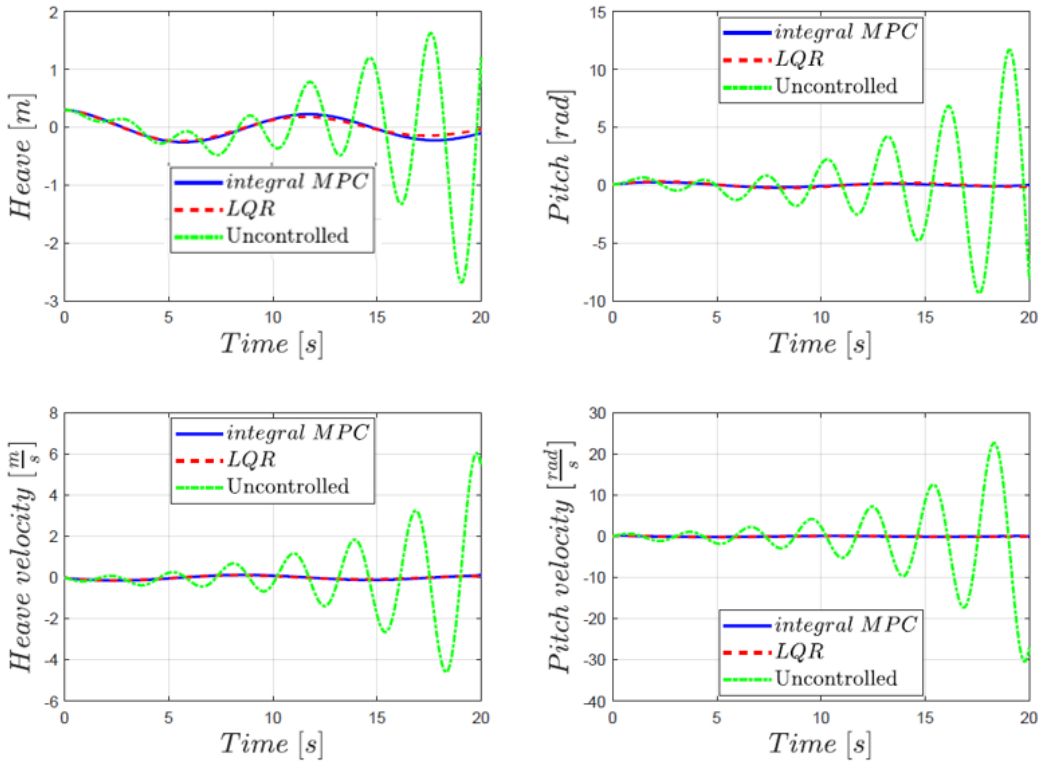

Figure 5.26. Control of fluttering instabilities: state

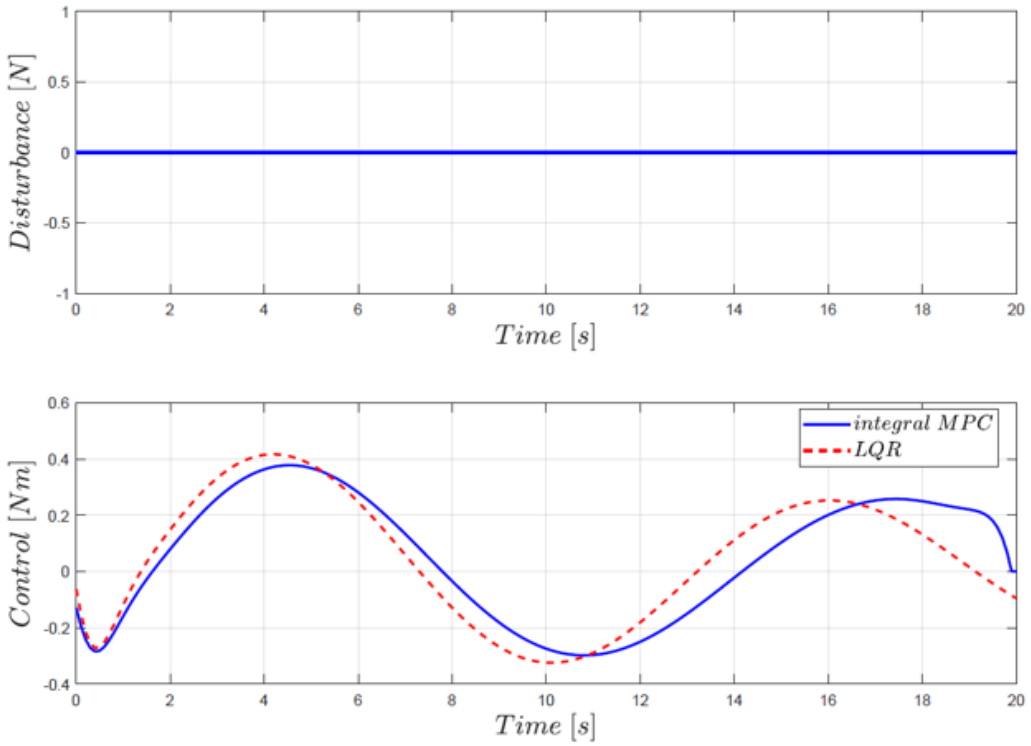

Figure 5.27. Control of fluttering instabilities: control law

Chapter 6

Conclusions

The “Optimal Control of systems with memory” is a PhD project that is borne from the collaboration between the Department of Mechanical and Aerospace Engineering of Sapienza University of Rome and the CNR-INM Institute of Marine Engineering Rome. This project is part of a larger EDA project called ETLAT: Evaluation of State of the Art Thin Line Array Technology (TLA).
A sonar TLA has been widely employed as an important tool for naval defence, ocean exploitation and ocean research. Two main operative limitations costrain the TLA design such as: a fixed immersion depth and the stabilization of its horizontal trim.
The entire system is composed by a towed vehicle and a towed line sonar array (TLA). The two subsystems are towed by a towing cable attached to the moving boat.
The role of the vehicle is to guarantee a TLA’s constant depth of navigation and the reduction of the entire system oscillations. The vehicle is also called "depressor" and its motion generates memory effects that influence the proper operation of the TLA.
In this thesis a simplified mathematical formulation of the system is considered. The presence of nonlinearities, stochastic operator and external forces have been neglected in the model. These mathematical complexities are due to the presence of cables and incident external waves, respectively. At this stage, only the effects of interaction between fluid and structure has been introduced in to the model.
The dynamic of underwater towed system is affected by memory effects induced by the fluid-structure interaction, namely: vortex shedding and added damping due to the presence of a free surface in the fluid. In time domain, memory effects are represented by convolution integral between special kernel functions and the state of the system.
The mathematical formulation of the underwater system, implies the use of integral-differential equations in the time domain. Two different IDEs models of the underwater vehicle motion affected by memory effects are proposed in this work. A prototype 1-Dof model in which both memory effects are included and the 2-Dof hydrofoil model by Theodorsen. The second model proposed takes inclusion of only the release of the vortex wake induced by the unsteady flow in which the hydrofoil is moving.
The goal of this work has been to develop an optimal control law for the underwater

depressor motion which guarantees the engineering costrains of the TLA's design. The presence of convolution terms in the model requires a nonstandard optimal control strategy.
Robust control techniques are often used to control underwater vehicle but they do not involve integral-differential equations. The optimal control applications applied to underwater vehicle present in literature normally do not take in account memory effects into the model. They are neglected or approximated by small external system perturbations. Others optimal control techniques applied on integral-differential equations present in literature are mainly based on direct methods. Direct optimal control methods imply the discretization of the optimal control problem to form a system of algebraic equations. The result is a nonlinear program (NLP) that can be solved using standard large-scale optimization algorithms.
In particular in this work, a new indirect variational control method applied to IDEs has been formalized. The control method proposed in this work, is an extension of the Pontryagin optimal solution, normally applied to differential equations. The first innovative result imply the extension of the variational calculus of the convolution term presents in the integral-differential equation of motion.
The implicit solution of the IDE optimal control problem is proposed by using the finite differences method from which derives the open loop control law. The open loop control reveals that the system response depends only on the initial condition of the system. As it is usual in optimal control problems, the solution is expressed in terms of a control program, i.e, through a prescribed time-dependent control.
Theoretically, this would not be a problem if the model of the physical investigated system is error-free. In this case the solution of the optimal control problem make use only of the past values of the state that are known: the initial conditions. All the remaing part of the trajectory is determined on this basis.
This way of solving the problem, has a strong engineering weakness. In fact, models are not perfect and the open loop control law determined by solving the Euler-Lagrange optimal control equations is based, at the end, only on the past known values and the theoretical model of the system represented. When sensor measurements are available, a technique that makes use of all the acquired information by the sensor over all the time history is much more robust.
This process modifies the exposed technique, switching from a control program to a feedback control. This allows the inclusion in the IDE model of external disturbances that are not known a priori. A feedback via model predictive control (MPC) is formulated for integral-differential system model. Normally the efficency of the MPC method is proportional to the computational costs of the numerical simulations. In the proposed applications the system is linear with a low number of degree of freedom precludind high computational costs.
Different numerical simulations have been developed applying the innovative integral MPC method to the two different IDE models. Different kinds of external disturbances have been applied: gaussian random and deterministic one.
The innovative method produces very interesting results, that show how even widely applied control methods (LQR) fail, while the present formulation exhibits the advantage of the optimal control theory based on integral-differential equations of motion.
The optimal control proposed is a general algorithm that can be applied to every sys-

tems which present memory effects represented by convolution terms (e.g.: floating bodies, materials with memory, surface vessels, etc.). The limitation of this method is its restriction to only linear integro-differential equations and the possible high computational cost of MPC method for high number of the degree of freedom of the system.
The last point could be not a real limitation, because it can be avoided by using dedicated online electronic boards normally used in control applications.
For these reasons, the future perspectives of this study will imply the extension of this optimal control theory to nonlinearities. In the next step the algorithm will be modified to control of the entire underwater mechanical system in analysis. The hydroelastic model of thin line array (TLA) and the presence of the external waves load that imply complexities in the mathematical model will be consider in the final model. The presence of cable involves nonlinearities in the model, the external waves loads give random external forces and the hydroelasticity of the TLA makes the model's operator random. In this way the integral optimal control strategy here proposed will be extend to the control of set of nonlinear partial differential equations and integro-differential equations with stochastic operator and stochastic external loads. Finally, the experimental validation of the control algorithm will be also perform on the already existing depressor prototype at CNR-INM Marine Institute of Rome.
The proposed algorithm will be also test when measurements by sensors are affected by uncertinities, that is an ongoing step of the study.

Appendix A

Matrix implicit formulation

The analitical form of the matrix that are involved in the implicit solution of the N-Dof variational optimal control IDE theory is here reported.
The matrix $\mathbf{\Omega}^{(0,N-2)}$ is composed by four quadratic matrix of $(N-1)\times(N-1)$ dimension:

$$\mathbf{\Omega}^{(0,N-2)} = \begin{bmatrix} \mathbf{\Omega_1} & \mathbf{\Omega_2} \\ \mathbf{\Omega_3} & \mathbf{\Omega_4} \end{bmatrix} \tag{A.1}$$

in which the expressions of each matrix are:

$$\mathbf{\Omega_1} = \begin{bmatrix} \mathbf{0} & \dots & \dots & \dots & \dots & \mathbf{0} \\ -\boldsymbol{Q} & \ddots & & & & \vdots \\ \mathbf{0} & \ddots & \ddots & & & \vdots \\ \vdots & \ddots & \ddots & \ddots & & \vdots \\ \vdots & & \ddots & \ddots & \ddots & \vdots \\ \mathbf{0} & \dots & \dots & 0 & -\boldsymbol{Q} & \mathbf{0} \end{bmatrix} \quad \mathbf{\Omega_4} = \begin{bmatrix} -\boldsymbol{B}\boldsymbol{R}^{-1}\boldsymbol{B}^T & \mathbf{0} & \dots & \dots & \dots & \mathbf{0} \\ \mathbf{0} & \ddots & \ddots & & & \vdots \\ \vdots & \ddots & \ddots & \ddots & & \vdots \\ \vdots & & \ddots & \ddots & \ddots & \vdots \\ \vdots & & & \ddots & \ddots & \mathbf{0} \\ \mathbf{0} & \dots & \dots & \dots & \mathbf{0} & -\boldsymbol{B}\boldsymbol{R}^{-1}\boldsymbol{B}^T \end{bmatrix} \tag{A.2}$$

$$\mathbf{\Omega_2} = \begin{bmatrix} -\frac{\boldsymbol{I}}{\Delta T} + \boldsymbol{A}^T + \mathbf{\Sigma_0}^T\Delta T & \frac{\boldsymbol{I}}{\Delta T} + \mathbf{\Sigma_1}^T\Delta T & \mathbf{\Sigma_2}^T\Delta T & \dots & \dots & \mathbf{\Sigma_{N-2}}^T\Delta T \\ \mathbf{0} & & \ddots & \ddots & \ddots & \\ \vdots & & \ddots & \ddots & \ddots & \ddots & \\ \vdots & & & \ddots & \ddots & \ddots & \mathbf{\Sigma_2}^T\Delta T \\ \vdots & & & & \ddots & \ddots & \frac{\boldsymbol{I}}{\Delta T} + \mathbf{\Sigma_1}^T\Delta T \\ \mathbf{0} & & \dots & \dots & \dots & \mathbf{0} & -\frac{\boldsymbol{I}}{\Delta T} + \boldsymbol{A}^T + \mathbf{\Sigma_0}^T\Delta T \end{bmatrix} \tag{A.3}$$

$$\mathbf{\Omega_3} = \begin{bmatrix} \frac{\boldsymbol{I}}{\Delta T} & \mathbf{0} & \dots & \dots & \dots & \mathbf{0} \\ -\frac{\boldsymbol{I}}{\Delta T} - \boldsymbol{A} - \mathbf{\Sigma_0}\Delta T & \ddots & \ddots & & & \vdots \\ -\mathbf{\Sigma_1}\Delta T & \ddots & \ddots & \ddots & & \vdots \\ \vdots & \ddots & \ddots & \ddots & \ddots & \vdots \\ \vdots & & \ddots & \ddots & \ddots & \mathbf{0} \\ -\mathbf{\Sigma_{N-3}}\Delta T & & -\mathbf{\Sigma_1}\Delta T & -\frac{\boldsymbol{I}}{\Delta T} - \boldsymbol{A} - \mathbf{\Sigma_0}\Delta T & \frac{\boldsymbol{I}}{\Delta T} \end{bmatrix} \tag{A.4}$$

$$\mathbf{\Lambda}^{(0,N-1)} = \begin{bmatrix} \boldsymbol{Q} & -\mathbf{\Sigma}_{\boldsymbol{N-1}}^{T}\Delta T \\ \mathbf{0} & -\mathbf{\Sigma}_{\boldsymbol{N-2}}^{T}\Delta T \\ \vdots & \vdots \\ \vdots & \vdots \\ \vdots & -\mathbf{\Sigma}_{\mathbf{0}}^{T}\Delta T \\ \mathbf{0} & -\frac{\boldsymbol{I}}{\Delta T} - \mathbf{\Sigma}_{\mathbf{1}}^{T}\Delta T \\ \frac{\boldsymbol{I}}{\Delta T} + \boldsymbol{A} + \mathbf{\Sigma}_{\mathbf{0}}\Delta T & \mathbf{0} \\ \mathbf{\Sigma}_{\mathbf{1}}\Delta T & \vdots \\ \vdots & \vdots \\ \vdots & \vdots \\ \vdots & \vdots \\ \mathbf{\Sigma}_{\boldsymbol{N-2}}\Delta T & \mathbf{0} \end{bmatrix} \tag{A.5}$$

Appendix B

Matrix MPC formulation

In this section the analitical expressions of the changing size matrix in the MPC method are illustred starting from the matrix defined in Appendix A.
The new matrix formulations are:

$$\mathbf{\Omega}_k^{(1,N-2)} = \begin{bmatrix} \mathbf{\Omega}_{k,1} & \mathbf{\Omega}_{k,2} \\ \mathbf{\Omega}_{k,3} & \mathbf{\Omega}_{k,4} \end{bmatrix} \tag{B.1}$$

The originary matrix $\mathbf{\Omega}^{(1,N-2)}$ and $\mathbf{\Phi}^{(1,N-1)}$ in Appendix A, shows the limit case when k=1, when the state evolves the new matrix $\mathbf{\Omega_{k,1}, \Omega_{k,2}, \Omega_{k,3}, \Omega_{k,4}}$ are created from the originary matrix (case k=1) when the only columns $(k, ..., N-1)$ are selected. The $\mathbf{\Omega_1, \Omega_2, \Omega_3, \Omega_4}$ from (A.2)-(A.4) can be divided into two submatrix:

$$\begin{aligned} \mathbf{\Omega_1} &= [\mathbf{\Omega_1}(\boldsymbol{N-1, 1, ..., k-1})\ \mathbf{\Omega_1}(\boldsymbol{N-1, k, ..., N-1})] \\ \mathbf{\Omega_2} &= [\mathbf{\Omega_2}(\boldsymbol{N-1, 1, ..., k-1})\ \mathbf{\Omega_2}(\boldsymbol{N-1, k, ..., N-1})] \\ \mathbf{\Omega_3} &= [\mathbf{\Omega_3}(\boldsymbol{N-1, 1, ..., k-1})\ \mathbf{\Omega_3}(\boldsymbol{N-1, k, ..., N-1})] \\ \mathbf{\Omega_4} &= [\mathbf{\Omega_4}(\boldsymbol{N-1, 1, ..., k-1})\ \mathbf{\Omega_4}(\boldsymbol{N-1, k, ..., N-1})] \end{aligned} \tag{B.2}$$

The matrix $\mathbf{\Omega_{k,1}, ..., \Omega_{k,4}}$ are the (k,N-1) selection of the $\mathbf{\Omega_1, ..., \Omega_4}$ matrix as (B.3) shows:

$$\begin{aligned} \mathbf{\Omega_{k,1}} &= [\mathbf{\Omega_1}(\boldsymbol{N-1, k, ..., N-1})] \\ \mathbf{\Omega_{k,2}} &= [\mathbf{\Omega_2}(\boldsymbol{N-1, k, ..., N-1})] \\ \mathbf{\Omega_{k,3}} &= [\mathbf{\Omega_3}(\boldsymbol{N-1, k, ..., N-1})] \\ \mathbf{\Omega_{k,4}} &= [\mathbf{\Omega_4}(\boldsymbol{N-1, k, ..., N-1})] \end{aligned} \tag{B.3}$$

The remaining part of the $\mathbf{\Omega_1, \Omega_2, \Omega_3, \Omega_4}$ columns $(1, ..., k-1)$ which have not been selected, take part of the composition of the new matrix $\mathbf{\Lambda}_k^{(1,N-1)}$. Defining as:

$$\begin{aligned} \mathbf{\Omega_{1,3}} &= \begin{bmatrix} \mathbf{\Omega_1}(\mathbf{N-1, 1, ..., k-1}) \\ \mathbf{\Omega_3}(\mathbf{N-1, 1, ..., k-1}) \end{bmatrix} \\ \mathbf{\Omega_{2,4}} &= \begin{bmatrix} \mathbf{\Omega_2}(\mathbf{N-1, 1, ..., k-1}) \\ \mathbf{\Omega_4}(\mathbf{N-1, 1, ..., k-1}) \end{bmatrix} \end{aligned} \tag{B.4}$$

The $\mathbf{\Lambda^{(1,N-1)}}$ matrix defined in (C.19) was composition of two vectors $\mathbf{\Lambda_1}$ and $\mathbf{\Lambda_2}$.

$$\begin{aligned} \mathbf{\Lambda}^{(1,N-1)} &= [\mathbf{\Lambda_1}\ \mathbf{\Lambda_2}] \\ \mathbf{\Lambda}_k^{(1,N-1)} &= [\mathbf{\Lambda_1}\ \mathbf{\Omega_{1,3}}\ \mathbf{\Omega_{2,4}}\ \mathbf{\Lambda_2}] \end{aligned} \tag{B.5}$$

Appendix C

Scalar optimal control formulation

In this appendix the optimal control algorithm proposed in this work is applied on the pototype 1-Dof integro-differential equation of motion shown in Section 3.3. The scalar formulation of the optimal control algorithm can be found in detail in [125].
The variational formulation of the control problem, the implicit solution of the problem and the extension to a feedback one by model MPC are here shown in detail for the particular scalar form of the integral-differential equation of motion. The integral control theory is formulated for the integral-differential equation of motion eq. (3.17) completed with the initial conditions $x(\tau)$=$x_0(\tau)$, $\tau \in (-\infty, t]$.

Scalar variational problem The cost function of the variational optimal control problem is described by the quadratic functional $\widetilde{J}$, and the optimal control problem is stated as:

$$\begin{aligned} &min\ \widetilde{J} = \int_{-\infty}^{T} \frac{1}{2} q x^2 + \frac{1}{2} r u^2\ dt \\ &\text{subjected to} \\ &\dot{x} = bu + bK * x \end{aligned} \tag{C.1}$$

where $*$ is the convolution product. Introducing the Lagrange multiplier λ, the cost function becomes:

$$J = \int_{-\infty}^{T} \frac{1}{2} q x^2 + \frac{1}{2} r u^2 + \lambda(\dot{x} - bu - bK * x)\ dt \tag{C.2}$$

where q and r are gain parameters. The minimization of the functional J implies:

$$\delta J = \delta \int_{-\infty}^{T} L(x, \dot{x}, \lambda, u)\ dt - \delta \int_{-\infty}^{T} \lambda bK * x\ dt \tag{C.3}$$

that when expressed in terms of the variations δx, $\delta \dot{x}$, $\delta \lambda$, δu, produces:

$$\delta J = \int_{-\infty}^{T} \frac{\partial L}{\partial x}\delta x + \frac{\partial L}{\partial \dot{x}}\delta \dot{x} + \frac{\partial L}{\partial \lambda}\delta \lambda + \frac{\partial L}{\partial u}\delta u\ dt - \int_{-\infty}^{T} \delta\lambda\ bK * x\ dt - \int_{-\infty}^{T} \lambda\ \delta\left(bK * x\right)\ dt = 0 \tag{C.4}$$

[127] or (using integration by parts of $\frac{\partial L}{\partial \dot{x}}\delta\dot{x}$)

$$\begin{aligned}\delta J = \int_{-\infty}^{T} \left(qx - \dot{\lambda}\right)\delta x + \left(\dot{x} - bu - K * x\right)\delta\lambda \quad &+ \left(ru - b\lambda\right)\delta u \; dt + \\ &- \textstyle\int_{-\infty}^{T} \lambda\delta\left(bK * x\right) \; dt = 0\end{aligned} \tag{C.5}$$

and $\lambda(T) = 0$.
The variations of the last term of equation (C.5) are now extended to the 1-Dof integral model starting from the variational matrix form in eq. (2.7). The variation of the convolution term in the scalar form are expressed by:

$$\int_{-\infty}^{T} \lambda(t)\left[\delta\int_{-\infty}^{t} K(t-\tau)x(\tau)\,d\tau\right]\,dt = \int_{-\infty}^{T}\int_{t}^{T} \lambda(\tau)K(\tau - t)\,d\tau\;\delta x(t)\,dt \tag{C.6}$$

So the stationary condition (C.5) for J becomes:

$$\begin{aligned}\delta J = \int_{-\infty}^{T}\Bigg[\left(qx - \dot{\lambda} - b\int_{t}^{T}\lambda(\tau)K(\tau-t)\,d\tau\right)\delta x \quad &+ \left(\dot{x} - bu - bK * x\right)\delta\lambda \\ &+ \left(ru - b\lambda\right)\delta u\Bigg]\;dt = 0\end{aligned} \tag{C.7}$$

and the associated Euler-Lagrange equations are:

$$\begin{cases} \dot{\lambda} = qx - b\displaystyle\int_{t}^{T}\lambda(\tau)K(\tau-t)\,d\tau \\ ru - b\lambda = 0 \\ \dot{x} = bu + b\displaystyle\int_{-\infty}^{t} K(t-\tau)x(\tau)\,d\tau = 0 \\ x(\tau) = x_0(\tau),\ \tau \in (-\infty, t] \\ \lambda(T) = 0 \end{cases} \tag{C.8}$$

The system (C.8) consists of two integral-differential equations (the first and the third) and one linear algebraic equation (the second), this last providing $u = \frac{b}{r}\lambda$, that permits to reduce the system as:

$$\begin{cases} \dot{\lambda} = qx - b\displaystyle\int_{t}^{T}\lambda(\tau)K(\tau-t)\,d\tau \\ \dot{x} = \lambda\dfrac{b^2}{r} + b\displaystyle\int_{-\infty}^{t} K(t-\tau)x(\tau)\,dt \\ x(\tau) = x_0(\tau),\ \tau \in (-\infty, t] \\ \lambda(T) = 0 \end{cases} \tag{C.9}$$

Implicit solution in the scalar case The implicit solution of the equations (C.9) implies a forward finite differences formulation of the problem:

$$\begin{cases} qx_i - \dfrac{\lambda_{i+1}}{\Delta T} + \dfrac{\lambda_i}{\Delta T} - \displaystyle\sum_{j=i}^{N} \lambda_j K_{j-i} \Delta t = 0 \\ \dfrac{x_{i+1}}{\Delta T} - \dfrac{x_i}{\Delta T} - \lambda_i \dfrac{b^2}{r} - \displaystyle\sum_{j=-\infty}^{i} x_j K_{i-j} \Delta t = 0 \\ x_j = x_0, \; j \in (-\infty, i] \\ \lambda_T = 0 \end{cases} \tag{C.10}$$

with $N = \frac{T}{\Delta t}$ and Δt the discretization time interval.
We start with the vector of unknowns as $\{\boldsymbol{\eta}_x^{(1,N)}, \boldsymbol{\eta}_\lambda^{(0,N-1)}\}^T$, $\boldsymbol{\eta}_x^{(1,N)}$=$\{x_1, ..., x_i, ..., x_N\}^T$, $\boldsymbol{\eta}_\lambda^{(0,N-1)}$=$\{\lambda_0, \lambda_1, ..., \lambda_i, ..., \lambda_{N-1}\}^T$, where the *(N,M)* indicates dependence on the time values of t_i for $i \in [N, M]$. Analogously, $\{\boldsymbol{\xi}_x^{(0)}, 0\}^T$ where $\boldsymbol{\xi}_x^{(0)}$=$\{x_0\}$. Equation (C.10) in matrix form becomes:

$$\boldsymbol{\Pi}^{(0,N-2)} \begin{Bmatrix} \boldsymbol{\eta}_x^{(1,N)} \\ \boldsymbol{\eta}_\lambda^{(0,N-1)} \end{Bmatrix} = \boldsymbol{\Phi}^{(0,N-1)} \begin{Bmatrix} \boldsymbol{\xi}_x^{(0)} \\ 0 \end{Bmatrix} \tag{C.11}$$

with obvious solution:

$$\begin{Bmatrix} \boldsymbol{\eta}_x^{(1,N)} \\ \boldsymbol{\eta}_\lambda^{(0,N-1)} \end{Bmatrix} = \boldsymbol{\Pi}^{(0,N-2)^{-1}} \boldsymbol{\Phi}^{(0,N-1)} \begin{Bmatrix} \boldsymbol{\xi}_x^{(0)} \\ 0 \end{Bmatrix} \tag{C.12}$$

the structures of the evolution matrices are shown in Appendix C.1.
The open loop control resulted by the implicit solution of the 1-Dof variational IDE problem has been switched into a feedback control via a model predictive method (integral MPC).

Scalar MPC application The key strategy does not implies the use of the complete solution $\{\boldsymbol{\eta}_x^{(1,N)}, \boldsymbol{\eta}_\lambda^{(0,N-1)}\}^T$ and $\boldsymbol{u} = \frac{b}{r}\boldsymbol{\eta}_\lambda^{(0,N-1)}$ along the time interval $[0, T]$ determined in the previous section, as for equation (C.12).
We use only the first output for $\boldsymbol{u}$, associated at the time $t = t_0$, to which is also associated the first output for the state at the time $t = t_1$. Therefore, at the time $t = t_1$ we know x_0, x_1, λ_0 (and u_0). This terms are collected into the vector $\{\boldsymbol{\xi}_x^{(0,1)}, \boldsymbol{\xi}_\lambda^{(0)}\}^T$ and the unknowns are reduced to $\{\boldsymbol{\eta}_x^{(2,N)}, \boldsymbol{\eta}_\lambda^{(1,N-1)}\}^T$=$\{x_2, x_3..., x_N, \lambda_1, ..., \lambda_{N-1}\}^T$. The matrix $\boldsymbol{\Pi}^{(1,N-2)}$ reduces obviously its dimensions, following the reduction of the number of the unknowns. The matrix $\boldsymbol{\Phi}^{(1,N-1)}$ increases its dimension, following the increase of the known term $\{\boldsymbol{\xi}_x^{(0,1)}, \boldsymbol{\xi}_\lambda^{(0)}\}^T$.
We can iterate this process and at the generic *k-th* step one obtains:

$$\begin{Bmatrix} \boldsymbol{\eta}_x^{(k,N)} \\ \boldsymbol{\eta}_\lambda^{(k-1,N-1)} \end{Bmatrix} = \boldsymbol{\Pi}^{(k-1,N-2)^{-1}} \boldsymbol{\Phi}^{(k-1,N-1)} \begin{Bmatrix} \boldsymbol{\xi}_x^{(0,k-1)} \\ \boldsymbol{\xi}_\lambda^{(0,k-2)} \\ 0 \end{Bmatrix} \tag{C.13}$$

The MPC matrix form is shown in Appendix C.2. An external disturbance $n_x(t)$ is introduced which models an error in the theoretical modelling of the system or/and an external not controllable force.
Introducing $n_x(t)$ equation (3.17) becomes:

$$\dot{x} = bu + b\int_{-\infty}^{t} K(t-\tau)x(\tau)\,dt + n_x(t) \tag{C.14}$$

with the initial condition $x(\tau) = x_0(\tau),\ \tau \in (-\infty, t]$. Equation (C.14) corresponds to the model of the system that includes the noise (model or/and disturbance), while equation (C.9), that is our best representation of the system, is used to determine the control law to be applied to equation (C.14). The scheme in Figure C.1 shows how the open loop optimal control has been converted into an integral feedback MPC, taking into account the past history of the state which represents the initial condition of (C.14).

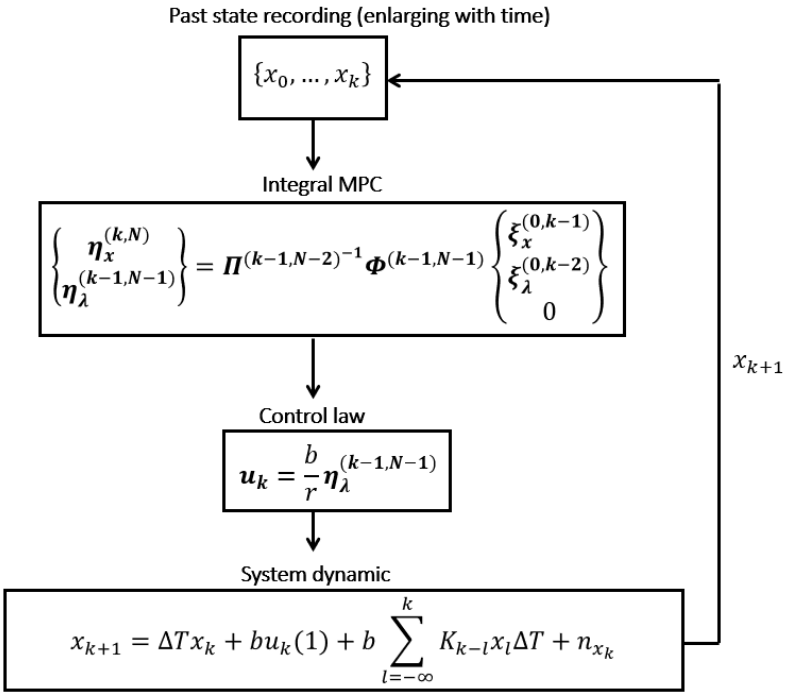

Figure C.1. Integral scalar MPC scheme

C.1 Matrix implicit formulation: scalar model

The matrix $\mathbf{\Pi}^{(0,N-2)}$ is composed by four quadratic matrix of $(N-1) \times (N-1)$ dimension:

$$\mathbf{\Pi}^{(0,N-2)} = \begin{bmatrix} \mathbf{\Pi_1} & \mathbf{\Pi_2} \\ \mathbf{\Pi_3} & \mathbf{\Pi_4} \end{bmatrix} \tag{C.15}$$

in which the expressions of each matrix are:

$$\mathbf{\Pi_1} = \begin{bmatrix} 0 & \dots & \dots & \dots & \dots & 0 \\ q & \ddots & & & & \vdots \\ 0 & \ddots & \ddots & & & \vdots \\ \vdots & \ddots & \ddots & \ddots & & \vdots \\ \vdots & & \ddots & \ddots & \ddots & \vdots \\ 0 & \dots & \dots & 0 & q & 0 \end{bmatrix} \quad \mathbf{\Pi_4} = \begin{bmatrix} -\frac{b^2}{r} & 0 & \dots & \dots & \dots & 0 \\ 0 & \ddots & \ddots & & & \vdots \\ \vdots & \ddots & \ddots & \ddots & & \vdots \\ \vdots & & \ddots & \ddots & \ddots & \vdots \\ \vdots & & & \ddots & \ddots & 0 \\ 0 & \dots & \dots & \dots & 0 & -\frac{b^2}{r} \end{bmatrix} \tag{C.16}$$

$$\mathbf{\Pi_2} = \begin{bmatrix} \frac{1}{\Delta T} - a + K_0\Delta T & -\frac{1}{\Delta T} + K_1\Delta T & K_2\Delta T & \dots & \dots & K_{N-2}\Delta T \\ 0 & \ddots & \ddots & \ddots & & \\ \vdots & \ddots & \ddots & \ddots & \ddots & \\ \vdots & & \ddots & \ddots & \ddots & K_2\Delta T \\ \vdots & & & \ddots & \ddots & -\frac{1}{\Delta T} + K_1\Delta t \\ 0 & \dots & \dots & \dots & 0 & \frac{1}{\Delta T} - a + K_0\Delta T \end{bmatrix} \tag{C.17}$$

$$\mathbf{\Pi_3} = \begin{bmatrix} \frac{1}{\Delta T} & 0 & \dots & \dots & \dots & 0 \\ -\frac{1}{\Delta T} - a + K_0\Delta T & \ddots & \ddots & & & \vdots \\ -K_1\Delta T & \ddots & \ddots & \ddots & & \vdots \\ \vdots & \ddots & \ddots & \ddots & \ddots & \vdots \\ \vdots & & \ddots & \ddots & \ddots & 0 \\ -K_{N-3}\Delta T & & & -K_1\Delta T & -\frac{1}{\Delta T} - a + K_0\Delta T & \frac{1}{\Delta T} \end{bmatrix} \tag{C.18}$$

$$\mathbf{\Phi}^{(0,N-1)} = \begin{bmatrix} -q & -K_{N-1}\Delta T \\ 0 & -K_{N-2}\Delta T \\ \vdots & \vdots \\ \vdots & \vdots \\ \vdots & -K_0\Delta T \\ 0 & -\frac{1}{\Delta T} - K_1\Delta T \\ -\frac{1}{\Delta T} + a + K_0\Delta T & 0 \\ K_1\Delta T & \vdots \\ \vdots & \vdots \\ \vdots & \vdots \\ \vdots & \vdots \\ K_{N-2}\Delta T & 0 \end{bmatrix} \tag{C.19}$$

C.2 Matrix MPC: scalar model

The new matrix formulations are:

$$\mathbf{\Pi}_k^{(1,N-2)} = \begin{bmatrix} \mathbf{\Pi}_{k,1} & \mathbf{\Pi}_{k,2} \\ \mathbf{\Pi}_{k,3} & \mathbf{\Pi}_{k,4} \end{bmatrix} \tag{C.20}$$

The originary matrix $\mathbf{\Pi}^{(1,N-2)}$ and $\mathbf{\Phi}^{(1,N-1)}$ in Appendix **??**, shows the limit case when k=1, when the state evolves the new matrix $\mathbf{\Pi_{k,1}, \Pi_{k,2}, \Pi_{k,3}, \Pi_{k,4}}$ are created from the originary matrix (case k=1) when the only columns $(k, ..., N-1)$ are selected. The $\mathbf{\Pi_1, \Pi_2, \Pi_3, \Pi_4}$ from (C.16)-(C.18) can be divided into two submatrix:

$$\begin{aligned} \mathbf{\Pi_1} &= [\mathbf{\Pi_1}(\boldsymbol{N-1, 1, ..., k-1})\ \mathbf{\Pi_1}(\boldsymbol{N-1, k, ..., N-1})] \\ \mathbf{\Pi_2} &= [\mathbf{\Pi_2}(\boldsymbol{N-1, 1, ..., k-1})\ \mathbf{\Pi_2}(\boldsymbol{N-1, k, ..., N-1})] \\ \mathbf{\Pi_3} &= [\mathbf{\Pi_3}(\boldsymbol{N-1, 1, ..., k-1})\ \mathbf{\Pi_3}(\boldsymbol{N-1, k, ..., N-1})] \\ \mathbf{\Pi_4} &= [\mathbf{\Pi_4}(\boldsymbol{N-1, 1, ..., k-1})\ \mathbf{\Pi_4}(\boldsymbol{N-1, k, ..., N-1})] \end{aligned} \tag{C.21}$$

The matrix $\mathbf{\Pi_{k,1}, ..., \Pi_{k,4}}$ are the (k,N-1) selection of the $\mathbf{\Pi_1, ..., \Pi_4}$ matrix as (C.22) shows:

$$\begin{aligned} \mathbf{\Pi_{k,1}} &= [\mathbf{\Pi_1}(\boldsymbol{N-1, k, ..., N-1})] \\ \mathbf{\Pi_{k,2}} &= [\mathbf{\Pi_2}(\boldsymbol{N-1, k, ..., N-1})] \\ \mathbf{\Pi_{k,3}} &= [\mathbf{\Pi_3}(\boldsymbol{N-1, k, ..., N-1})] \\ \mathbf{\Pi_{k,4}} &= [\mathbf{\Pi_4}(\boldsymbol{N-1, k, ..., N-1})] \end{aligned} \tag{C.22}$$

The remaining part of the $\mathbf{\Pi_1, \Pi_2, \Pi_3, \Pi_4}$ columns $(1, ..., k-1)$ which have not been selected, take part of the composition of the new matrix $\mathbf{\Phi}_k^{(1,N-1)}$. Defining as:

$$\begin{aligned} \mathbf{\Pi_{1,3}} &= \begin{bmatrix} \mathbf{\Pi_1}(\boldsymbol{N-1, 1, ..., k-1}) \\ \mathbf{\Pi_3}(\boldsymbol{N-1, 1, ..., k-1}) \end{bmatrix} \\ \mathbf{\Pi_{2,4}} &= \begin{bmatrix} \mathbf{\Pi_2}(\boldsymbol{N-1, 1, ..., k-1}) \\ \mathbf{\Pi_4}(\boldsymbol{N-1, 1, ..., k-1}) \end{bmatrix} \end{aligned} \tag{C.23}$$

The $\mathbf{\Phi}^{(1,N-1)}$ matrix defined in (C.19) was composition of two vectors $\mathbf{\Phi_1}$ and $\mathbf{\Phi_2}$.

$$\begin{aligned} \mathbf{\Phi}^{(1,N-1)} &= [\mathbf{\Phi_1}\ \mathbf{\Phi_2}] \\ \mathbf{\Phi}_k^{(1,N-1)} &= [\mathbf{\Phi_1}\ \mathbf{\Pi_{1,3}}\ \mathbf{\Pi_{2,4}}\ \mathbf{\Phi_2}] \end{aligned} \tag{C.24}$$

Appendix D

Stability Analysis

The question of the stability of the controlled integral-differential dynamics is not the key point of the present work. In fact, we are investigating finite time horizon with a two-points boundary value problem, one at the initial time, another at the final time, solved by an implicit numerical scheme over a finite time interval. A stability problem emerges in general only when considering the infinite time horizon. However, the question shows some analogies with the problem of stability approached in the frame of the LQR. In that case, when the Euler-Lagrange equations are determined, as the conditions for the quadratic functional minimization, the linear differential equations in terms of the state and co-state variables are set. This system is characterized by the Hamilton matrix **H** (see later). The Euler-Lagrange equations produce an open-loop time dependent solution for the control, and both the state and the control variables are characterized by pairs of decaying exponentials and exponentially diverging terms. Namely, it is a known result that the Hamilton matrix admits pair of symmetric eigenvalues, i.e. for each negative-real-part eigenvalue, a symmetric corresponding positive-real-part exists. The diverging terms do not cause any problem for the finite time horizon, rather they help in fitting the boundary values (at initial and final times). For the infinite time horizon case, it is known that, when the steady algebraic Riccati's equation is set finding a closed-loop feedback solution, the determined gain matrix, when inserted into the system dynamics, produces only the set of negative-real-part exponentials of the Hamiltonian matrix, and the controlled system is asymptotically stable.
In the present Appendix we demonstrated the stability analysis of the integral-differential optimal control (4.13) starting from its scalar form. We determined the Euler-Lagrange equations (C.9) associated to the optimal control of the integral-differential problem (C.1), that are solved only for the finite time horizon case. In fact, we have not an analogous of the algebraic Riccati's equation to solve directly the closed-loop problem, and for this reason the stability problem is not crucial in this context. However, the chance of determining an analogous of the Riccati's equation, even for the integral-differential problem (C.9), is interesting and will the subject of further investigations.
Let us make the point about the Euler-Lagrange equation (C.9) in the infinite horizon case, analyzing the properties of a generalized Hamilton matrix that shows some analogies with the Hamilton matrix **H** associated to the LQR theory.

Assume initial conditions, $x(\tau)$=0, $\tau \in (-\infty, 0]$. Without loss of generality we have:

$$\begin{cases} \dot{x} = ax + \lambda\dfrac{b^2}{r} + b\displaystyle\int_0^t K(t-\tau)x(\tau)\,d\tau \\ \dot{\lambda} = qx - a\lambda - b\displaystyle\int_t^T K(\tau-t)\lambda(\tau)\,d\tau \\ \lambda(T) = 0 \end{cases} \tag{D.1}$$

Consider, additionally, an infinite time horizon $T \to \infty$ and constant values for a, b, q, r. Moreover, since the kernel $K(t) = 0$ for t<0, finally we have:

$$\begin{cases} \dot{x} = ax + \lambda\dfrac{b^2}{r} + b\displaystyle\int_0^\infty K(t-\tau)x(\tau)\,d\tau \\ \dot{\lambda} = qx - a\lambda - b\displaystyle\int_0^\infty K(\tau-t)\lambda(\tau)\,d\tau \\ \lim\limits_{t\to\infty} \lambda(t) = 0 \end{cases} \tag{D.2}$$

The two integrals are reduced to convolutions: the first of $K(t)$ and $x(t)$, the second of $K(-t)$ and $\lambda(t)$. Introducing the two matrices:

$$\boldsymbol{H} = \begin{bmatrix} a & \frac{b^2}{r} \\ q & -a \end{bmatrix} \quad \boldsymbol{K}(t) = \begin{bmatrix} K(t) & 0 \\ 0 & K(-t) \end{bmatrix} \tag{D.3}$$

the problem shows the compact form:

$$\dot{\boldsymbol{\zeta}} = \boldsymbol{H}\boldsymbol{\zeta} + \boldsymbol{K} * \boldsymbol{\zeta} \qquad \boldsymbol{\zeta} = \begin{Bmatrix} x \\ \lambda \end{Bmatrix} \tag{D.4}$$

Passing to the Laplace transform $\hat{\cdot}$

$$s\hat{\boldsymbol{\zeta}}(s) = \boldsymbol{H}\hat{\boldsymbol{\zeta}}(s) + \hat{\boldsymbol{K}}(s)\hat{\boldsymbol{\zeta}}(s) \tag{D.5}$$

i.e.

$$\boldsymbol{M}(s)\hat{\boldsymbol{\zeta}}(s) = \left[s\boldsymbol{I} - \boldsymbol{H} - \hat{\boldsymbol{K}}(s)\right]\hat{\boldsymbol{\zeta}}(s) = \boldsymbol{0} \tag{D.6}$$

The matrix $\boldsymbol{M} = s\boldsymbol{I} - \boldsymbol{H} - \hat{\boldsymbol{K}}(s)$ is a generalized Hamilton matrix associated to integral-differential problem. In the absence of $\hat{\boldsymbol{K}}(s)$, $\boldsymbol{M} = \boldsymbol{H}$. Its eigenvalues are determined solving the equation $det\left(s\boldsymbol{I} - \boldsymbol{H} - \hat{\boldsymbol{K}}(s)\right) = 0$. Considering elemental properties of the Laplace transform, the generalized Hamilton matrix is:

$$\boldsymbol{M}(s) = \begin{bmatrix} s - a - \hat{\boldsymbol{K}}(s) & -\frac{b^2}{r} \\ -q & s + a - \hat{\boldsymbol{K}}(-s) \end{bmatrix} \tag{D.7}$$

and

$$det\,(\boldsymbol{M}) = 0 \to \left(s - a - \hat{\boldsymbol{K}}(s)\right)\left(s + a - \hat{\boldsymbol{K}}(-s)\right) - \frac{qb^2}{r} = 0 \tag{D.8}$$

A direct inspection of this expression shows that if p is an eigenvalue, then $-p$ is also an eigenvalue. Therefore, the generalized Hamilton matrix $\boldsymbol{M}$ shares this eigenvalues symmetry with the Hamilton matrix $\boldsymbol{H}$. This implies that certainly, a

direct time-marching solution over an infinite time horizon of the equation (D.4) produces diverging terms. However, this is not the case of the solution proposed in Appendix C, because it is based on an implicit numerical scheme. Nevertheless, these diverging terms affect also equation (D.4) for $\hat{\boldsymbol{K}}(s) = 0$ as it appears in the LQR Hamilton equation, i.e. $\dot{\boldsymbol{\zeta}} = \boldsymbol{H}\boldsymbol{\zeta}$, that is well known produces instability when integrated over an unlimited time domain with a marching scheme. To go more in depth, consider that in hydrodynamics the Wagner function can be approximated by a series of exponentials, so that:

$$K(t) = \sum_{i=1}^{N} A_i e^{-\beta_i t} \qquad K(-t) = \sum_{i=1}^{N} A_i e^{\beta_i t} \tag{D.9}$$

with $\beta_i < 0$ and $\hat{\boldsymbol{K}}(s)$ shows the explicit form:

$$\hat{\boldsymbol{K}}(s) = \begin{bmatrix} \sum_{i=1}^{N} \frac{A_i}{s+\beta_i} & 0 \\ 0 & \sum_{i=1}^{N} \frac{A_i}{s-\beta_i} \end{bmatrix} \tag{D.10}$$

$$\boldsymbol{M}(s) = s\boldsymbol{I} - \boldsymbol{H} - \hat{\boldsymbol{K}}(s) = \begin{bmatrix} s - a - \sum_{i=1}^{N} \frac{A_i}{s+\beta_i} & -\frac{b^2}{r} \\ -q & s + a - \sum_{i=1}^{N} \frac{A_i}{s-\beta_i} \end{bmatrix} \tag{D.11}$$

The eigenvalues are determined solving the secular equation:

$$\left(s - a - \sum_{i=1}^{N} \frac{A_i}{s+\beta_i} \right) \left(s + a + \sum_{i=1}^{N} \frac{A_i}{s-\beta_i} \right) - \frac{qb^2}{r} = 0 \tag{D.12}$$

This theory is the same also for the general N-Dof integral-differential model, however it is not here reported.

Bibliography

[1] Jiaming Wu and Allen T. Chwang. "Investigation on a two-part underwater manoeuvrable towed system". In: *Ocean Engineering* 28.8 (Aug. 2001), pp. 1079–1096.

[2] Jie Wu et al. "Vortex-induced vibration of a flexible cylinder: Interaction of the in-line and cross-flow responses". In: *Journal of Fluids and Structures* 63 (May 2016), pp. 238–258.

[3] Joël V. Sanders. "A three-dimensional dynamic analysis of a towed system". In: *Ocean Engineering* 9.5 (Jan. 1982), pp. 483–499.

[4] B. Buckham et al. "Dynamics and control of a towed underwater vehicle system, part I: model development". In: *Ocean Engineering* 30.4 (Mar. 2003), pp. 453–470.

[5] S.G. Lemon. "Towed-Array History, 1917–2003". In: *IEEE Journal of Oceanic Engineering* 29.2 (Apr. 2004), pp. 365–373.

[6] M. Lasky, R.D. Doolittle, B.D. Simmons, and S.G. Lemon. "Recent Progress in Towed Hydrophone Array Research". In: *IEEE Journal of Oceanic Engineering* 29.2 (Apr. 2004), pp. 374–387.

[7] Chengyan Peng and Xueliang Zhang. "A dynamic depth estimation method for towed optical fiber hydrophone array". In: *The Journal of the Acoustical Society of America* 143.5 (May 2018), EL399–EL404.

[8] Autun Purser et al. "Ocean Floor Observation and Bathymetry System (OFOBS): A new Towed Camera/Sonar System for Deep-Sea Habitat Surveys". In: *IEEE Journal of Oceanic Engineering* (2018), pp. 1–13.

[9] A.S. Gadre et al. "Cooperative localization of an acoustic source using towed hydrophone arrays". In: *2008 IEEE/OES Autonomous Underwater Vehicles*. IEEE, Oct. 2008.

[10] Tina M. Yack et al. "Passive acoustic monitoring using a towed hydrophone array results in identification of a previously unknown beaked whale habitat". In: *The Journal of the Acoustical Society of America* 134.3 (Sept. 2013), pp. 2589–2595.

[11] A. M. von Benda-Beckmann, S. P. Beerens, and S. P. van IJsselmuide. "Effect of towed array stability on instantaneous localization of marine mammals". In: *The Journal of the Acoustical Society of America* 134.3 (Sept. 2013), pp. 2409–2417.

[12] H.O. Berteaux. *Buoy Engineering*. Ocean Engineering; a Wiley Series. Wiley, 1976. ISBN: 9780835774765. URL: https://books.google.it/books?id=vp6fPQAACAAJ.

[13] Antonio Culla and Antonio Carcaterra. "Statistical moments predictions for a moored floating body oscillating in random waves". In: *Journal of Sound and Vibration* 308.1-2 (Nov. 2007), pp. 44–66.

[14] T. Huang and S. Chucheepsakul. "Large Displacement Analysis of a Marine Riser". In: *Journal of Energy Resources Technology* 107.1 (1985), p. 54.

[15] N. Yoshizawa and T. Yabuta. "Study on submarine cable tension during laying". In: *IEEE Journal of Oceanic Engineering* 8.4 (Oct. 1983), pp. 293–299.

[16] Marco D. Masciola, Meyer Nahon, and Frederick R. Driscoll. "Static Analysis of the Lumped Mass Cable Model Using a Shooting Algorithm". In: *Journal of Waterway, Port, Coastal, and Ocean Engineering* 138.2 (Mar. 2012), pp. 164–171.

[17] Elena Paifelman. "A comparison between mathematical models of stationary configuration of an underwater towed system with experimental validations". In: *OCEANS 2017 - Aberdeen*. IEEE, June 2017.

[18] Chunying Xu, Jiawang Chen, Dongxu Yan, and Jian Ji. "Review of Underwater Cable Shape Detection". In: *Journal of Atmospheric and Oceanic Technology* 33.3 (Mar. 2016), pp. 597–606.

[19] J. Ketchman. "Vibration induced in towed linear underwater array cables". In: *IEEE Journal of Oceanic Engineering* 6.3 (July 1981), pp. 77–87.

[20] W.-J. Kim and N.C. Perkins. "Two-Dimensional Vortex-Induced Vibration Of Cable Suspensions". In: *Journal of Fluids and Structures* 16.2 (Feb. 2002), pp. 229–245.

[21] A. Cigada et al. "Vortex shedding and wake-induced vibrations in single and bundle cables". In: *Journal of Wind Engineering and Industrial Aerodynamics* 72 (Nov. 1997), pp. 253–263.

[22] F.S. Hover, S.N. Miller, and M.S. Triantafyllou. "Vortex-Induced Vibration Of Marine Cables: Experiments Using Force Feedback". In: *Journal of Fluids and Structures* 11.3 (Apr. 1997), pp. 307–326.

[23] S.K. Bhattacharyya, C.P. Vendhan, and K. Sudarsan. "The Finite Element Method For Hydroelastic Instability Of Underwater Towed Cylindrical Structures". In: *Journal of Sound and Vibration* 237.1 (Oct. 2000), pp. 119–143.

[24] M. Kheiri, M.P. Païdoussis, and M. Amabili. "An experimental study of dynamics of towed flexible cylinders". In: *Journal of Sound and Vibration* 348 (July 2015), pp. 149–166.

[25] F.S. Hover, M.A. Grosenbaugh, and M.S. Triantafyllou. "Calculation of dynamic motions and tensions in towed underwater cables". In: *IEEE Journal of Oceanic Engineering* 19.3 (July 1994), pp. 449–457.

[26] E. E. Zajac. "Dynamics and Kinematics of the Laying and Recovery of Submarine Cable". In: *Bell System Technical Journal* 36.5 (Sept. 1957), pp. 1129–1207.

[27] H. M. Irvine and J. H. Griffin. "On the dynamic response of a suspended cable". In: *Earthquake Engineering & Structural Dynamics* 4.4 (Apr. 1976), pp. 389–402.

[28] Young-il Choo and Mario J. Casarella. "A Survey of Analytical Methods for Dynamic Simulation of Cable-Body Systems." In: *Journal of Hydronautics* 7.4 (Oct. 1973), pp. 137–144.

[29] H.I. Park, D.H. Jung, and W. Koterayama. "A numerical and experimental study on dynamics of a towed low tension cable". In: *Applied Ocean Research* 25.5 (Oct. 2003), pp. 289–299.

[30] Sylvie Marcos. "Calibration of a distorted towed array using a propagation operator". In: *The Journal of the Acoustical Society of America* 93.4 (Apr. 1993), pp. 1987–1994.

[31] John L Butler and Charles H Sherman. *Transducers and arrays for underwater sound*. Springer, 2016.

[32] Stergios Stergiopoulos. "Limitations on towed-array gain imposed by a nonisotropic ocean". In: *The Journal of the Acoustical Society of America* 90.6 (Dec. 1991), pp. 3161–3172.

[33] P. Vinod, Roni Francis, P. Prabhasuthan, and O.R. Nandagopan. "Depth Enhancement of an Underwater Towed System using Hydrodynamic Depressor". In: *Defence Science Journal* 66.5 (Sept. 2016), p. 546.

[34] N. E. Jeffrey. "Influence of Design Features on Underwater Towed System Stability". In: *Journal of Hydronautics* 2.4 (Oct. 1968), pp. 205–213.

[35] Kai Zhou, Junkao Liu, and Weishan Chen. "Numerical studies on hydrodynamics of flapping foils". In: *2015 IEEE International Conference on Information and Automation*. IEEE, Aug. 2015.

[36] Hadar Ben-Gida, Alex Liberzon, and Roi Gurka. "A stratified wake of a hydrofoil accelerating from rest". In: *Experimental Thermal and Fluid Science* 70 (Jan. 2016), pp. 366–380.

[37] Junshi Wang et al. "Effects of flapping waveforms on the performance of intermittent swimming in viscous flows". In: *2018 AIAA Aerospace Sciences Meeting*. American Institute of Aeronautics and Astronautics, Jan. 2018.

[38] Arkadiusz Mystkowski. "Piezo-stack vortex generators for boundary layer control of a delta wing micro-aerial vehicle". In: *Mechanical Systems and Signal Processing* 40.2 (Nov. 2013), pp. 783–790.

[39] Joel E. Guerrero. "Wake Signature and Strouhal Number Dependence of Finite-Span Flapping Wings". In: *Journal of Bionic Engineering* 7 (Sept. 2010), S109–S122.

[40] J.D. Holmes et al. "An autonomous underwater vehicle towed array for ocean acoustic measurements and inversions". In: *Europe Oceans 2005*. IEEE, 2005.

[41] Alan Jennings, Michael Mayhew, and Jonathan Black. "Video measurements of instantaneous forces of flapping wing vehicles". In: *Mechanical Systems and Signal Processing* 64-65 (Dec. 2015), pp. 325–336.

[42] Yiming Jin and Ping Dong. "A novel Wake Oscillator Model for simulation of cross-flow vortex induced vibrations of a circular cylinder close to a plane boundary". In: *Ocean Engineering* 117 (May 2016), pp. 57–62.

[43] B.H. Huynh and T. Tjahjowidodo. "Experimental chaotic quantification in bistable vortex induced vibration systems". In: *Mechanical Systems and Signal Processing* 85 (Feb. 2017), pp. 1005–1019.

[44] Thomas Battista, Craig Woolsey, Tristan Perez, and Francis Valentinis. "A Dynamic Model for Underwater Vehicle Maneuvering Near a Free Surface". In: *IFAC-PapersOnLine* 49.23 (2016), pp. 68–73.

[45] Sh. Mansoorzadeh and E. Javanmard. "An investigation of free surface effects on drag and lift coefficients of an autonomous underwater vehicle (AUV) using computational and experimental fluid dynamics methods". In: *Journal of Fluids and Structures* 51 (Nov. 2014), pp. 161–171.

[46] Ali Nematollahi, Abdolrahman Dadvand, and Mazyar Dawoodian. "An axisymmetric underwater vehicle-free surface interaction: A numerical study". In: *Ocean Engineering* 96 (Mar. 2015), pp. 205–214.

[47] S. Khalil Shariati and S. Hossein Mousavizadegan. "The effect of appendages on the hydrodynamic characteristics of an underwater vehicle near the free surface". In: *Applied Ocean Research* 67 (Sept. 2017), pp. 31–43.

[48] T. Theodorsen. *General theory of aerodynamic instabilities and the meccanism of flutter*. Vol. 496. 413-433. Naca report, 1935.

[49] Y.C. Fung. *An introduction to the Theory of Aeroleasticity*. Ed. by New York Dover. 1969.

[50] R.T. Jones. *The unsteady lift of a wing of finite aspect ratio*. Vol. 681. 31-36. Naca report, 1940.

[51] Minsung Kim, Hangil Joe, Jinwhan Kim, and Son-cheol Yu. "Integral sliding mode controller for precise manoeuvring of autonomous underwater vehicle in the presence of unknown environmental disturbances". In: *International Journal of Control* 88.10 (July 2015), pp. 2055–2065.

[52] Y. Nasuno et al. "A controller design for autonomous underwater vehicle "MR-X1" using linear matrix inequalities". In: *International Journal of Control* 80.7 (July 2007), pp. 1125–1135.

[53] Dimitra Panagou and Kostas J. Kyriakopoulos. "Dynamic positioning for an underactuated marine vehicle using hybrid control". In: *International Journal of Control* 87.2 (Sept. 2013), pp. 264–280.

[54] Michael R. Benjamin et al. "Autonomous Control of an Autonomous Underwater Vehicle Towing a Vector Sensor Array". In: *Proceedings 2007 IEEE International Conference on Robotics and Automation*. IEEE, Apr. 2007.

[55] R. K. Lea, R. Allen, and S. L. Merry. "A comparative study of control techniques for an underwater flight vehicle". In: *International Journal of Systems Science* 30.9 (Jan. 1999), pp. 947–964.

[56] Sahar Sedaghati, Farzaneh Abdollahi, and Khashayar Khorasani. "Model predictive and non-cooperative dynamic game fault recovery control strategies for a network of unmanned underwater vehicles". In: *International Journal of Control* (Aug. 2017), pp. 1–29.

[57] J. E. Refsnes, A. J. Sørensen, and K. Y. Pettersen. "Output feedback control of slender body underwater vehicles with current estimation". In: *International Journal of Control* 80.7 (July 2007), pp. 1136–1150.

[58] Brian S. Thomas and Paul D. Sclavounos. "Optimal-control theory applied to ship maneuvering in restricted waters". In: *Journal of Engineering Mathematics* 58.1-4 (Feb. 2007), pp. 301–315.

[59] Paul D Sclavounos. "Intersections between marine hydrodynamics and optimal control theory". In: *Proceedings of the 21st International Workshop on Water Waves and Floating Bodies*. 2006.

[60] Thor I Fossen. *Handbook of marine craft hydrodynamics and motion control*. John Wiley & Sons, 2011.

[61] Iason Hatzakis and Paul D Sclavounos. "Active motion control of high-speed hydrofoil vessels by state-space methods". In: *Journal of ship research* 50.1 (2006), pp. 49–62.

[62] K. Maleknejad and M. Hadizadeh. "A new computational method for Volterra-Fredholm integral equations". In: *Computers & Mathematics with Applications* 37.9 (May 1999), pp. 1–8.

[63] K. Maleknejad, S. Sohrabi, and Y. Rostami. "Numerical solution of nonlinear Volterra integral equations of the second kind by using Chebyshev polynomials". In: *Applied Mathematics and Computation* 188.1 (May 2007), pp. 123–128.

[64] S.A. Belbas. "A new method for optimal control of Volterra integral equations". In: *Applied Mathematics and Computation* 189.2 (June 2007), pp. 1902–1915.

[65] V. R. Vinokurov. "Optimal Control of Processes Described by Integral Equations. I". In: *SIAM Journal on Control* 7.2 (May 1969), pp. 324–336.

[66] S.A. Belbas. "A reduction method for optimal control of Volterra integral equations". In: *Applied Mathematics and Computation* 197.2 (Apr. 2008), pp. 880–890.

[67] Eduardo D Sontag. *Mathematical control theory: deterministic finite dimensional systems*. Vol. 6. Springer Science & Business Media, 2013.

[68] Leonard David Berkovitz. *Optimal control theory*. Vol. 12. Springer Science & Business Media, 2013.

[69] Lorenz T Biegler. *Nonlinear programming: concepts, algorithms, and applications to chemical processes*. Vol. 10. Siam, 2010.

[70] Oskar Von Stryk. "Numerical solution of optimal control problems by direct collocation". In: *Optimal Control*. Springer, 1993, pp. 129–143.

[71] John T Betts. *Practical methods for optimal control and estimation using nonlinear programming*. Vol. 19. Siam, 2010.

[72] Gamal N Elnagar. "Optimal control computation for integro-differential aerodynamic equations". In: *Mathematical methods in the applied sciences* 21.7 (1998), pp. 653–664.

[73] Mordecai Avriel. *Nonlinear programming: analysis and methods*. Courier Corporation, 2003.

[74] Ashok D. Belegundu and Jasbir S. Arora. "A study of mathematical programmingmethods for structural optimization. Part II: Numerical results". In: *International Journal for Numerical Methods in Engineering* 21.9 (Sept. 1985), pp. 1601–1623.

[75] M. J. D. Powell. "An efficient method for finding the minimum of a function of several variables without calculating derivatives". In: *The Computer Journal* 7.2 (Feb. 1964), pp. 155–162.

[76] James T. Allison, Tinghao Guo, and Zhi Han. "Co-Design of an Active Suspension Using Simultaneous Dynamic Optimization". In: *Journal of Mechanical Design* 136.8 (June 2014), p. 081003.

[77] Yurii Alekseevich Kochetkov and VK Tomshin. "Optimal control of deterministic systems described by integro-differential equations". In: *Avtomatika i Telemekhanika* 1 (1978), pp. 5–11.

[78] M. Y. Chou and James R. Chelikowsky. "First-principles study of hydrogen adsorption on Ru(0001): Possible occupation of subsurface sites". In: *Physical Review Letters* 59.15 (Oct. 1987), pp. 1737–1740.

[79] Dong-Her Shih and Lai-Fwu Wang. "Optimal control of deterministic systems described by integrodifferential equations". In: *International Journal of Control* 44.6 (Dec. 1986), pp. 1737–1745.

[80] Anil V Rao. "A survey of numerical methods for optimal control". In: *Advances in the Astronautical Sciences* 135.1 (2009), pp. 497–528.

[81] Lakshmi Gururaja Rao and James T. Allison. "Generalized Viscoelastic Material Design With Integro-Differential Equations and Direct Optimal Control". In: *Volume 2B: 41st Design Automation Conference*. ASME, Aug. 2015.

[82] Uri M Ascher and Linda R Petzold. *Computer methods for ordinary differential equations and differential-algebraic equations*. Vol. 61. Siam, 1998.

[83] Giorgio Bacelli and John V. Ringwood. "Numerical Optimal Control of Wave Energy Converters". In: *IEEE Transactions on Sustainable Energy* 6.2 (Apr. 2015), pp. 294–302.

[84] F. Khellat. "Optimal Control of Linear Time-Delayed Systems by Linear Legendre Multiwavelets". In: *Journal of Optimization Theory and Applications* 143.1 (May 2009), pp. 107–121.

[85] Mohsen Razzaghi and Hamid-Reza Marzban. "Direct method for variational problems via hybrid of block-pulse and chebyshev functions". In: *Mathematical Problems in Engineering* 6.1 (2000), pp. 85–97.

[86] R. Y. Chang and M. L. Wang. "Shifted Legendre direct method for variational problems". In: *Journal of Optimization Theory and Applications* 39.2 (Feb. 1983), pp. 299–307.

[87] Gamal N Elnagar and Mohsen Razzaghi. "A collocation-type method for linear quadratic optimal control problems". In: *Optimal Control Applications and Methods* 18.3 (1997), pp. 227–235.

[88] C. Hwang and Y. P. Shih. "Optimal control of delay systems via block pulse functions". In: *Journal of Optimization Theory and Applications* 45.1 (Jan. 1985), pp. 101–112.

[89] Mamdouh M. El-Kady and Hachem Moussa. "Monic Chebyshev Approximations for Solving Optimal Control Problem with Volterra Integro Differential Equations". In: 2013.

[90] Rong Horng and Horng Chou. "Shifted Chebyshev direct method for solving variational problems". In: *International Journal of Systems Science* 16.7 (July 1985), pp. 855–861.

[91] M. Tavassoli Kajani and A. Hadi Vencheh. "Solving second kind integral equations with Hybrid Chebyshev and Block-Pulse functions". In: *Applied Mathematics and Computation* 163.1 (Apr. 2005), pp. 71–77.

[92] Xing Tao Wang and Yuan Min Li. "Numerical solutions of integrodifferential systems by hybrid of general block-pulse functions and the second Chebyshev polynomials". In: *Applied Mathematics and Computation* 209.2 (Mar. 2009), pp. 266–272.

[93] H.R. Marzban and M. Razzaghi. "Optimal control of linear delay systems via hybrid of block-pulse and Legendre polynomials". In: *Journal of the Franklin Institute* 341.3 (May 2004), pp. 279–293.

[94] Chun-Hui Hsiao. "Hybrid function method for solving Fredholm and Volterra integral equations of the second kind". In: *Journal of Computational and Applied Mathematics* 230.1 (Aug. 2009), pp. 59–68.

[95] V. B. Singh, P. K. Kapur, and Abhishek Tandon. "Measuring reliability growth of software by considering fault dependency, debugging time Lag functions and irregular fluctuation". In: *ACM SIGSOFT Software Engineering Notes* 35.3 (May 2010), p. 1.

[96] Khosrow Maleknejad and A. Ebrahimzadeh. "Optimal Control of Volterra Integro-Differential Collocation Method". In: 2014.

[97] H. R. Marzban and M. Razzaghi. "Analysis of Time-delay Systems via Hybrid of Block-pulse Functions and Taylor Series". In: *Modal Analysis* 11.12 (Dec. 2005), pp. 1455–1468.

[98] H.R. Marzban and M. Razzaghi. "Solution of multi-delay systems using hybrid of block-pulse functions and Taylor series". In: *Journal of Sound and Vibration* 292.3-5 (May 2006), pp. 954–963.

[99] V. Yen and M. Nagurka. "Linear Quadratic Optimal Control Via Fourier-Based State Parameterization". In: *Journal of Dynamic Systems, Measurement, and Control* 113.2 (1991), p. 206.

[100] S. Mashayekhi, Y. Ordokhani, and M. Razzaghi. "Hybrid functions approach for optimal control of systems described by integro-differential equations". In: *Applied Mathematical Modelling* 37.5 (Mar. 2013), pp. 3355–3368.

[101] K. Maleknejad and H. Almasieh. "Optimal control of Volterra integral equations via triangular functions". In: *Mathematical and Computer Modelling* 53.9-10 (May 2011), pp. 1902–1909.

[102] Wanfang Shen, Liang Ge, and Danping Yang. "Finite Element Methods For Optimal Control Problems Governed By Linear Quasi-Parabolic Integro-Differential Equations." In: *International Journal of Numerical Analysis & Modeling* 10.3 (2013).

[103] Wanfang Shen, Danping Yang, and Wenbin Liu. "Optimal control problem governed by a linear hyperbolic integro-differential equation and its finite element analysis". In: *Boundary Value Problems* 2014.1 (2014), p. 173.

[104] Wanfang Shen, Liang Ge, Danping Yang, and Wenbin Liu. "A priori error estimates of finite element methods for linear parabolic integro-differential optimal control problems". In: *Advances in Applied Mathematics and Mechanics* 6.4 (2014), pp. 552–569.

[105] Wanfang Shen, Liang Ge, Danping Yang, and Wenbin Liu. "Sharp a posteriori error estimates for optimal control governed by parabolic integro-differential equations". In: *Journal of Scientific Computing* 65.1 (2015), pp. 1–33.

[106] Hermann Brunner and Ningning Yan. "Finite element methods for optimal control problems governed by integral equations and integro-differential equations". In: *Numerische Mathematik* 101.1 (2005), pp. 1–27.

[107] Akylbek Kerimbekov. "On the solvability of a nonlinear optimal control problem for the thermal processes described by fredholm integro-differential equations". In: *Current Trends in Analysis and Its Applications*. Springer, 2015, pp. 803–821.

[108] G. Pepe and A. Carcaterra. "VFC – Variational Feedback Controller and its application to semi-active suspensions". In: *Mechanical Systems and Signal Processing* 76-77 (Aug. 2016), pp. 72–92.

[109] A. Carcaterra G. Pepe N. Roveri. "Prototyping a new car semi-active suspension by variational feedback controller". In: *Proceedings of ISMA 2016 - International Conference on Noise and Vibration Engineering and USD2016 - International Conference on Uncertainty in Structural Dynamics, pp. 231-245.* 2016.

[110] G Pepe, A Carcaterra, I Giorgio, and D Del Vescovo. "Variational Feedback Control for a nonlinear beam under an earthquake excitation". In: *Mathematics and Mechanics of Solids* 21.10 (Aug. 2016), pp. 1234–1246.

[111] S. Pensalfini et al. "Optimal control theory based design of elasto-magnetic metamaterial". In: *Procedia Engineering* 199 (2017), pp. 1761–1766.

[112] A. Carcaterra G. Pepe. "Semi-active damping by variational control algorithms". In: *Proceedings of the International Conference on Structural Dynamic , EURODYN, 2014-January, pp. 1721-1727*. 2014.

[113] G. Pepe and A. Carcaterra. "A new semi-active variational based damping control". In: *2014 IEEE/ASME 10th International Conference on Mechatronic and Embedded Systems and Applications (MESA)*. IEEE, Sept. 2014.

[114] Eduardo F Camacho and Carlos Bordons Alba. *Model predictive control*. Springer Science & Business Media, 2013.

[115] D.Q. Mayne, J.B. Rawlings, C.V. Rao, and P.O.M. Scokaert. "Constrained model predictive control: Stability and optimality". In: *Automatica* 36.6 (June 2000), pp. 789–814.

[116] Pedro Abreu et al. "Marine Vehicles with Streamers for Geotechnical Surveys: Modeling, Positioning and Control". In: *IFAC-PapersOnLine* 49.23 (2016), pp. 458–464.

[117] Filippo Arrichiello, Gianluca Antonelli, and Elbert Kelholt. "Shape estimate of a streamer of hydrophones towed by an Autonomous Underwater Vehicle". In: *IFAC - PaperOnLine* 49.23 (2016), pp. 181–186.

[118] Jaye Falls, Sarah E. Mouring, Ananth Sridharan, and Jean Loomis. "Measured and predicted response of a submerged towed sonar array to maneuvering input". In: *OCEANS 2015 - MTS/IEEE Washington*. IEEE, Oct. 2015.

[119] Hejia Pan and Ming Xin. "Depth control of autonomous underwater vehicles using indirect robust control method". In: *International Journal of Control* 85.1 (Jan. 2012), pp. 98–113.

[120] Z. Feng and R. Allen. "Evaluation of the effects of the communication cable on the dynamics of an underwater flight vehicle". In: *Ocean Engineering* 31.8-9 (June 2004), pp. 1019–1035.

[121] J.N. Newmann. *Marine hydrodynamics*. MIT Press, Cambridge, 1978.

[122] T Francis Ogilvie. "Singular perturbation problems in ship hydrodynamics". In: *Adv. Appl. Mech* 17 (1977), pp. 91–188.

[123] WE Cummins. *The impulse response function and ship motions*. Tech. rep. David Taylor Model Basin Washington DC, 1962.

[124] A. E. Bryson. *Applied Optimal Control*. 1975.

[125] E. Paifelman, G. Pepe, and A. Carcaterra. "Control of fluctuations of a tethered unmanned-underwater-vehicle". In: *ISMA Conference 2018*. 2018.

[126] Steven De Lannoy. "Method to determine correction factors for Section Modulus and Bending Inertia Equations of Wings". In: ().

[127] Halil Akçakaya and Leyla Gören Sümer. "Robust control of variable speed autonomous underwater vehicle". In: *Advanced Robotics* (Jan. 2014), pp. 1–11.